

***IN VIVO* PROTEIN LABELING FOR STRUCTURAL AND
FUNCTIONAL INVESTIGATION OF THE 5-HT_{3A}
NEUROTRANSMITTER RECEPTOR**

THÈSE N° 3016 (2004)

PRÉSENTÉE À LA FACULTÉ SCIENCES DE BASE

Institut des sciences et ingénierie chimiques

SECTION DE CHIMIE ET GÉNIE CHIMIQUE

ÉCOLE POLYTECHNIQUE FÉDÉRALE DE LAUSANNE

POUR L'OBTENTION DU GRADE DE DOCTEUR ÈS SCIENCES

PAR

Erwin ILEGEMS

chimiste diplômé de l'Université de Lausanne
et de nationalité belge

acceptée sur proposition du jury:

Prof. H. Vogel, directeur de thèse
Dr K. Lundstrom, rapporteur
Dr G. Turcatti, rapporteur
Prof. F. Wurm, rapporteur

Lausanne, EPFL
2004

Table of contents

Version abrégée.....	1
Summary.....	2
Abbreviations.....	3
Protein labeling and its applications	5
0.1.1 Introduction	6
0.1.2 References	9
Part I Protein labeling via genetic fusion to fluorescent proteins	13
I.1.1 Introduction	14
I.1.2 References	17
I.2 Noninvasive imaging of 5-HT ₃ receptor trafficking in live cells: from biosynthesis to endocytosis.....	19
I.2.1 Abstract	20
I.2.2 Introduction	21
I.2.3 Experimental procedures.....	22
I.2.4 Results	26
I.2.5 Discussion.....	38
I.2.6 References	40
I.3 Probing the 5-HT ₃ receptor function in single native vesicles.....	45
I.3.1 Abstract	46
I.3.2 Introduction	47
I.3.3 Experimental procedures.....	48
I.3.4 Results	50
I.3.5 Discussion.....	53
I.3.6 References	54

I.4	GFPs at the intracellular side of the 5-HT ₃ receptor sense transmembrane mediated conformational changes induced by extracellular binding of agonist.....	57
I.4.1	Abstract	58
I.4.2	Introduction	59
I.4.3	Experimental procedures.....	60
I.4.4	Results	64
I.4.5	Discussion.....	74
I.4.6	References	77
Part II Protein labeling using mis-acylated suppressor tRNA technology		81
II.1.1	Introduction	82
II.1.2	References	86
II.2	mRNA transfection as a mean to achieve homogeneous protein expression: uptake and expression profiles	93
II.2.1	Abstract	94
II.2.2	Introduction	95
II.2.3	Experimental procedures.....	96
II.2.4	Results	98
II.2.5	Discussion.....	102
II.2.6	References	103
II.3	Monitoring mis-acylated tRNA suppression efficiency in mammalian cells via EGFP fluorescence recovery.....	105
II.3.1	Abstract	106
II.3.2	Introduction	107
II.3.3	Experimental procedures.....	108
II.3.4	Results	112
II.3.5	Discussion.....	116
II.3.6	References	118
II.4	Quantification of natural nonsense codon suppression in mammalian cells using an EGFP reporter assay.....	121
II.4.1	Abstract	122
II.4.2	Introduction	123
II.4.3	Experimental procedures.....	124

II.4.4	Results	127
II.4.5	Discussion.....	131
II.4.6	References	133
II.5	RNA interference targeting eRF1 in human cells increases mis-acylated tRNA suppression efficiency.....	137
II.5.1	Abstract	138
II.5.2	Introduction	139
II.5.3	Experimental procedures.....	140
II.5.4	Results	145
II.5.5	Discussion.....	150
II.5.6	References	152
III	Conclusions and outlook	155
III.1.1	Conclusions and outlook.....	156
III.1.2	References	159
IV	Appendix.....	161
IV.1	Murine 5-HT _{3A} receptor cDNA.....	162
IV.2	Bioluminescent proteins cDNAs	164
IV.3	Subcellular targeting sequences	167
IV.4	References.....	172

Dans le cadre de cette thèse, je présente deux techniques de marquage de protéines par fluorescence, afin d'étudier *in vivo* les fonctions du récepteur de la sérotonine 5-HT₃ (5-HT₃R). Cette protéine membranaire contient cinq sous-unités formant un canal ionique dont l'ouverture est induite par la fixation d'un neurotransmetteur spécifique au 5-HT₃R.

La première technique, décrite dans la première partie de cette thèse, consiste au marquage du récepteur par fusion génétique à une protéine fluorescente. J'ai développé des chimères du 5-HT₃R contenant une protéine fluorescente (GFP) par sous-unité, et qui conservent leurs fonctionnalités biologiques de fixation de ligand et de canal ionique. L'addition d'une dimension visuelle à ce récepteur permet une grande variété d'expériences, parmi lesquelles je présente la possibilité de suivre en détail son cycle de vie, de l'assemblage de ses cinq sous-unités dans le réticulum endoplasmique, sa disposition sur la membrane cellulaire, jusqu'à son internalisation induite par un ligand. L'imagerie multicolore par microscopie confocale permet en outre de dévoiler l'importance du cytosquelette pour le transport du récepteur vers la membrane et sa répartition.

La destruction partielle des filaments d'actine engendre la production de fractions de cellules sous forme de vésicules de diamètres s'échelonnant entre 0.1 et quelques micromètres. La fluorescence émise par la GFP attachée au 5-HT₃R permet d'observer que ces "vésicules natives" contiennent à leur surface les protéines membranaires originant de la cellule. Je montre que l'activité ionique liée à ces récepteurs peut être mesurée par fluorescence sur les vésicules, et que ces dernières peuvent potentiellement remplacer les cellules entières pour analyser les fonctions de base du récepteur.

Je démontre également que la fixation extracellulaire d'un ligand sur le récepteur induit un changement de conformation transmembranaire du récepteur mesurable par la fluorescence des protéines de marquage situées dans le domaine intracellulaire du récepteur.

Dans la deuxième partie de cette thèse, j'étudie une technique basée sur l'utilisation d'ARNt suppresseurs mis-acylés permettant l'incorporation d'acides aminés artificiels fluorescents dans une protéine. Je parviens à adapter cette technique à une utilisation dans des cellules CHO, et obtiens une efficacité d'incorporation de l'ordre de 15%. Une méthode originale est également développée afin de quantifier dans différentes cellules la suppression naturelle, permettant de définir pour chaque lignée cellulaire la paire codon-anticodon la mieux adaptée à la technique d'ARNt suppresseur. Finalement, je présente une nouvelle stratégie permettant d'améliorer l'efficacité d'incorporation d'acides aminés artificiels en diminuant *in vivo* la quantité d'eRF1 par le biais d'ARN interférents.

Summary

In this thesis, two different fluorescent labeling techniques for *in vivo* investigations on the 5-HT₃ receptor (5-HT₃R) functions are presented. This plasma membrane protein contains five subunits surrounding an ion channel that opens after binding of a 5-HT₃-specific neurotransmitter.

The first technique, described in the first part of this report, focuses on receptor labeling via genetic fusion to spectral variants of the green fluorescent protein. I found that the resulting chimeras containing one fluorescent protein per subunit exhibit preserved ligand binding and channel activity, opening a wide range of biological research applications. Among these, I present the possibility to follow the 5-HT₃R trafficking and localization during its entire life cycle by multicolor imaging in live cells, starting with its cytoplasmic biogenesis and ending with its ligand-induced internalization. The intracellular subunit assembly is shown to occur in the endoplasmic reticulum, and the importance of the cytoskeleton microtubules for proper membrane targeting is unraveled.

The utility of bioluminescent 5-HT₃R constructs was also demonstrated in another approach using the chemical disruption of cellular actin filaments to produce vesicular fractions of cells, in the order of 0.1 to a few micrometers in diameter. These so-called native vesicles, containing the labeled receptors in their membrane, were shown to be suitable for measurements using fluorescence confocal microscopy of ligand binding and of ion influx, opening new possibilities for miniaturized bioanalytics.

In a third approach, I demonstrated that after detergent-solubilization of the receptor, the green fluorescent protein (GFP) inserted into the receptor sequence permitted to monitor ligand binding via fluorescence resonance energy transfer (FRET). Furthermore, I could observe a spatial reorientation of the receptor GFPs upon binding an agonist to the receptor.

In the second part of this thesis, I adapted the mis-acylated suppressor tRNA technology to mammalian cells, permitting the introduction of unnatural amino acids at specific positions in the protein of interest. I achieved an efficiency of amino acid incorporation using *in vitro* aminoacylated suppressor tRNA in the order of 15% in CHO cells. A novel methodology for the quantification of background natural nonsense codon readthrough in different cell lines was also developed, permitting to select the most suitable codon-anticodon pair for this suppressor tRNA technique in various cell lines. Finally, I present a general strategy to increase the aforementioned artificial incorporation efficiency by down-regulating the competing eukaryotic release factor 1 (eRF1) using small interfering RNAs.

Abbreviations

5-HT ₃ R	5-hydroxytryptamine (serotonin) 3 receptor
AARS	aminoacyl RNA synthetase
AMA	human epithelial amnion cells
C12E9	nonethyleneglycol monodecyl ether
CAT	chloramphenicol acetyltransferase
CD	circular dichroism
cDNA	complementary DNA
CHO	Chinese hamster ovary cell
cmc	critical micellar concentration
COS1	African green monkey kidney cells
DEPC	diethylpyrocarbonate
DHFR	dehydrofolate reductase
DMSO	dimethylsulfoxide
DNA	deoxyribonucleic acid
DOTAP	N-[1-(2,3-Dioleoyloxy)]-N,N,N-trimethylammonium propane methylsulfate
EC50	half maximal effective concentration
ECFP	enhanced cyan fluorescent protein
EDTA	ethylenediaminetetraacetic acid
EGFP	enhanced green fluorescent protein
EGTA	ethylene glycol-bis(2-aminoethylether)-N,N,N',N'-tetraacetic acid
ER	endoplasmic reticulum
eRF1	eukaryotic release factor 1
EYFP	enhanced yellow fluorescent protein
FACS	fluorescence activated cell sorting
FCS	fetal calf serum
FLASH	4',5'-bis(1,3,2-dithioarsolan-2-yl)fluorescein
FRET	fluorescence resonance energy transfer
GABA _A	γ-aminobutyric acid receptor
GAPDH	glyceraldehyde-3-phosphate dehydrogenase
GFP	green fluorescent protein
hAGT	human O ⁶ -alkylguanine-DNA alkyltransferase
HEK293	human embryonic kidney cell
HeLa	human cervical carcinoma cells
Hepes	4-(2-hydroxyethyl)-1-piperazineethanesulfonic acid
IC50	half maximal inhibitory concentration
K _d	dissociation constant
K _i	inhibition constant
LGIC	ligand-gated ion channel
mCPBG	1-(<i>m</i> -chlorophenyl)-biguanide
mRNA	messenger RNA
N1E-115	murine neuroblastoma cell
nAChR	nicotinic acetylcholine receptor
NaOAc	sodium acetate
NaPi	NaH ₂ PO ₄ -Na ₂ HPO ₄
NMR	nuclear magnetic resonance
NTA	nitrilotriacetate
PBS	phosphate-buffered saline
RNA	ribonucleic acid
siRNA	short interfering RNA
THF	tetrahydrofuran
tRNA	transfer RNA

Thesis

***In vivo* protein labeling for structural and functional investigation of the 5-HT_{3A} neurotransmitter receptor**

Thesis - General introduction on protein labeling and its applications

0.1.1 Introduction

Understanding the functions and interactions of proteins can be of great benefit for advances in pharmaceutical research. Indeed, proteins such as ligand-gated ion channels act as important drug targets by activating or blocking of their channel via the submission of ligands. A complete study of a specific protein would require deciphering its function and localization *in vivo* as well as its structure and activities. However, specific investigations are confronted to the large number of other molecules present in the living cell. The studied protein would require a specific “tag” to be distinguishable from the thousands of different endogenous proteins.

Fluorescent labels equip proteins under investigation with a unique property that can be exploited for both spatial and temporal monitoring of the proteins functions. Such labeling permits the study of a wide range of intracellular processes – including gene expression [1-4] or cytoskeleton network visualization [5-7] – by the specific detection of single cellular elements.

Absorption of a photon by a fluorescent molecule causes a transition to an excited state that decays back to ground state by the emission of a lower energy photon, generating a fluorescent signal. This entire fluorescence process is cyclical: unless the fluorophore is irreversibly destroyed in the excited state (photobleaching), the same fluorophore can be repeatedly excited and detected, generating many thousands of detectable photons. This fluorescence emission can be visualized quantitatively by various ways. For example fluorescence spectrofluorometers and microplate readers allow to measure the average signal emitted by molecules in solution, while the use of a confocal microscope permits *in situ* detection of fluorescent probes in live cells, producing optical sections by excluding out-of-focus light.

An evident prerequisite for high detection sensitivity is that the labeled protein must be strongly fluorescent and distinguishable from the background signals originating from endogenous sample constituents. A wise selection of the fluorescent label in respect to its extinction coefficient, quantum yield and resistance to photobleaching, as well as a refinement of the detection specificity by the use of appropriate filter sets is therefore crucial to proper application of fluorescence quantification techniques.

The main objection towards labeling of proteins is the possibility that the tag might interfere with the function of the investigated protein and that therefore this protein might not reflect anymore the behavior of its unmodified form. It is hence of utmost importance to probe the basic functions of the engineered protein under study.

In addition to spatial distribution and colocalization studies, multiple site-specific fluorescent labeling of proteins permits in some cases the determination of inter- or intramolecular distances by experiments based on fluorescence resonance energy transfer (FRET). This process of radiationless energy transfer from a fluorescent donor molecule to a fluorescent acceptor in very close proximity occurs when the emission spectrum of the donor overlaps that of the acceptor excitation, and results in the reduction in the donor fluorescence intensity and an increase in the acceptor emission intensity. The efficiency of this process depends on the inverse sixth power of the distance between donor and acceptor as described by Förster [8,9]. Hence FRET provides a “molecular ruler” for determining distances between a donor and an acceptor when they are in the order of 10 to 100 Å apart, making it ideal for short-range protein interaction studies [10] and a valuable complement to x-ray diffraction and NMR structure determination.

During the past decade a number of new tools were developed for labeling proteins within cells, providing high sensitivity and versatility while trying to minimize perturbation of the host cell. Post-translational fluorescent labeling techniques are based on labeling of the protein itself (using for instance antibodies [11,12] or ligands [13]), or on the labeling of a peptide genetically fused to the protein of interest (e.g. bi-arsenic labeling of tetracysteine motifs [14-18], alkyltransferase labeled with enzymatic substrate derivatives [19], peptide biotinylation by biotin ligases [20-22], dihydrofolate reductase (DHFR) labeled with fluorescent derivatives of methotrexate [23-25], metal-ion-chelating nitrilotriacetate (NTA) labeling of oligohistidine sequences [26], semiconductor nanocrystals (quantum dots) [27-29]).

Another strategy consists on the site-specific labeling of the protein under investigation at an earlier stage, while it is being translated. This can be achieved via genetic fusion to an autofluorescent protein [2] or via unnatural fluorescent amino acid incorporation using mis-acylated suppressor tRNAs [30], techniques approached respectively in the first and second parts of this thesis. The main advantage of a fluorescent tag integration occurring directly during translation resides in the fact that it potentially allows for quantitative labeling of the protein under investigation. Also, the protein can then be observed in live cells without further fixation and labeling procedures, circumventing any background fluorescence related to unbound or nonspecifically bound probes.

In this report, different labeling and visualization technologies have been optimized in the prospect of biological, bioanalytical and biophysical analysis of the pharmacologically important 5-HT₃ neurotransmitter receptor (5-HT₃R). In that sense and as an initial approach towards fluorescent labeling at an early stage of the nascent protein I genetically modified its sequence by the insertion of bioluminescent proteins. The obtained chimeras were probed to be functionally active in terms of ligand binding and channel activation and offered a wide range of research possibilities, some of which being presented in the first part of this thesis. In addition, the limitations of this labeling technique are discussed.

I then focused on a technique permitting the site-specific incorporation of much smaller fluorescent probes than obtained via protein fusion. This mis-acylated suppressor tRNA method is based on the integration of unnatural amino acids, which can be autofluorescent or fluorescently-labeled at a later stage. While technically more challenging, this procedure permits potentially to introduce small probes at specific positions where protein fusion would structurally or functionally alter the original protein. However, this technique was originally developed as an *in vitro* method [31,32], and later applied *in vivo* in *Xenopus oocytes* [30] and *Escherichia coli* [33]. In the second part of this thesis, I aimed to expand the suppressor tRNA technology to cultured mammalian cells, generally more suitable for structural and functional studies of human derived proteins such as the 5-HT₃R.

0.1.2 References

1. Chalfie, M., Tu, Y., Euskirchen, G., Ward, W.W. and Prasher, D.C. (1994) Green fluorescent protein as a marker for gene expression. *Science*, **263**, 802-805.
2. Kain, S.R., Adams, M., Kondepudi, A., Yang, T.T., Ward, W.W. and Kitts, P. (1995) Green fluorescent protein as a reporter of gene expression and protein localization. *Biotechniques*, **19**, 650-655.
3. Li, X., Zhao, X., Fang, Y., Jiang, X., Duong, T., Fan, C., Huang, C.C. and Kain, S.R. (1998) Generation of destabilized green fluorescent protein as a transcription reporter. *J Biol Chem*, **273**, 34970-34975.
4. Pick, H.M., Meissner, P., Preuss, A.K., Tromba, P., Vogel, H. and Wurm, F.M. (2002) Balancing GFP reporter plasmid quantity in large-scale transient transfections for recombinant anti-human Rhesus-D IgG1 synthesis. *Biotechnol Bioeng*, **79**, 595-601.
5. Presley, J.F., Cole, N.B., Schroer, T.A., Hirschberg, K., Zaal, K.J. and Lippincott-Schwartz, J. (1997) ER-to-Golgi transport visualized in living cells. *Nature*, **389**, 81-85.
6. Toomre, D., Keller, P., White, J., Olivo, J.C. and Simons, K. (1999) Dual-color visualization of trans-Golgi network to plasma membrane traffic along microtubules in living cells. *J Cell Sci*, **112 (Pt 1)**, 21-33.
7. Kimble, M., Kuzmiak, C., McGovern, K.N. and de Hostos, E.L. (2000) Microtubule organization and the effects of GFP-tubulin expression in dictyostelium discoideum. *Cell Motil Cytoskeleton*, **47**, 48-62.
8. Forster, T. (1946) Energiewanderung Und Fluoreszenz. *Naturwissenschaften*, **33**, 166-175.
9. Forster, T. (1948) Zwischenmolekulare Energiewanderung Und Fluoreszenz. *Annalen Der Physik*, **2**, 55-75.
10. Lankiewicz, L., Malicka, J. and Wiczak, W. (1997) Fluorescence resonance energy transfer in studies of inter-chromophoric distances in biomolecules. *Acta Biochim Pol*, **44**, 477-489.
11. Ng, T., Squire, A., Hansra, G., Bornancin, F., Prevostel, C., Hanby, A., Harris, W., Barnes, D., Schmidt, S., Mellor, H. *et al.* (1999) Imaging protein kinase Calpha activation in cells. *Science*, **283**, 2085-2089.
12. Verveer, P.J., Wouters, F.S., Reynolds, A.R. and Bastiaens, P.I. (2000) Quantitative imaging of lateral ErbB1 receptor signal propagation in the plasma membrane. *Science*, **290**, 1567-1570.
13. McGrath, J.C., Arribas, S. and Daly, C.J. (1996) Fluorescent ligands for the study of receptors. *Trends Pharmacol Sci*, **17**, 393-399.

14. Griffin, B.A., Adams, S.R. and Tsien, R.Y. (1998) Specific covalent labeling of recombinant protein molecules inside live cells. *Science*, **281**, 269-272.
15. Gaietta, G., Deerinck, T.J., Adams, S.R., Bouwer, J., Tour, O., Laird, D.W., Sosinsky, G.E., Tsien, R.Y. and Ellisman, M.H. (2002) Multicolor and electron microscopic imaging of connexin trafficking. *Science*, **296**, 503-507.
16. Adams, S.R., Campbell, R.E., Gross, L.A., Martin, B.R., Walkup, G.K., Yao, Y., Llopis, J. and Tsien, R.Y. (2002) New biarsenical ligands and tetracysteine motifs for protein labeling in vitro and in vivo: synthesis and biological applications. *J Am Chem Soc*, **124**, 6063-6076.
17. Rice, M.C., Czymmek, K. and Kmiec, E.B. (2001) The potential of nucleic acid repair in functional genomics. *Nat Biotechnol*, **19**, 321-326.
18. Stroffekova, K., Proenza, C. and Beam, K.G. (2001) The protein-labeling reagent FLASH-EDT2 binds not only to CCXXCC motifs but also non-specifically to endogenous cysteine-rich proteins. *Pflugers Arch*, **442**, 859-866.
19. Keppler, A., Gendreizig, S., Gronemeyer, T., Pick, H., Vogel, H. and Johnsson, K. (2003) A general method for the covalent labeling of fusion proteins with small molecules in vivo. *Nat Biotechnol*, **21**, 86-89.
20. Cronan, J.E., Jr. (1990) Biotination of proteins in vivo. A post-translational modification to label, purify, and study proteins. *J Biol Chem*, **265**, 10327-10333.
21. Cronan, J.E., Jr. and Reed, K.E. (2000) Biotinylation of proteins in vivo: a useful posttranslational modification for protein analysis. *Methods Enzymol*, **326**, 440-458.
22. Cull, M.G. and Schatz, P.J. (2000) Biotinylation of proteins in vivo and in vitro using small peptide tags. *Methods Enzymol*, **326**, 430-440.
23. Israel, D.I. and Kaufman, R.J. (1993) Dexamethasone negatively regulates the activity of a chimeric dihydrofolate reductase/glucocorticoid receptor protein. *Proc Natl Acad Sci U S A*, **90**, 4290-4294.
24. Remy, I. and Michnick, S.W. (1999) Clonal selection and in vivo quantitation of protein interactions with protein-fragment complementation assays. *Proc Natl Acad Sci U S A*, **96**, 5394-5399.
25. Remy, I. and Michnick, S.W. (2001) Visualization of biochemical networks in living cells. *Proc Natl Acad Sci U S A*, **98**, 7678-7683.
26. Guignet, E.G., Hovius, R. and Vogel, H. (2004) Reversible site-selective labeling of membrane proteins in live cells. *Nat Biotechnol*.

-
27. Wu, X., Liu, H., Liu, J., Haley, K.N., Treadway, J.A., Larson, J.P., Ge, N., Peale, F. and Bruchez, M.P. (2003) Immunofluorescent labeling of cancer marker Her2 and other cellular targets with semiconductor quantum dots. *Nat Biotechnol*, **21**, 41-46.
 28. Jaiswal, J.K., Mattoussi, H., Mauro, J.M. and Simon, S.M. (2003) Long-term multiple color imaging of live cells using quantum dot bioconjugates. *Nat Biotechnol*, **21**, 47-51.
 29. Dubertret, B., Skourides, P., Norris, D.J., Noireaux, V., Brivanlou, A.H. and Libchaber, A. (2002) In vivo imaging of quantum dots encapsulated in phospholipid micelles. *Science*, **298**, 1759-1762.
 30. Turcatti, G., Nemeth, K., Edgerton, M.D., Meseth, U., Talabot, F., Peitsch, M., Knowles, J., Vogel, H. and Chollet, A. (1996) Probing the structure and function of the tachykinin neurokinin-2 receptor through biosynthetic incorporation of fluorescent amino acids at specific sites. *J Biol Chem*, **271**, 19991-19998.
 31. Kurzchalia, T.V., Wiedmann, M., Breter, H., Zimmermann, W., Bauschke, E. and Rapoport, T.A. (1988) tRNA-mediated labelling of proteins with biotin. A nonradioactive method for the detection of cell-free translation products. *Eur J Biochem*, **172**, 663-668.
 32. Noren, C.J., Anthony-Cahill, S.J., Suich, D.J., Noren, K.A., Griffith, M.C. and Schultz, P.G. (1990) In vitro suppression of an amber mutation by a chemically aminoacylated transfer RNA prepared by runoff transcription. *Nucleic Acids Res*, **18**, 83-88.
 33. Liu, D.R., Magliery, T.J., Pastrnak, M. and Schultz, P.G. (1997) Engineering a tRNA and aminoacyl-tRNA synthetase for the site-specific incorporation of unnatural amino acids into proteins in vivo. *Proc Natl Acad Sci U S A*, **94**, 10092-10097.

Chapter I.1

Part I: protein labeling via genetic fusion to fluorescent proteins

Part I - Protein labeling via genetic fusion to fluorescent proteins

I.1.1 Introduction

The advent of genetically encoded dyes began with the discovery of the green fluorescent protein (GFP), originally isolated from the light-emitting organ of the jellyfish *Aequorea victoria* in 1962 [1]. About 30 years later its encoding complementary DNA was characterized [2], permitting to expand the expression of this protein to a wide variety of tissues and organisms, which revolutionized modern cell biology.

The green light emitted by *A. victoria* is the result of an energy transfer between the photoprotein aequorin – producing blue light after calcium binding – and the GFP. Activation of the green fluorescent protein alone *in vitro* or in heterologous cells can be achieved via light excitation of its immanent fluorophore. The GFP structure consists of an 11-stranded β -barrel with a coaxial helix; its centrally-located chromophore is formed by autocatalytic internal cyclization and oxidation of the Ser-Tyr-Gly sequence at positions 65-67 within the 238 amino-acid polypeptide [3,4] (Figure I.1.1).

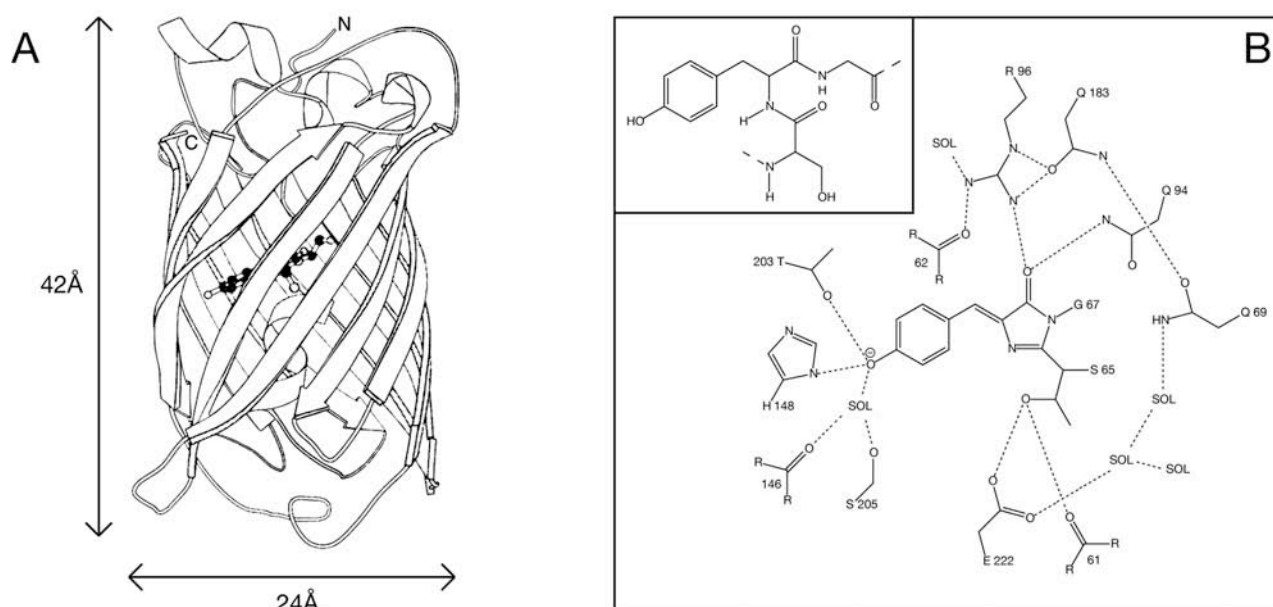


Figure I.1.1 (A) Structure of the green fluorescent protein (GFP) and (B) interactions between the encaged fluorophore and its surrounding amino acids and water solvent (“SOL”). Inset in B represents the centrally located Ser-Tyr-Gly sequence before its cyclization (Figures adapted from Ormö et al. [4]).

As the GFP is intrinsically fluorescent, chimeric *in situ* expressed fusion proteins can be monitored *in vivo*. Depending on the protein under investigation, its GFP-tagging can be the result of a simple amino or carboxyl terminus sequence fusion or a more complex genetic incorporation of the GFP. Functionality of the obtained protein fusion can generally be assessed by proper localization and by its biochemical activity. In addition to specific protein labeling GFP fusions can be localized to particular sites within the cell by appropriate targeting signals [5], enlightening the spatial distribution of all major organelles (see Appendix IV.3).

The engineering of mutated versions of the *Aequorea* GFP permitted the expansion of the color repertoire covered by this fluorescent protein. Extensive mutagenesis – mostly near the central chromophore position – created a number of GFP variants with differing excitation and emission properties (Appendix IV.2.1). Additionally, the recent discovery of novel GFP-like proteins originating from other organisms such as *Discosoma* and *Anthozoa* have furthermore expanded the range of available colors, virtually covering the whole visible spectra. As a result, the family of autofluorescent proteins now includes approximately 30 significantly different members [6,7], which can be used in conjunction [8] or in combination with other fluorescent molecules for both multicolor labeling and fluorescent resonance energy transfer experiments.

In the first part of this thesis, I focus on the fluorescent labeling of the 5-HT₃ receptor (5-HT₃R) type A via genetic fusion to bioluminescent proteins. This particular ligand-gated ion channel inducing fast depolarizing neuronal responses after binding of the 5-hydroxytryptamine (5-HT or serotonin) neurotransmitter secreted from the presynaptic membrane [9] has been shown to be of medical and pharmaceutical interest by specific ligand administration, in particular for suppression of the emesis caused by anticancer chemotherapy and radiation [10], or for treating schizophrenia and other psychiatric disorders [11-14]. An accrued knowledge of cellular trafficking, ligand binding and channel gating of such neurotransmitter receptors would be beneficial to advances in drug research.

As an initial step, I found a suitable genetic position for the insertion of GFP-like protein sequences into that of the receptor under investigation, which resulted in chimeric proteins presenting preserved ligand binding and channel activity. I first show in chapter I.2 that the autofluorescence of the resulting receptor permits to monitor its trafficking and membrane organization *in vivo* after transient expression. In combination with a spectrally distinguishable variant of the green fluorescent protein targeted to different specific cytoplasmic organelles and with 5-HT₃R-specific fluorescent ligands, this labeling allows for the determination of subcellular assembly of the

receptor by multicolor imaging, and permits a better understanding of the cellular cytoskeleton function for receptor trafficking and localization.

In the two following chapters, I investigate different *in vitro* techniques to measure ligand binding as well as channel activation on sub-cellular systems, potentially applicable for multiarray bioanalytical drug screening methodologies. In chapter I.3, I show that the vesicles protruding from the plasma membrane after chemical disruption of actin filaments in cells expressing the fluorescently-labeled 5-HT₃R contain the chimera receptor. These so-called “native vesicles” permit additionally to observe calcium influx after agonist-induced receptor activation, as measured by confocal fluorescence microscopy using a calcium sensitive dye. In the last chapter of this first part, I demonstrate that detergent-solubilized labeled receptors – completely separated from their originating cell – also allow for both ligand binding affinity and channel activation measurements via fluorescence resonance energy transfer quantification, and we discuss the possibility to obtain precise resulting structural information using GFP as an energy donor and acceptor.

I.1.2 References

1. Shimomura, O., Johnson, F.H. and Saiga, Y. (1962) Extraction, purification and properties of aequorin, a bioluminescent protein from the luminous hydromedusan, *Aequorea*. *J Cell Comp Physiol*, **59**, 223-239.
2. Prasher, D.C., Eckenrode, V.K., Ward, W.W., Prendergast, F.G. and Cormier, M.J. (1992) Primary structure of the *Aequorea victoria* green-fluorescent protein. *Gene*, **111**, 229-233.
3. Heim, R., Prasher, D.C. and Tsien, R.Y. (1994) Wavelength mutations and posttranslational autoxidation of green fluorescent protein. *Proc Natl Acad Sci U S A*, **91**, 12501-12504.
4. Ormö, M., Cubitt, A.B., Kallio, K., Gross, L.A., Tsien, R.Y. and Remington, S.J. (1996) Crystal structure of the *Aequorea victoria* green fluorescent protein. *Science*, **273**, 1392-1395.
5. Blobel, G. (2000) Protein targeting. *Biosci Rep*, **20**, 303-344.
6. Matz, M.V., Fradkov, A.F., Labas, Y.A., Savitsky, A.P., Zaraisky, A.G., Markelov, M.L. and Lukyanov, S.A. (1999) Fluorescent proteins from nonbioluminescent Anthozoa species. *Nat Biotechnol*, **17**, 969-973.
7. Labas, Y.A., Gurskaya, N.G., Yanushevich, Y.G., Fradkov, A.F., Lukyanov, K.A., Lukyanov, S.A. and Matz, M.V. (2002) Diversity and evolution of the green fluorescent protein family. *Proc Natl Acad Sci U S A*, **99**, 4256-4261.
8. Rizzuto, R., Brini, M., De Giorgi, F., Rossi, R., Heim, R., Tsien, R.Y. and Pozzan, T. (1996) Double labelling of subcellular structures with organelle-targeted GFP mutants in vivo. *Curr Biol*, **6**, 183-188.
9. Mott, D.D., Erreger, K., Banke, T.G. and Traynelis, S.F. (2001) Open probability of homomeric murine 5-HT_{3A} serotonin receptors depends on subunit occupancy. *J Physiol*, **535**, 427-443.
10. Walton, S.M. (2000) Advances in use of the 5-HT₃ receptor antagonists. *Expert Opin Pharmacother*, **1**, 207-223.
11. Kilpatrick, G.J. and Tyers, M.B. (1992) Inter-species variants of the 5-HT₃ receptor. *Biochem Soc Trans*, **20**, 118-121.
12. Zoldan, J., Friedberg, G., Livneh, M. and Melamed, E. (1995) Psychosis in advanced Parkinson's disease: treatment with ondansetron, a 5-HT₃ receptor antagonist. *Neurology*, **45**, 1305-1308.

13. Brunello, N., Masotto, C., Steardo, L., Markstein, R. and Racagni, G. (1995) New insights into the biology of schizophrenia through the mechanism of action of clozapine. *Neuropsychopharmacology*, **13**, 177-213.
14. Jones, B.J. and Blackburn, T.P. (2002) The medical benefit of 5-HT research. *Pharmacol Biochem Behav*, **71**, 555-568.

Chapter I.2

Noninvasive imaging of 5-HT₃ receptor trafficking in live cells: from biosynthesis to endocytosis

I.2 Noninvasive imaging of 5-HT₃ receptor trafficking in live cells: from biosynthesis to endocytosis

I.2.1 Abstract

Sequential stages in the life cycle of the ionotropic 5-HT₃ receptor were resolved temporally and spatially in live cells by multi-color fluorescence confocal microscopy. The insertion of the enhanced cyan fluorescent protein into the large intracellular loop delivered a fluorescent 5-HT₃R, fully functional in terms of ligand binding specificity and channel activity, which allowed for the first time to monitor *in vivo* expression, membrane targeting and ligand mediated endocytosis of a receptor. The dynamics of subcellular localizations of the fluorescent 5-HT₃R were investigated by imaging simultaneously the receptor and spectrally distinguishable variants of the green fluorescent protein targeted to particular cytoplasmic organelles. The intracellular delivery of fluorescent 5-HT₃R-specific antagonists allowed the study of ligand binding site formation at an early stage of receptor expression. After novel protein synthesis was chemically blocked, the 5-HT₃ receptor populations in the endoplasmic reticulum and Golgi cisternae moved quantitatively to the cell surface, indicating efficient receptor folding and subunit assembly. The intracellular 5-HT₃ receptors, which were trafficking in vesicle-like structures along microtubules, inserted into the cell membrane in a characteristic cluster distribution overlapping with actin-rich domains. Extracellular agonist application induced rapid internalization of 5-HT₃ receptors. The time course of the disappearance of 5-HT₃ receptors from the cell surface was monitored by measuring the binding of receptor-specific fluorescent ligands at the extracellular membrane surface at different time points after agonist application.

The results of this chapter have been submitted for publication:

Ilegems, E., Pick, H.M., Deluz, C., Kellenberger, S. and Vogel, H.: Noninvasive imaging of 5-HT₃ receptor trafficking in live cells: from biosynthesis to endocytosis.

I.2.2 Introduction

A fundamental interest in neurobiology is the study of processes involved in expression, assembly and subcellular trafficking of neurotransmitter receptors. These receptors are members of a large molecular family of ligand-gated ion channels (LGIC) that include nicotinic acetylcholine (AChRs), serotonin (5-HT₃R), γ -aminobutyric acid (GABA_A), glycine, and ionotropic glutamate receptors [1,2]. All of them are oligomeric membrane proteins composed of subunits surrounding an ion channel that opens upon neurotransmitter binding to the receptor. The structural relationship between the different LGICs suggests that their assembly and trafficking involves similar molecular events [3]. In general, it is thought that subunit assembly occurs shortly after biosynthesis in the endoplasmic reticulum (ER) followed by trafficking to the plasma membrane [4-8]. Methodologies allowing the dynamic observation of these processes have still to be elaborated. In the present study, we focus on the ionotropic 5-HT₃R as a representative member of the LGICs and explore new strategies for following receptor biogenesis in real time starting with the delivery of their coding DNA into living cells. We aim at dissecting events, which occur after their “birth” leading to cell membrane insertion of mature receptors and finally their ligand-induced re-absorption into the cell reflecting the endpoint of their lifespan. Improved understanding of these processes can be expected to provide valuable information for the therapeutic targeting of LGICs at specific stages in their life cycle.

The ionotropic 5-HT₃R type A is known to mediate fast signal transduction across synapses in the nervous system. Homo-pentameric complexes of recombinant 5-HT_{3A} receptors exhibit high cell surface expression levels in heterologous systems [9] and share substantial pharmacological and functional properties with native neuronal 5-HT₃R [10-12]. To date the direct intracellular analysis of 5-HT₃ receptors has been limited to antibody labeling methods [8]. However these technologies are not adequate for visualizing receptors in live cells and cannot be used to label intracellular receptors in non-permeabilized cells. Here we fuse the enhanced cyan fluorescent protein (ECFP) to the 5-HT₃R to visualize the entire sequence of stages in the life of the receptor. The green fluorescent protein and its spectral variants are becoming widely used as molecular reporters to monitor gene expression, localization and intracellular protein trafficking in living cells [13-15]. GFP-tagged proteins often retain their biological activity and have the same trafficking pattern as native proteins [16-20]. The combination of tagging 5-HT₃ receptors with autofluorescent proteins and the parallel use of fluorescent 5-HT₃R specific ligands [21] will be demonstrated as a powerful tool allowing the multicolor analysis of receptor biosynthesis, trafficking and ligand-dependent receptor internalization.

1.2.3 Experimental procedures

Materials

Synthetic oligonucleotides were purchased from MWG-Biotech AG (Ebersberg, Germany), kits for plasmid and DNA-fragment purification from QIAGEN GmbH (Hilden, Germany), restriction endonucleases (*ClaI*, *HindIII* and *NotI*) from New England Biolabs (Massachusetts, USA). The radioligand 3-(5-methyl-1H-imidazol-4-yl)-1-(1-[³H]methyl-1H-indol-3-yl)propanone ([³H]-GR65630; 85.5 Ci/ mmol) was from NEN-DuPont (Boston, MA); the agonist serotonin (5HT) was obtained from Sigma (Buchs, Switzerland), and quipazine and 1-(*m*-chlorophenyl)biguanide (mCPBG) from Tocris-Cookson (Langford, UK). The fluorescent ligands GR-Cy5 (1,2,3,9-tetrahydro-3-[(5-methyl-1H-imidazol-4-yl)methyl]-9-[3-amino-[N-(Cy5)amido]propyl]-4H-carbazol-4-one), GR-Flu (1,2,3,9-tetrahydro-3-[(5methyl-1H-imidazol-4-yl)methyl]-9-(3-amino-(N-fluorescein-thiocarbamoyl)-propyl)-4H-carbazol-4-one) and GR-Rho (1,2,3,9-tetrahydro-3-[(5-methyl-1H-imidazol-4-yl)methyl]-9-[3-amino-[N-(rhodamineB)thiocarbamoyl]-propyl]-4H-carbazol-4-one) were prepared as described elsewhere [21,22]. Triton-X100 was from Fluka (Buchs, Switzerland). The plasmids pEYFP-ER, pEYFP-Golgi, pEYFP-Tub and pEYFP-Actin were purchased from Clontech (California, USA). Other chemicals were from Sigma-Aldrich (Missouri, USA).

DNA constructs

All constructs are based on a vector containing the short splicing variant of the murine 5-hydroxytryptamine type 3A subunit cDNA preceded by the human cytomegalovirus gene promoter, as described before [9].

The vector p5HT3R-ECFP, containing the ECFP-labeled receptor, was obtained as follows: the original vector was first mutated using the oligos 5'-CTG ATG ACT GCT CAA TCG ATG CCA TGG GAA ACC-3' and 5'-GGT TTC CCA TGG CAT CGA TTG AGC AGT CAT CAG-3', adding a *ClaI* restriction site in the large cytoplasmic loop sequence between the 3rd and 4th predicted membrane-spanning domains. The ECFP insert was obtained by PCR amplification on the template pECFP-N1 (Clontech, California, USA) using the synthetic oligonucleotides 5'- CCA TCG ATA TGG TGA GCA AGG GCG AGG -3' and 5'- CCA TCG ATC TTG TAC AGC TCG TCC ATG CCG -3', and ligated into the receptor *ClaI* restriction site. The restriction sites *HindIII* and *NotI* were added to the 5' and 3' ends of the 5-HT3R-EGFP sequence by PCR amplification using the oligonucleotides 5'- CGA TAA GCT TCA CCA TGC GGC TCT GCA TCC CGC AGG TG -3'

and 5'- GCT GTG CCC ACG CGG CCG CTC AAG AAT AAT GCC AAA TGG ACC AGAG -3', and the purified 2197 bp fragment was sub-cloned into the *HindIII/NotI* cut vector pEAK8 (Edge BioSystems, Gaithersburg, MD, USA), giving rise to the vector p5HT3R-ECFP.

The vector p5HT3R was obtained by sub-cloning the non-mutated receptor gene into the plasmid pEAK8 between *HindIII* and *NotI*, using the same oligos as for constructing p5HT3R-ECFP.

The plasmid constructs were confirmed by restriction mapping and DNA sequencing.

Cell culture, transfections and permeabilization

Adherent human embryonic kidney (HEK293) and N1E-115 cells were grown in DMEM/F12 (Dulbecco's modified Eagle medium; GIBCO BRL, Rockville, USA) supplemented with 2.2 % and 10 % fetal calf serum (GIBCO BRL) respectively, using plastic flasks from TPP (Trasadingen, Switzerland). The cultures were split regularly and kept at 37 °C in a humidified atmosphere with 5 % CO₂.

For electrophysiology, confocal microscopy measurements and membrane purification respectively, cells were seeded in 35 mm cell culture dishes, six-well plates containing 22 mm-diameter glass cover slips and 150 cm² flasks at a density of 150'000 cells/ml and transfected using Lipofectamine 2000 reagent (Invitrogen, Carlsbad, California, USA), according to the manufacturer's instructions. An amount of 4 g of pelleted cells was used for the membrane solubilization.

Fixation of cells was achieved by 10 minutes incubation at room temperature in a solution containing 3.7 % formaldehyde in PBS. Subsequent permeabilization was performed by 5 minutes incubation in presence of 0.1 % Triton-X100 in PBS. Cells were washed three times with PBS between incubations.

Membrane solubilization

All following manipulations were performed on ice or at 4 °C, to avoid degradation of the receptor. The cell pellets were resuspended in 10 ml of a solution containing 10 mM HEPES and 1 mM EDTA at a pH of 7.4, and homogenized for 90 seconds with an Ultra-Turrax T25 (IKA, Staufen, Germany). The membrane fraction was collected by centrifugation at 27'000 g for 40 minutes, and the membrane proteins were solubilized by resuspending and incubating the pellet in 20 ml of 50 mM NaPi (NaH₂PO₄-Na₂HPO₄), 300 mM NaCl and 50 cmc C₁₂E₉ (Anatrace, Maumee, USA) at pH 8.0. A final centrifugation at 100'000 g for 60 minutes served to remove the remaining membrane fraction, and the resulting supernatant was collected and stored at -80 °C until use.

Radioactive binding assays

Receptor concentrations as well as ligand affinities were measured by radioligand binding assay. 100 μ l of cells resuspended in 10 mM Hepes pH7.4 were incubated for 30 minutes at room temperature in solutions of 10 mM Hepes pH7.4 with varying concentrations of the specific antagonist [3 H]-GR65630 in a final volume of 1ml. A rapid filtration through Whatman GF/B filters (presoaked for 15 min in 0.5% (w/v) polyethylenimine) followed by two washes with 3 mL of ice-cold 10 mM Hepes at pH 7.4 terminated the incubation. Filters were then transferred into scintillation vials and 4 mL of Ultima Gold (Packard, Meridan, CT) was added. The radioactivity was measured in a Tri-Carb 2200CA liquid scintillation counter (Packard). Nonspecific binding was determined in the presence of 1 μ M quipazine. All experiments were performed in triplicate. The dissociation constant K_d of [3 H]-GR65630 and the Hill coefficient n were calculated by fitting the experimental data to the binding equation:

$$[GR65630]_{bound} = \frac{[5 - HT_3R]}{1 + (K_d / [GR65630]_{free})^n} \quad [I.2.1]$$

Binding assay on permeabilized cells were processed as above, but the cells were pre-treated with 0.1 % saponin in 10 mM Hepes pH 7.4 for 5 minutes at room temperature before radioligand binding. All experiments were done in triplicate.

Electrophysiology

We used the standard patch-clamp technique in whole-cell voltage-clamp to -60 mV employing an EPC-9 patch-clamp amplifier (HEKA Elektronik Dr. Schulze GmbH, Lambrecht, Germany). For data acquisition and storage the software PULSE 8.3 (HEKA) was used. Borosilicate glass pipettes were heat polished and had resistances of 2-5 M Ω . Pipettes were filled with 140 mM KCl, 5 mM MgCl₂, 10 mM EGTA, 10 mM HEPES-KOH, pH 7.3. The external solution was 147 mM NaCl, 12 mM glucose, 2 mM KCl, 2 mM CaCl₂, 1 mM MgCl₂, 10 mM HEPES-NaOH, pH 7.4. Ligands dissolved in the external solution were applied with a RSC-200 or the MSC-200 perfusion system (Bio-Logic, Claix, France). During experiments the cells were continuously perfused. All experiments were performed at room temperature.

Data were evaluated by fitting to the Hill Equations:

$$I = I_{\max} / \{1 + (EC_{50} / [\text{agonist}])^n\} \quad [\text{I.2.2}]$$

and

$$I = I_0 / \{1 + (IC_{50} / [\text{antagonist}])^{-n}\} \quad [\text{I.2.3}]$$

where I is the peak current at a certain ligand concentration, I_{\max} is the maximal peak current achievable, I_0 is the peak current in absence of any antagonist, EC_{50} and IC_{50} are the half maximal effective and inhibitory concentrations, respectively, and n is the Hill coefficient.

For antagonist-agonist competition experiments, cells were perfused with granisetron containing solutions for three minutes before the addition of serotonin (5-HT) at a concentration of 30 μM .

Laser scanning confocal microscopy and fluorescence measurements

Laser-scanning confocal micographs were recorded using 458 and 488 nm Argon/Krypton and 543 nm HeNe laser lines on a Zeiss LSM 510 microscope (Carl Zeiss AG) equipped with a 63x water (1.2 numerical aperture) objective. Detection and distinction of fluorescence signals was achieved by appropriate filter sets using a multitracking mode. Scanning speed and laser intensity were adjusted to avoid photobleaching of the fluorescent probes, and damage or morphological changes of the cells. The microscope was equipped with a microcultivation system (Incubator S, CTI controller 3700 digital, Zeiss) to control temperature, humidity and CO_2 for maintaining physiological conditions during long term experiments.

Fluorescence measurements on detergent-solubilized 5-HT₃R-ECFP were performed on a SPEX Fluorolog II (Instruments S.A., Stanmore, U.K.), using quartz cuvettes of 1x1 cm² (Hellma, Müllheim, Germany) and 1.5 nm excitation and emission bandwidths for data acquisition.

I.2.4 Results

We investigated the time course of 5-HT₃R plasma membrane expression by analyzing non-permeabilized HEK293 cell samples at different time points after transfection via radioligand binding assay. 5-HT₃R cell surface expression increased over time and reached a maximum number of about 2.6×10^6 receptors per cell 34 hours after transfection (Figure I.2.1).

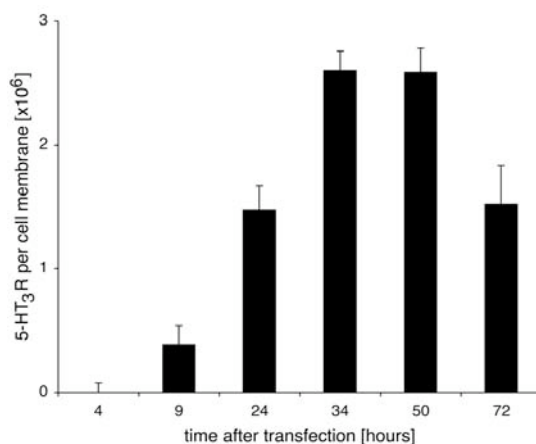


Figure I.2.1 5-HT₃R cell surface expression measured at different time points after transfection via radioligand binding assays on populations of HEK293 cells. The obtained values were divided by the number of cells before transfection, which were in the order of 1×10^6 per assay.

When these cells were permeabilized with saponin it was possible to detect in addition to cell surface receptors also 5-HT₃R-specific ligand binding activity inside the cytoplasm, which accounted to about 40 % of the total ligand binding sites. In N1E-115 cells, which endogenously express the 5-HT₃ receptor, about 60 % of the ligand binding activity was localized inside the cell (Table I.2.1).

	Non-transfected N1E-115 cells	p5HT3R-transfected HEK293 cells
Receptor binding sites per cell on membrane	$5.0 \pm 0.6 \times 10^4$	$2.6 \pm 0.2 \times 10^6$
Total number of receptor binding sites per cell	$1.2 \pm 0.2 \times 10^5$	$4.4 \pm 0.2 \times 10^6$
Percentage of receptor binding sites localized on membrane	$42 \pm 12 \%$	$59 \pm 7 \%$

Table I.2.1 Radioactive binding assays to 5-HT₃R performed on cell membrane and on saponin-permeabilized cells. The values represent average number of 5-HT₃Rs on populations of 1×10^6 cells as measured 34 hours after transient transfection of HEK293 cells or on non-transfected N1E-115 cells.

These results indicate that a substantial fraction of intracellular receptors is capable of binding 5-HT₃R-specific ligands before plasma membrane integration. At this point we decided to analyze intracellular 5-HT₃R formation and trafficking in more detail. In order to observe in real time 5-HT₃R biosynthesis after cell delivery of its coding DNA, we inserted the coding sequence of the enhanced cyan fluorescent protein (ECFP) into the large cytoplasmic loop between the 3rd and 4th predicted membrane-spanning domains in the short splicing variant of the receptor, at the position where in comparison to the large splicing variant six amino acids are missing (homology alignment in Figure I.2.2A).

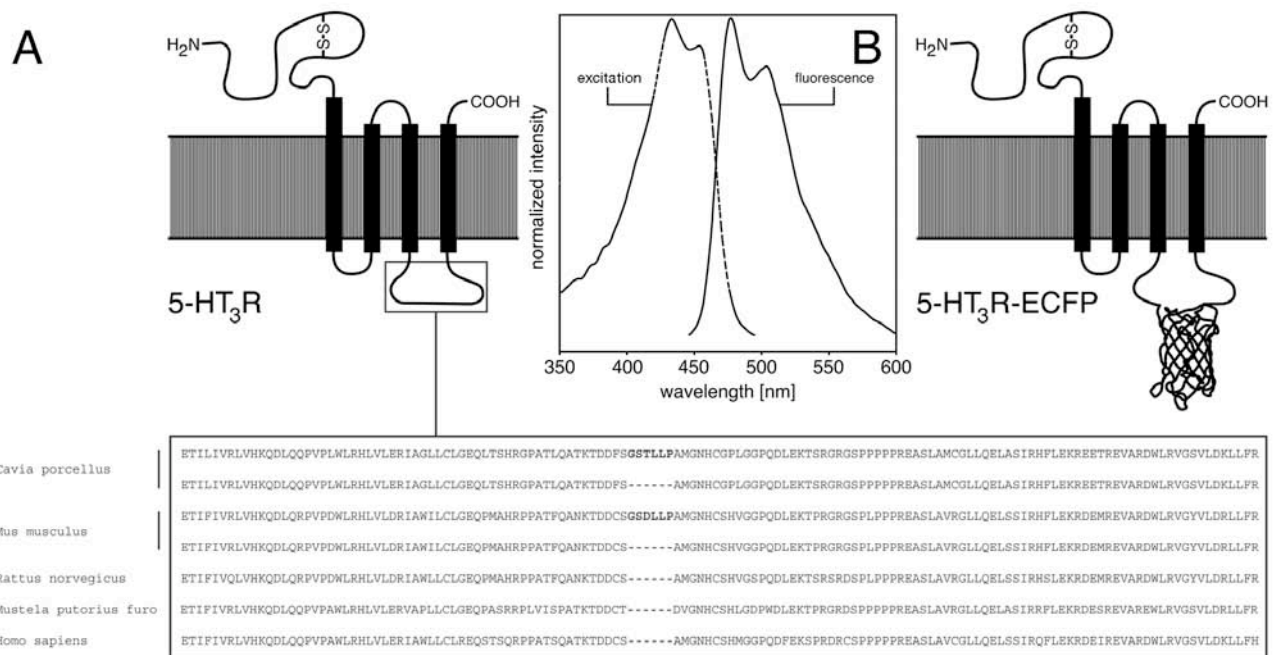


Figure I.2.2 Fusion of ECFP to the 5-HT₃R. (A) Scheme of the folding of the membrane integrated 5-HT₃R and 5-HT₃R-ECFP: the ECFP coding sequence is genetically fused into the large cytoplasmic loop between the 3rd and 4th transmembrane domains, replacing the amino acids present in the long splicing variant of the receptor (shown in bold letters in the amino acid homology sequence alignment of the large cytoplasmic loop). (B) Excitation and fluorescence emission of the detergent-solubilized 5-HT₃R-ECFP after transient expression in human cells, permitting to spectrally differentiate the receptor from EYFP-based subcellular markers.

The preserved functionality of the fusion construct was confirmed by radioligand binding assay and whole cell patch clamp measurements (Table I.2.2).

			5HT ₃ R	5HT ₃ R-ECFP
Binding assay	[³ H]-GR65630	K _d [nM]	0.3 ± 0.1	0.6 ± 0.1
		Hill	0.8 ± 0.2	1.1 ± 0.2
Electrophysiology	Serotonin	EC ₅₀ [μM]	0.97 ± 0.02	0.62 ± 0.06
		Hill	3.1 ± 0.2	1.8 ± 0.3
	mCPBG	EC ₅₀ [μM]	0.4 ± 0.1	0.20 ± 0.03
		Hill	1.0 ± 0.2	1.5 ± 0.3
	Granisetron inhibition	IC ₅₀ [nM]	0.17 ± 0.01	0.26 ± 0.02
		Hill	0.92 ± 0.03	1.04 ± 0.05

Table I.2.2 Radioligand binding and electrophysiology on wild-type and ECFP-labeled 5-HT₃R revealed the preserved functionalities of the receptor chimera. For antagonist-agonist competition experiments, cells were perfused with granisetron containing solutions for three minutes before the addition of serotonin (5-HT) at a concentration of 30 μM.

Using laser scanning confocal microscopy we found that the ECFP-labeled receptors start to form in the endoplasmic reticulum about 3 hours after transfection. The receptor-derived fluorescence signal could be overlapped with a spectrally distinguishable (Figure I.2.2B) enhanced yellow fluorescent ER marker (Figure I.2.3A), which was transfected together with the ECFP-tagged receptor DNA. In parallel experiments, we were able to overlap the chimeric receptor bioluminescence with an EYFP marker targeted to the Golgi apparatus at approximately 4 hours after transfection (Figure I.2.3B). The complete receptor trafficking from the appearance in the Golgi and processing to plasma membrane targeting occurred in about 30 minutes (Figure I.2.3C). The integration of mature receptors into the plasma membrane could be confirmed by binding of a fluorescent labeled 5-HT₃-specific antagonist (Figure I.2.3C inset).

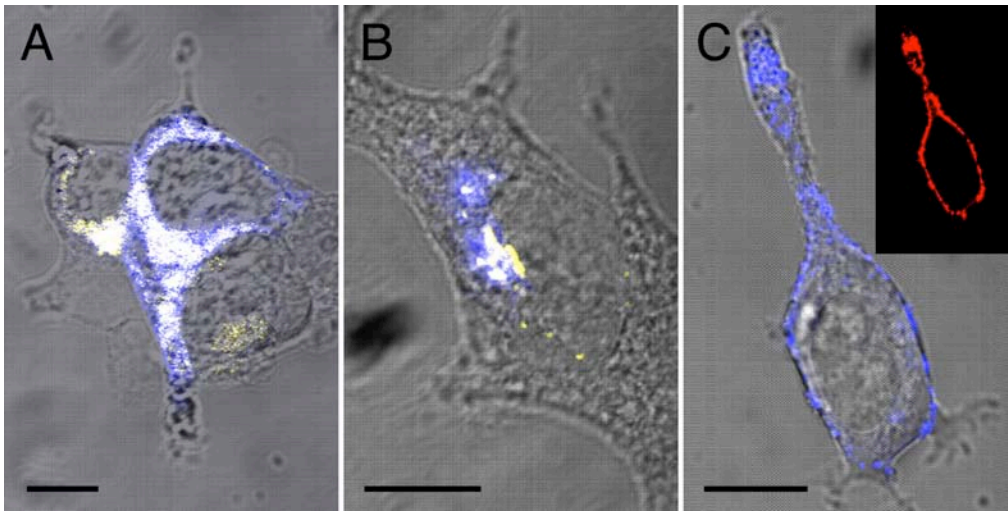


Figure I.2.3 Trafficking of the 5-HT₃R-ECFP followed over time in HEK293 cells by co-transfection with EYFP-labeled subcellular localization vectors. Images were acquired 3 hours (A), 4 hours (B) and 5 hours (C) after transfection. The endoplasmic reticulum and Golgi apparatus are labeled by co-transfection with pEYFP-ER (A) and pEYFP-Golgi (B), respectively. Inset in C shows the membrane integrated receptors by labeling the non-permeabilized cell with the fluorescent ligand GR-Cy5 (red) [22]. Co-localization of ECFP (blue) and EYFP (yellow) is indicated in white. Size bar is 10 μ m.

Though the fluorescence emitted from the 5-HT₃R-ECFP is primarily an indication for ECFP label folding completion, it allows also to monitor 5-HT₃ receptor biogenesis, since the ECFP label is directly integrated into the receptor sequence. Information about the assembly of 5-HT₃R subunits can be assessed via detection of the formation of the ligand binding sites. Indeed, it has been shown for the structurally related acetylcholine receptor [23] as well as by amino acid sequence homology studies on the 5-HT₃R [24,25] that the ligand binding sites are located between neighboring subunits; in consequence, ligand binding can only be observed once the subunits are fully assembled to a functional pentameric receptor.

After monitoring 5-HT₃R biosynthesis in cytoplasmic compartments we started to investigate the formation of intracellular 5-HT₃-specific ligand binding sites indicating the assembly of receptor subunits. Subcellular receptor ligand binding was assessed by first permeabilizing fixed HEK293 cells at different times after transfection, and subsequently labeling the receptor with 5-HT₃-specific fluorescent ligands. Triton-X100 was used for cell permeabilization because this detergent was shown not to interfere with ligand binding affinity [12,26].

ECFP-labeled 5-HT₃R were localized in the endoplasmic reticulum or Golgi apparatus by overlap with corresponding EYFP organelle markers as described above. The delivery of a Cy5-labeled 5-HT₃R-specific antagonist (GR-Cy5) into permeabilized cells allowed the detection of ligand binding activity in ER and Golgi apparatus (Figure I.2.4). This is an indication for receptor assembly at an early stage of expression in the ER. The GR-Cy5 fluorescence signal located in the Golgi was stronger than in the ER indicating substantially higher amounts of assembled 5-HT₃ receptors in the Golgi.

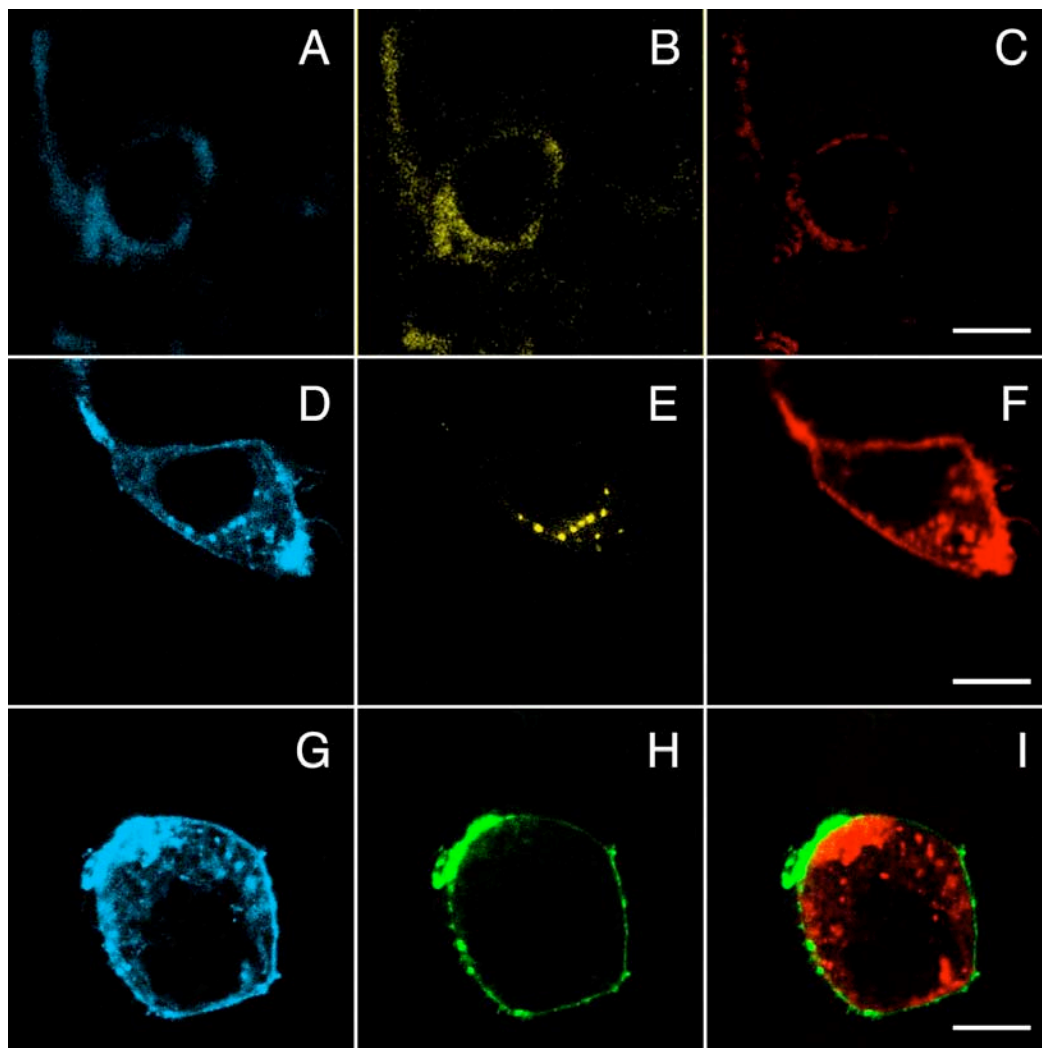


Figure I.2.4 Study of ligand binding site activity at different stages of receptor expression.

The 5-HT₃R-ECFP (cyan) was co-expressed with EYFP (yellow) targeted to the endoplasmic reticulum (A-C) and Golgi apparatus (D-F). After cell fixation and membrane permeabilization, the overlap with the fluorescent ligand GR-Cy5 (red) demonstrated the presence of active ligand binding sites of the receptor in these organelles (C, F).

(G-I): GR-Rho (green) and GR-Cy5 were applied, respectively, before and after permeabilization to investigate the percentage of membrane as compared to whole cell binding receptors. Size bars = 5 μ m.

The percentage of cell surface receptors as compared to intracellularly formed ligand binding sites was then evaluated by double ligand labeling (Figure I.2.4, G-I): 2 nM of the fluorescent rhodamine-labeled antagonist GR-Rho was applied to non-permeabilized 5-HT₃R-ECFP expressing cells 34 hours after transfection to label the receptors located on the plasma membrane. After fixation and permeabilization of the cells, the antagonist GR-Cy5 was added at a concentration of 12 nM in order to label the receptors inside the cell. Due to particular high affinity of the fluorescent antagonist GR-Rho to the 5-HT₃R, the latter was not replaced by GR-Cy5, as described before [9], and allowed to visualize the distribution of extra- and intracellular ligand binding activity. Subsequent image analysis consisting in pixel quantification of Cy5- and rhodamine-derived fluorescence in consecutive confocal sections covering the whole cell volume revealed that about 43 ± 14 % of the binding-active receptors were located in the plasma membrane. This mean value was obtained from analysing 20 different cells, and were in the same range as the values obtained from radioligand binding assays on cell suspensions.

The specificity of GR-Cy5 ligand binding to 5-HT₃ receptors in intracellular compartments was confirmed by ligand displacement experiments. On fixed and permeabilized HEK293 cells expressing the 5-HT₃R in ER and Golgi, the GR-Cy5 labeling could be replaced by an excess of a fluorescein-labeled antagonist (GR-Flu), which exhibits a strong affinity for the 5-HT₃R (Figure I.2.5).

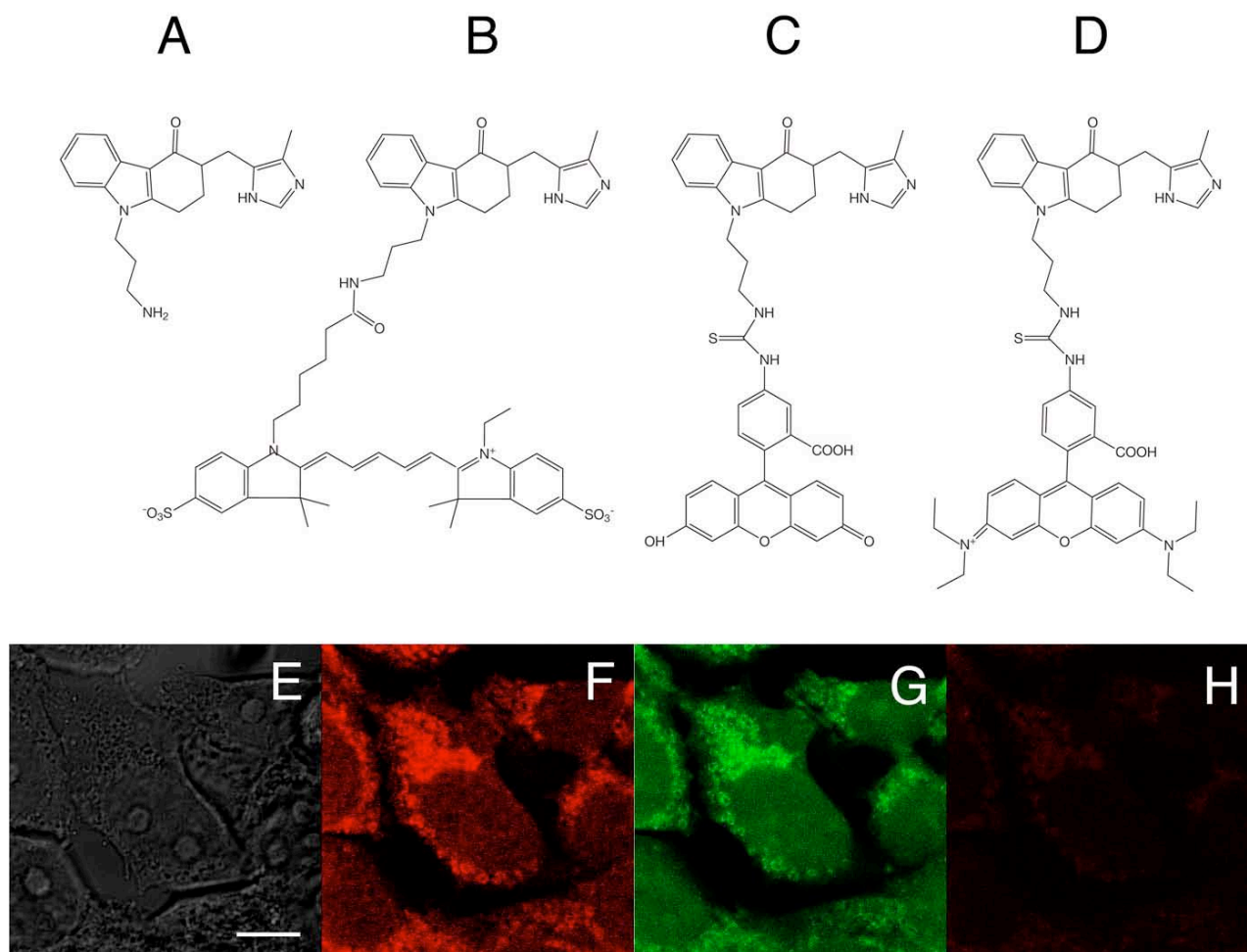


Figure I.2.5 Fluorescent ligands and their specificity for the 5-HT₃R in permeabilized cells.

Chemical structures of the fluorescent antagonists: the pharmacophore GR119566 (A) was labeled with Cy5, fluorescein and rhodamine B, yielding GR-Cy5 (B), GR-Flu (C) and GR-Rho (D) respectively.

HEK293 cells stably expressing the non-labeled 5-HT₃R were fixed with 10% formaldehyde and detergent-permeabilized (E). The receptors were then labeled for 3 minutes with the 5-HT₃R-specific ligand GR-Cy5 (F, red) at a concentration of 12 nM, and the excess was washed three times with PBS. This fluorescent antagonist was then replaced by the ligand GR-Flu, which shows a higher affinity for the receptor (G). Absence of GR-Cy5 signal after replacement shows the specificity of the ligand in permeabilized cells (H). Size bar is 5 μ m.

Receptor trafficking from the Golgi apparatus to the plasma membrane was then more precisely analyzed by imaging 5-HT₃R-ECFP expressing HEK293 cells (frame rate of 2 images/s; Figure I.2.6). The ECFP label allowed us to detect vesicle-like structures carrying 5-HT₃ receptors in their membrane, which moved inside the cytoplasm. The velocity of these carrier vesicles was generally below 1 μm per second, measured as the distance between the pixel coordinates in consecutive images. The receptor-carrying vesicles seemed to be located in tubulin-rich regions as visualized by cotransfection with a EYFP-labeled tubulin marker (pEYFP-Tub).

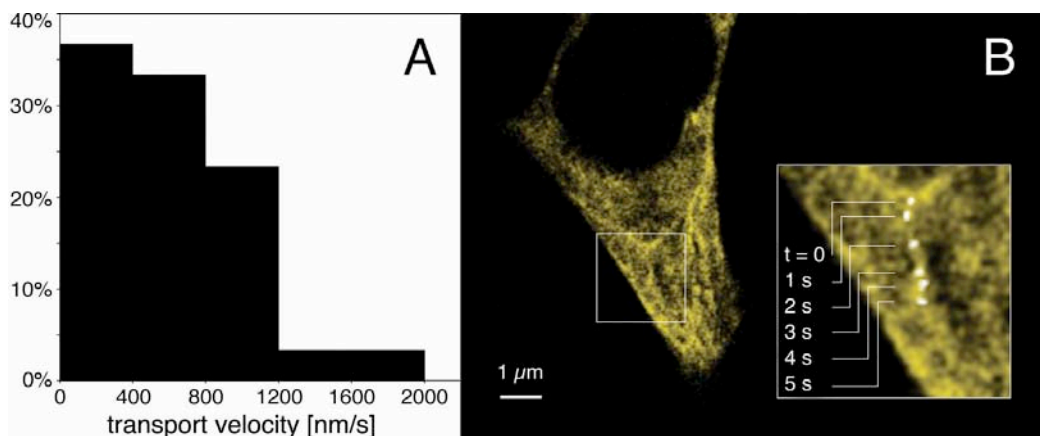


Figure I.2.6 Spatial and temporal resolution in live HEK293 cells of post-Golgi carriers containing the 5-HT₃R-ECFP by confocal microscopy.

(A) average speed as measured by consecutive image acquisition tracking 10 individual receptor carriers. (B) cotransfection of HEK293 cells with 5-HT₃R-ECFP and EYFP-labeled tubulin shows the movement of carrier vesicles along tubulin-rich domains (white dots in inlet enlargement).

In order to verify whether tubulin filaments are of required for 5-HT₃ receptor transport to the plasma membrane, we studied the influence of colchicine on receptor trafficking, which is known to inhibit microtubule formation [27-29] (Figure I.2.7). 5 hours after addition of 100 μg/ml cycloheximide, known to interfere with the translation machinery [30], the receptors were almost completely located on the cell membrane. However, prior treatment of the cells for 2 hours with 50 μg/ml colchicine did not lead to a complete membrane localization of the receptors, demonstrating the tubulin requirement for proper receptor trafficking.

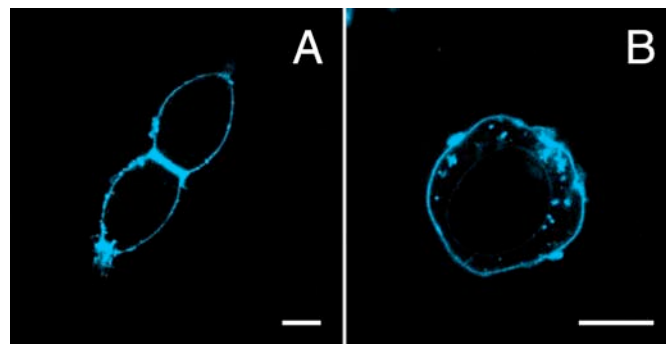


Figure I.2.7 Influence of cycloheximide and colchicine on receptor localization.

(A) 100 $\mu\text{g/ml}$ cycloheximide administrated to the cells 5 hours prior to imaging. (B) Pretreatment with 50 $\mu\text{g/ml}$ colchicine for 2 hours before cycloheximide administration did not lead to complete cell surface localization of the receptors 5 hours later. Size bars = 5 μm .

We then investigated the effects of agonist application on the subcellular distribution of 5-HT₃ receptors. 34 hours after transient 5-HT₃R-ECFP expression, HEK293 cells were treated with 100 $\mu\text{g/ml}$ cycloheximide for 5 hours in order to stop new protein synthesis allowing delivery of intracellular receptors to the cell membrane and thus to avoid intracellular fluorescence background. Subsequent incubation of non-permeabilized cells with 12 nM GR-Cy5 led to a complete spatial overlap of the receptors ECFPs and the ligands Cy5 fluorescence signals on the cell surface (Figure I.2.8, A-E). The fluorescent antagonist was then replaced by adding an excess of the non-fluorescent 5-HT₃R-specific agonist 1-(*m*-chlorophenyl)-biguanide (mCPBG, 500 nM). After incubation at room temperature for 30 min, the cells were intensively washed with PBS buffer. Then we applied the fluorescent antagonist GR-Cy5 for a second time using the same concentration as before (Figure I.2.8, F-J). The absence of fluorescence labeling on the cell surface was a first indication that agonist-induced internalization of the 5-HT₃R might have occurred. The fact that the ECFP fluorescence was still located near the plasma membrane might indicate receptor internalization in early endosomes located closely below the cell surface. This hypothesis was studied in more detail in the following.

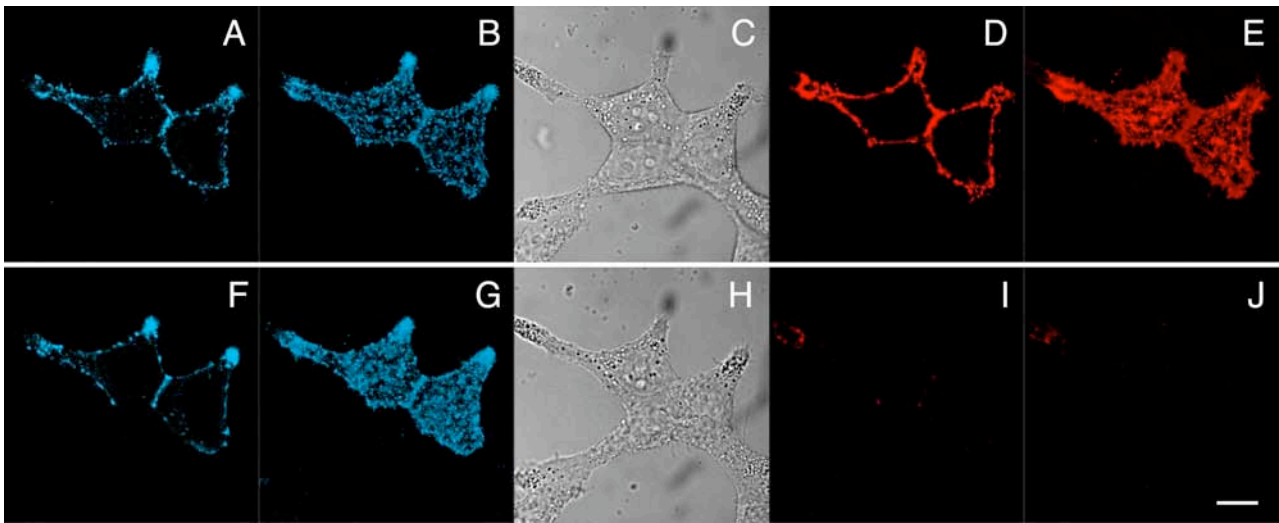


Figure I.2.8 Internalization of the 5-HT₃R visualized by fluorescent antagonist accessibility. (A-E): The 5-HT₃R-ECFP chimera (cyan) was labeled with the fluorescent antagonist GR-Cy5 (red). The cells were then washed with PBS, and the agonist mCPBG was applied for 30 minutes, leading to the internalization of the receptors. (F-J): Incubation of internalized receptors with the fluorescent antagonist GR-Cy5 reflected the inaccessibility of the binding sites. (A, F, D, I): confocal imaging; (B, G, E, J): tridimensional projection of confocal images; (C, H): transmission channel; 5-HT₃R-ECFP and GR-Cy5 fluorescence signals are represented in cyan and red respectively. Size bar = 10 μ m.

Quantification of fluorescence intensities arising from 5-HT₃R-ECFP on one hand and from the receptor-bound antagonist GR-Cy5 on the other, allowed to estimate the number of binding sites on the cell surface receptors accessible for the ligand. The time-course of receptor internalization was studied by exposing the cells to 500 nM mCPBG for increasing periods of time at 37°C. The agonist was then quickly removed by three washes with PBS buffer. Subsequent labeling with GR-Cy5 allowed to visualize remaining 5-HT₃ receptors on the cell surface. We observed that more than half of the receptors were internalized after 5 minutes constant exposure to the agonist (Figure I.2.9A). The internalized receptors progressively moved away from the cell surface after endocytosis, and after 2 hours of constant exposure to the agonist, labeling of the plasma membrane with R18 clearly revealed no overlap of the ECFP signal with the membrane dye indicating complete internalization of the receptor (Figure I.2.9, B-D).

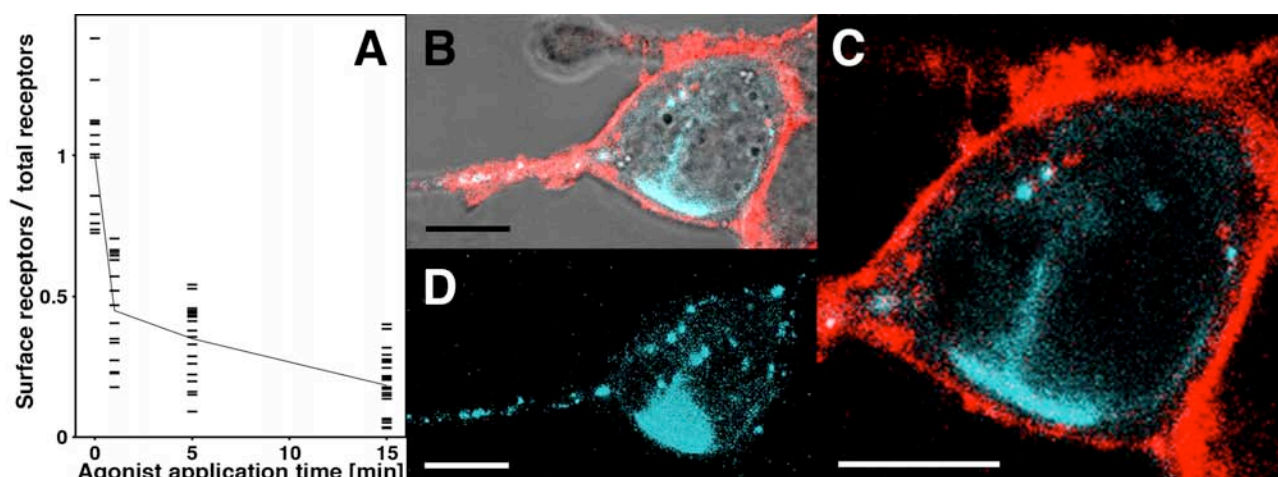


Figure I.2.9 Time-course of agonist-induced decrease in cell-surface binding of GR-Cy5 and internalization imaged by membrane labeling with R18.

(A) Live HEK293 cells expressing the 5-HT₃R-ECFP chimera were exposed to 500 nM mCPBG for the indicated lengths of time. Subsequent washing with PBS and incubation with 12 nM GR-Cy5 allowed to quantify non-internalized receptors by comparing ECFP and Cy5 fluorescence intensities. Each bar represents values measured on one cell and the line shows the average values. (B) After 2 hours constant exposure to the agonist, the cells were membrane-labeled with R18 (red) and imaged by confocal microscopy. (C) The receptors fluorescence (cyan) clearly revealed no overlap with the membrane-labeled dye. (D) The tridimensional projection of confocal images of the ECFP label showed a partial clustered organization of the internalized receptors. Size bars represent 5 μm.

During receptor internalization we observed a progressive disappearance of its cluster distribution on the membrane upon agonist binding. By coexpression of 5-HT₃R-ECFP together with the actin marker EYFP-Actin, we could observe that these clusters were colocalized with the actin marker, suggesting the involvement of actin filaments in the membrane organization of the 5-HT₃R (Figure I.2.10). Image treatment of a 5-HT₃R-ECFP-expressing cell over time indicated that its fraction of receptors in cluster form, which was originally almost 50% of total membrane receptors, dropped by a factor of two after approximately 4 minutes incubation with 500 nM mCPBG, a time frame comparable to that of internalization as measured conjointly with the fluorescent antagonist.

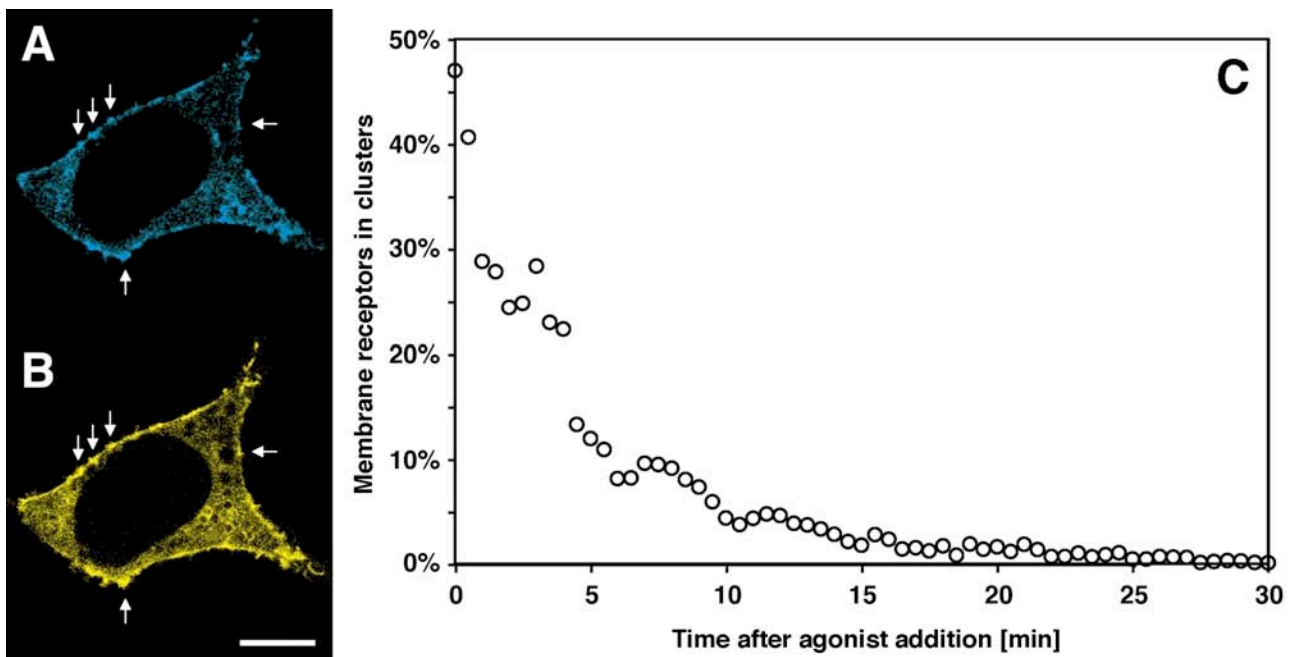


Figure I.2.10 Colocalization of 5-HT₃R clusters with actin filaments and cluster disappearance during agonist-induced desensitization. (A) The 5-HT₃R-ECFP chimera has a cluster distribution on the plasma membrane (arrows). (B) Clusters colocalize with actin-rich domains visualized by co-expression of EYFP-Actin (arrows). (C) After adding 500 nM of the agonist mCPBG, the percentage of membrane receptors in cluster form is rapidly decreasing and leads to a more homogeneous distribution of the receptors below the cell membrane. Size bar = 5 μ m.

1.2.5 Discussion

Receptor labeling by genetic fusion with the enhanced version of the cyan fluorescent protein (ECFP) allowed monitoring of 5-HT₃R expression, trafficking, plasma membrane targeting and ligand-induced endocytosis in real time in living cells. The fluorescent receptor retained ligand binding and channel activity, and permitted *in vivo* observation of its “birth” after delivery of its coding DNA into HEK293 cells, used as host system for this trafficking study because these cells allow efficient cell surface expression of 5HT₃ receptors [9].

By colocalization with EYFP-labeled subcellular markers, it was possible to monitor the receptor’s successive appearance in different organelles over time. Furthermore, the formation of ligand binding sites was observable *in situ* at an early step in 5-HT₃R synthesis in the endoplasmic reticulum as visualized by labeling with fluorescent antagonists on permeabilized cells. Recent studies on the ligand binding domain of nicotinic receptors indicated that the assembly of subunits was required for proper functioning of its binding site [23]. Homology studies between acetylcholine receptor and 5-HT₃R amino acid sequences point to the fact that the ligand binding site might be located at the interface between two subunits [24,25,31] indicating that assembly of the 5-HT₃ subunits might be required for proper functioning of the binding site. Thus this present study indicates that the assembly of the 5-HT₃R subunits to a functional receptor is likely to occur in the endoplasmic reticulum, since the labeling with the 5-HT₃R-specific antagonist GR-Cy5 correlates in time and space with the fluorescence signal of the 5-HT₃R-ECFP in this subcellular compartment. Thus, we provide the first evidence obtained *in situ* on individual live cells that the first formation of functional 5-HT₃R specific binding sites occurs in the ER. So far there were only indirect indications for 5-HT_{3A}R subunit assembly based on radioligand binding in cell fractions [12]. For the case of the nAChR assembly the formation of alpha-bungarotoxin binding sites was also found to occur in the endoplasmic reticulum [32]. The recent discovery of an ER retention signal in 5-HT_{3B} subunits [33] and the fact that these subunits can only be “rescued” from the ER and assemble to functional receptors by coexpression of 5-HT₃ type A subunits in COS 7 cells [8], are complementary indirect indications in support of our observations.

We were able to follow receptor trafficking from intracellular compartments up to the plasma membrane as a microtubule-based transport; receptor-containing vesicles leaving the Golgi apparatus could not reach the membrane when the microtubule formation was blocked for 2 hours by colchicine treatment. Another support for this hypothesis was provided by velocity measurements on these vesicles carrying 5-HT₃R-ECFP chimeras inside living cells. We obtained values of 220 to 1850 nm/s by consecutive fluorescence imaging, which is similar as for the Golgi-

to-plasma membrane transport via post-Golgi carriers on microtubules measured by others [34-38]. The first appearance of receptors on the plasma membrane occurred about 4-5 hours after transfection onset and exhibited a cluster distribution, which is in agreement with precedent experiments on the 5-HT₃R [9]. By fluorescent overlap with an actin marker, we observed that these receptor clusters colocalized with actin-rich membrane domains, suggesting an actin-dependent membrane localization. Moreover, we could observe high receptor densities on cell-cell interfaces, corroborating with the large quantity of actin present in these domains [39].

It has been shown for other ligand-gated channels such as nicotinic acetylcholine [40], GABA_A [41], P2X₁ [42] receptors that long time-course desensitization provoke internalization by endocytosis. This property, which could furnish a pathway for receptor down-regulation in response to tonic levels of agonist, was so far not observed for the 5-HT₃R. We could monitor ligand-evoked endocytosis by concerted imaging of 5-HT₃R-ECFP and the antagonist GR-Cy5 after application of the potent specific agonist mCPBG for different time lapses. We observed that after 5 minutes incubation the number of receptors present on the plasma membrane diminished by a factor of three, and in parallel that its cluster organization was consistently overtaken by a more homogeneous distribution, presumably in endosomes located below the cell membrane. The loss of cell surface binding of GR-Cy5 was the first indication for 5-HT₃R internalization. The localization of internalized receptors below the plasma membrane could be confirmed by employing a lipophilic membrane dye, which did not overlap with the bioluminescence signal of the receptor.

In conclusion, the functionally silent insertion of ECFP into the 5-HT₃R proved to be a valuable tool enabling spatial and temporal examination of the receptor trafficking pattern in single living cells. We have demonstrated that multicolor imaging could be used to study the receptor translocation to the plasma membrane after biosynthesis, appearing to follow the microtubule cytoskeleton in post-Golgi carriers whereas its localization and clustering on the plasma membrane would involve actin filaments. Furthermore, this is the first report to demonstrate *in situ* the ER-localized formation of the 5-HT₃R ligand binding sites. We could additionally track dynamic changes in the receptor localization by direct observation of ligand-induced internalization of the receptor in response to a 5-HT₃R-specific agonist. We believe the same methodology using multicolor dynamic tracking in living cells could be applied to a variety of other receptors in order to elucidate number of unraveled cellular mechanisms.

I.2.6 References

1. Betz, H. (1990) Ligand-gated ion channels in the brain: the amino acid receptor superfamily. *Neuron*, **5**, 383-392.
2. Barnard, E.A. (1992) Receptor classes and the transmitter-gated ion channels. *Trends Biochem Sci*, **17**, 368-374.
3. Green, W.N. and Millar, N.S. (1995) Ion-channel assembly. *Trends Neurosci*, **18**, 280-287.
4. Blount, P. and Merlie, J.P. (1990) Mutational analysis of muscle nicotinic acetylcholine receptor subunit assembly. *J Cell Biol*, **111**, 2613-2622.
5. Gu, Y., Forsayeth, J.R., Verrall, S., Yu, X.M. and Hall, Z.W. (1991) Assembly of the mammalian muscle acetylcholine receptor in transfected COS cells. *J Cell Biol*, **114**, 799-807.
6. Chavez, R.A., Maloof, J., Beeson, D., Newsom-Davis, J. and Hall, Z.W. (1992) Subunit folding and alpha delta heterodimer formation in the assembly of the nicotinic acetylcholine receptor. Comparison of the mouse and human alpha subunits. *J Biol Chem*, **267**, 23028-23034.
7. Hall, Z.W. (1992) Recognition domains in assembly of oligomeric membrane proteins. *Trends Cell Biol*, **2**, 66-68.
8. Boyd, G.W., Low, P., Dunlop, J.I., Robertson, L.A., Vardy, A., Lambert, J.J., Peters, J.A. and Connolly, C.N. (2002) Assembly and cell surface expression of homomeric and heteromeric 5-HT₃ receptors: the role of oligomerization and chaperone proteins. *Mol Cell Neurosci*, **21**, 38-50.
9. Pick, H., Preuss, A.K., Mayer, M., Wohland, T., Hovius, R. and Vogel, H. (2003) Monitoring expression and clustering of the ionotropic 5HT₃ receptor in plasma membranes of live biological cells. *Biochemistry*, **42**, 877-884.
10. Maricq, A.V., Peterson, A.S., Brake, A.J., Myers, R.M. and Julius, D. (1991) Primary structure and functional expression of the 5HT₃ receptor, a serotonin-gated ion channel. *Science*, **254**, 432-437.
11. Boess, F.G., Beroukhim, R. and Martin, I.L. (1995) Ultrastructure of the 5-hydroxytryptamine₃ receptor. *J Neurochem*, **64**, 1401-1405.
12. Green, T., Stauffer, K.A. and Lummis, S.C. (1995) Expression of recombinant homo-oligomeric 5-hydroxytryptamine₃ receptors provides new insights into their maturation and structure. *J Biol Chem*, **270**, 6056-6061.

13. Chalfie, M., Tu, Y., Euskirchen, G., Ward, W.W. and Prasher, D.C. (1994) Green fluorescent protein as a marker for gene expression. *Science*, **263**, 802-805.
14. Cubitt, A.B., Heim, R., Adams, S.R., Boyd, A.E., Gross, L.A. and Tsien, R.Y. (1995) Understanding, improving and using green fluorescent proteins. *Trends Biochem Sci*, **20**, 448-455.
15. Kain, S.R., Adams, M., Kondepudi, A., Yang, T.T., Ward, W.W. and Kitts, P. (1995) Green fluorescent protein as a reporter of gene expression and protein localization. *Biotechniques*, **19**, 650-655.
16. Ogawa, H., Inouye, S., Tsuji, F.I., Yasuda, K. and Umesono, K. (1995) Localization, trafficking, and temperature-dependence of the *Aequorea* green fluorescent protein in cultured vertebrate cells. *Proc Natl Acad Sci U S A*, **92**, 11899-11903.
17. Stauber, R., Gaitanaris, G.A. and Pavlakis, G.N. (1995) Analysis of trafficking of Rev and transdominant Rev proteins in living cells using green fluorescent protein fusions: transdominant Rev blocks the export of Rev from the nucleus to the cytoplasm. *Virology*, **213**, 439-449.
18. Naray-Fejes-Toth, A. and Fejes-Toth, G. (1996) Subcellular localization of the type 2 11beta-hydroxysteroid dehydrogenase. A green fluorescent protein study. *J Biol Chem*, **271**, 15436-15442.
19. Sengupta, P., Chou, J.H. and Bargmann, C.I. (1996) odr-10 encodes a seven transmembrane domain olfactory receptor required for responses to the odorant diacetyl. *Cell*, **84**, 899-909.
20. Htun, H., Barsony, J., Renyi, I., Gould, D.L. and Hager, G.L. (1996) Visualization of glucocorticoid receptor translocation and intranuclear organization in living cells with a green fluorescent protein chimera. *Proc Natl Acad Sci U S A*, **93**, 4845-4850.
21. Tairi, A.P., Hovius, R., Pick, H., Blasey, H., Bernard, A., Surprenant, A., Lundstrom, K. and Vogel, H. (1998) Ligand binding to the serotonin 5HT₃ receptor studied with a novel fluorescent ligand. *Biochemistry*, **37**, 15850-15864.
22. Wohland, T., Friedrich, K., Hovius, R. and Vogel, H. (1999) Study of ligand-receptor interactions by fluorescence correlation spectroscopy with different fluorophores: evidence that the homopentameric 5-hydroxytryptamine type 3A_s receptor binds only one ligand. *Biochemistry*, **38**, 8671-8681.
23. Brejc, K., van Dijk, W.J., Klaassen, R.V., Schuurmans, M., van Der Oost, J., Smit, A.B. and Sixma, T.K. (2001) Crystal structure of an ACh-binding protein reveals the ligand-binding domain of nicotinic receptors. *Nature*, **411**, 269-276.

24. Maksay, G., Bikadi, Z. and Simonyi, M. (2003) Binding interactions of antagonists with 5-hydroxytryptamine_{3A} receptor models. *J Recept Signal Transduct Res*, **23**, 255-270.
25. Reeves, D.C., Sayed, M.F., Chau, P.L., Price, K.L. and Lummis, S.C. (2003) Prediction of 5-HT₃ Receptor Agonist-Binding Residues Using Homology Modeling. *Biophys J*, **84**, 2338-2334.
26. Hovius, R., Tairi, A.P., Blasey, H., Bernard, A., Lundstrom, K. and Vogel, H. (1998) Characterization of a mouse serotonin 5-HT₃ receptor purified from mammalian cells. *J Neurochem*, **70**, 824-834.
27. Weisenberg, R.C., Borisy, G.G. and Taylor, E.W. (1968) The colchicine-binding protein of mammalian brain and its relation to microtubules. *Biochemistry*, **7**, 4466-4479.
28. Sherline, P., Leung, J.T. and Kipnis, D.M. (1975) Binding of colchicine to purified microtubule protein. *J Biol Chem*, **250**, 5481-5486.
29. Sackett, D.L. and Varma, J.K. (1993) Molecular mechanism of colchicine action: induced local unfolding of beta-tubulin. *Biochemistry*, **32**, 13560-13565.
30. Wettstein, F.O., Noll, H. and Penman, S. (1964) Effect of Cycloheximide on Ribosomal Aggregates Engaged in Protein Synthesis in Vitro. *Biochim Biophys Acta*, **87**, 525-528.
31. Schreiter, C., Hovius, R., Costioli, M., Pick, H., Kellenberger, S., Schild, L. and Vogel, H. (2003) Characterization of the Ligand-binding Site of the Serotonin 5-HT₃ Receptor: THE ROLE OF GLUTAMATE RESIDUES 97, 224, AND 235. *J Biol Chem*, **278**, 22709-22716.
32. Mitra, M., Wanamaker, C.P. and Green, W.N. (2001) Rearrangement of nicotinic receptor alpha subunits during formation of the ligand binding sites. *J Neurosci*, **21**, 3000-3008.
33. Boyd, G.W., Doward, A.I., Kirkness, E.F., Millar, N.S. and Connolly, C.N. (2003) Cell surface expression of 5-HT₃ receptors is controlled by an endoplasmic reticulum retention signal. *J Biol Chem*.
34. Lippincott-Schwartz, J. (2001) The secretory membrane system studied in real-time. Robert Feulgen Prize Lecture, 2001. *Histochem Cell Biol*, **116**, 97-107.
35. Hirschberg, K., Miller, C.M., Ellenberg, J., Presley, J.F., Siggia, E.D., Phair, R.D. and Lippincott-Schwartz, J. (1998) Kinetic analysis of secretory protein traffic and characterization of golgi to plasma membrane transport intermediates in living cells. *J Cell Biol*, **143**, 1485-1503.
36. Nakata, T., Terada, S. and Hirokawa, N. (1998) Visualization of the dynamics of synaptic vesicle and plasma membrane proteins in living axons. *J Cell Biol*, **140**, 659-674.

-
37. Toomre, D., Keller, P., White, J., Olivo, J.C. and Simons, K. (1999) Dual-color visualization of trans-Golgi network to plasma membrane traffic along microtubules in living cells. *J Cell Sci*, **112 (Pt 1)**, 21-33.
 38. Lauf, U., Giepmans, B.N., Lopez, P., Braconnot, S., Chen, S.C. and Falk, M.M. (2002) Dynamic trafficking and delivery of connexons to the plasma membrane and accretion to gap junctions in living cells. *Proc Natl Acad Sci U S A*, **99**, 10446-10451.
 39. Vasioukhin, V., Bauer, C., Yin, M. and Fuchs, E. (2000) Directed actin polymerization is the driving force for epithelial cell-cell adhesion. *Cell*, **100**, 209-219.
 40. St John, P.A. and Gordon, H. (2001) Agonists cause endocytosis of nicotinic acetylcholine receptors on cultured myotubes. *J Neurobiol*, **49**, 212-223.
 41. Barnes, E. (2000) Intracellular trafficking of GABA(A) receptors. *Life Sciences*, **66**, 1063-1070.
 42. Dutton, J.L., Poronnik, P., Li, G.H., Holding, C.A., Worthington, R.A., Vandenberg, R.J., Cook, D.I., Barden, J.A. and Bennett, M.R. (2000) P2X(1) receptor membrane redistribution and down-regulation visualized by using receptor-coupled green fluorescent protein chimeras. *Neuropharmacology*, **39**, 2054-2066.

Chapter I.3

Probing the 5-HT₃ receptor function in single native vesicles via fluorescence measurements

I.3 Probing the 5-HT₃ receptor function in single native vesicles via fluorescence measurements

I.3.1 Abstract

Cytochalasin induces live biological cells to extrude from their plasma membranes native vesicles. These (sub-)micrometer-sized vesicles comprise functional cell surface receptors exposing their originally extracellular ligand binding sites on the outer vesicle surface and retain cytosolic proteins in the vesicle interior. This was demonstrated coexpressing the ionotropic serotonin 5HT₃ receptor and cytosolic GFP in HEK293 cells from which native vesicles were produced. Agonist application induced cellular transient calcium signaling in native vesicles proving functional preservation of both vesicular 5HT₃ receptors (calcium ion influx) and ion pumps (restoration of initial calcium concentration). Such vesicles are the smallest autonomous containers capable of performing cellular signaling reactions. They open new possibilities for multiple analyses of the functions of single live cells, which especially in the case of primary cells were hampered by limited availability.

The results of this chapter are part of the submitted publication: Pick, H.M., Schmid, E.L., Tairi, A.P., Ilegems, E., Preuss, A., Hovius, R. and Vogel, H.: Downscaling bioanalytics to the submicrometer and attoliter range by probing cellular signaling reactions in single native vesicles

I.3.2 Introduction

Understanding cellular signaling mediated by cell surface receptors is key to modern biological research and central to drug development [1,2]. Facing the rapidly growing number of (i) molecular targets discovered by functional genomics [3] and (ii) potential therapeutic compounds produced by combinatorial chemical synthesis [4], the need of downscaling assay formats is of utmost importance for accelerating functional-screening, and reducing costs and reagent consumption [5]. Cellular responses upon activation of cell surface receptors such as intracellular calcium ion signals or ion fluxes are typically investigated measuring optical or electrical properties of either single cells or cell populations in microliter volumes [6]. On the other hand, most bioanalytical approaches on the micro- and nanometer scale are limited to investigations of selected molecular interactions under artificially reconstituted, non-physiological conditions [7-14].

In the present study, transmembrane signaling reactions on membrane receptors were monitored in single (sub-)micrometer sized vesicles derived from biological cells. Such native vesicles are the smallest autonomous containers capable to perform cellular signaling reactions under physiological conditions, thus downscaling cellular functions to the micrometer and femtoliter level. This ultimate miniaturization opens novel routes in functional proteomics such as multiplexing single cell bioanalytics or investigating receptor mediated signaling in multiarray format.

We describe the production of native vesicles and demonstrate that in these vesicles cell surface receptors and cytoplasmic proteins retain their original cellular location, orientation and function. Preserved ligand binding functionality and transmembrane calcium ion flux show that native vesicles may be used as a universal, efficient and cheap bio-analytical reagent for investigating cellular signaling reactions in a highly parallel format, replacing live cells within many applications.

I.3.3 Experimental procedures

Chemicals.

Cytochalasin B and Dulbecco's PBS containing 1 mM CaCl₂ were obtained from Sigma (Buchs, Switzerland); [³H]-GR65630 from NEN-Dupont (Boston, MA); quipazine and mCPBG from Tocris-Cookson (Langford, UK); granisetron from the Glaxo Institute for Molecular Biology (Geneva, Switzerland). All other products were of highest quality available.

5-HT₃R constructs

The vector containing the short splice variant of the murine 5-hydroxytryptamine type 3A subunit cDNA preceded by the human cytomegalovirus gene promoter was described elsewhere [15].

The vector p5HT3R-EGFP, containing the receptor fused to EGFP, was obtained the following way: the original vector was first mutated using the oligos 5'-CTG ATG ACT GCT CAA TCG ATG CCA TGG GAA ACC-3' and 5'-GGT TTC CCA TGG CAT CGA TTG AGC AGT CAT CAG-3', adding a *Cla*I restriction site in the large cytoplasmic loop sequence between the 3rd and 4th predicted membrane-spanning domains. The EGFP insert was obtained by PCR amplification on the template pEGFP-N1 (Clontech, California, USA) using the synthetic oligonucleotides 5'-CCA TCG ATA TGG TGA GCA AGG GCG AGG -3' and 5'- CCA TCG ATC TTG TAC AGC TCG TCC ATG CCG -3', and ligated into the receptor's *Cla*I restriction site. The restriction sites *Hind*III and *Not*I were added to the 5' and 3' ends of the 5-HT3R-EGFP sequence by PCR amplification using the oligonucleotides 5'- CGA TAA GCT TCA CCA TGC GGC TCT GCA TCC CGC AGG TG -3' and 5'- GCT GTG CCC ACG CGG CCG CTC AAG AAT AAT GCC AAA TGG ACC AGA G -3', and the purified 2197 bp fragment was sub-cloned into the *Hind*III/*Not*I cut vector pEAK8 (Edge BioSystems, Gaithersburg, MD, USA), giving rise to the vector p5HT3R-EGFP, confirmed by restriction mapping and DNA sequencing.

Cell culture and transfection

Adherent human embryonic kidney HEK293 cells were grown in DMEM/F12 (Dulbecco's modified Eagle medium) supplemented with either 2.2 % or 10 % fetal calf serum FCS), using plastic flasks from TPP (Trasadingen, Switzerland). Cultures were kept at 37 °C in humidified, 5 % CO₂ atmosphere. Exponentially growing HEK293 cells were seeded (10⁵ cells/ml) into 6-well plates, and transfected after 16 - 20 h using Effectene (Qiagen, Hilden, Germany). After 4 h the transfection solution was replaced by fresh medium. To obtain a stable expression of the receptor, the growth media of transfected cells was supplemented with 1 µg/ml of puromycin for 3 weeks.

Vesicle formation

Native vesicles were produced from HEK293 cells expressing either the 5HT₃R or the 5-HT₃R-EGFP by a 10-20 min incubation at 37°C with cytochalasin B (10 µg/ml) in serum-free DMEM/F12 medium. Cells were first separated from vesicles by centrifugation at 50 g for 5 minutes (Eppendorf 5810, Hamburg, Germany). Vesicles were then collected by centrifugation at 800 g for 20 min and resuspended in PBS and either used directly or stored in 10 % DMSO at –80 °C for several weeks without loss of ligand binding activity.

Calcium signaling in native vesicles

HEK293 cells stably expressing 5-HT₃R-EGFP were loaded at 37 °C for 30 min with 10 µM Fura-Red-AM (Molecular Probes, Oregon, USA) in serum-free DMEM/F12 medium. Cells were washed with PBS and incubated in DMEM/F12 medium containing 10 % FCS for 30 minutes to allow complete hydrolysis of intracellular Fura Red-AM. Subsequently, cells were treated with cytochalasin B as described above. Vesicles containing Fura-Red were transferred to 8-well chambered coverglass slides (grade 1 thickness, Lab-Tek®, Nalge Nunc International, Naperville, IL, USA) precoated with 0.1 mg/l poly-L-lysine (Sigma) to ensure electrostatic binding of the vesicles to the glass surface, and investigated by confocal fluorescence microscopy (LSM 510, Zeiss, Oberkochen, Germany) using a water immersion objective (Zeiss Achroplan 63 NA 1.2). Excitation was at 488 nm (Ar⁺ laser) using either 505-530 nm band pass or 650 nm long pass emission filters to image EGFP and Fura Red, respectively. Vesicles expressing the 5-HT₃R-EGFP receptor, but not loaded with Fura Red were used as control to ensure that no crosstalk did occur from the green to the red measuring channel. Generally, individual responses to the 5-HT₃R-specific agonist mCPBG were recorded for 100 s.

Radioligand Binding

The total amount of the radioligand [³H]-GR65630 bound to 5HT₃R in native vesicles and in whole cells was determined as described in chapter I.2.

Binding fluorescent ligands to native vesicles

400 µl of native vesicle preparation was added per well of a 6-well plate in which a coverslide had been placed at the bottom. After vesicle immobilization, the coverslides were transferred to a microscope chamber and covered with 200-300 µl PBS buffer. Fluorescence intensity measurements were performed employing a Zeiss LSM510 confocal microscope and evaluated from regions of interest (ROI) using the microscope software.

I.3.4 Results

Formation of native vesicles made from cell membranes

Formation of native vesicles was monitored and characterized using HEK293 cells expressing the serotonin-gated 5-HT₃R-EGFP as a prototypic cell membrane receptor. This chimeric receptor is genetically identical to the one presented in chapter I.2 (5-HT₃R-ECFP), except for the labeling fluorescent protein. Here, the enhanced version of the green fluorescent protein (EGFP) is preferred to the cyan version because of its higher quantum yield and extinction coefficient [16], and because it appeared to be less sensitive to photobleaching, important properties especially when studying low numbers of receptors in very small spatial regions. Treatment of cells with cytochalasin B leads to the appearance of tubular extensions, which upon agitation bud off as (sub)micrometer sized vesicles. When treated cells are expressing the 5-HT₃R-EGFP fusion protein, produced vesicles contain the receptor on their membrane as demonstrated by fluorescence confocal microscopy (Figure I.3.1A).

Receptor activity and orientation is maintained throughout native vesicle production

Native vesicle production was quantified by measuring binding of radioactive ligands to the 5HT₃R. HEK293 cells transiently expressing 5HT₃Rs at average level of $1.2 \pm 0.2 \times 10^6$ receptors on the surface of live cells were used as starting material. Live cells were incubated with cytochalasin B and vesicles were released from the cells by agitation. Low speed centrifugation yielded a homogeneous preparation of 0.5 - 1 μm diameter vesicles (Figure I.3.1B). Typically, a single live cell delivered 50 ± 10 vesicles. From radioactive ligand binding experiments 15 ± 4 % of the original average cellular receptor activity was found in vesicles, which corresponds to an average number of about 3500 receptors per vesicle. If we alternatively compare the average surface area of the native vesicles ($2.0 \pm 0.6 \mu\text{m}^2$, histogram in Figure I.3.1B) with the average surface area of a live cell ($580 \pm 20 \mu\text{m}^2$, see Chapter II.3 for more details), we yield a number of 17 ± 6 % of the cell membrane transformed to native vesicles, in accord with the number calculated above from ligand binding experiments.

The topology of the plasma membrane of the originating cells is maintained in native vesicles. Indeed, after cellular co-transfection with wild-type 5-HT₃R and cytosolic GFP DNAs the fluorescent antagonist GR-Rho binds specifically to native vesicles when added from the bulk aqueous phase (Figure I.3.1B, inset), indicating that the ligand-binding sites of the 5HT₃R are accessible on the outer vesicle surface. Moreover, cytosolic components are enclosed in vesicles as demonstrated by the presence of cellular cytosolic GFP. Hence vesicles are formed from live cells

blistering from the plasma membrane without reorientation, thus enclosing parts of the cellular cytoplasm in the vesicle lumen. Native vesicles therefore represent miniaturized replications of a living cell.

These findings are important because only those native vesicles are of interest for bioanalytical applications, which retain both the membrane topology and cytosolic components.

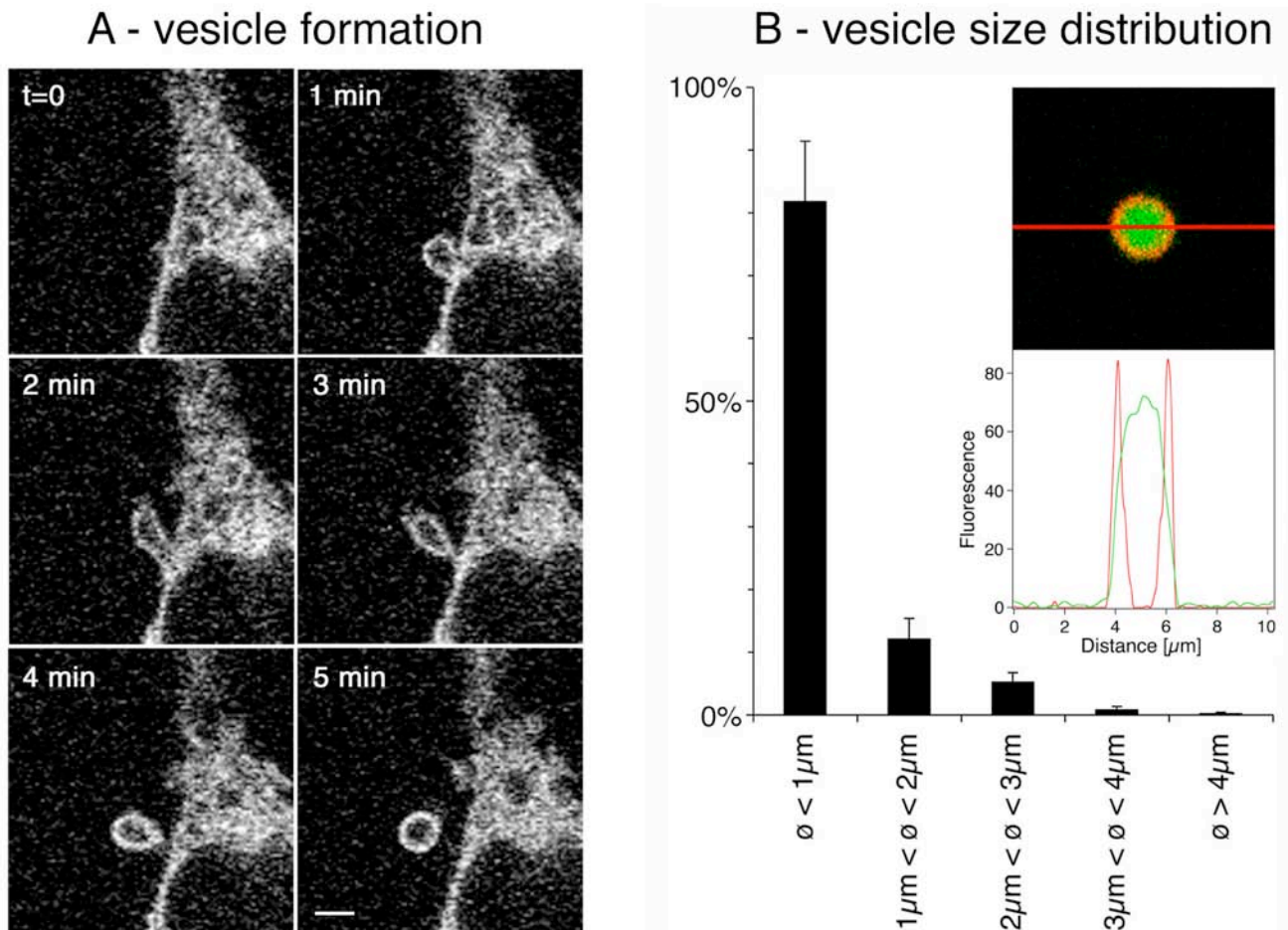


Figure I.3.1 Formation and characterization of native vesicles from HEK293 cells.

(A) Addition of cytochalasin B to HEK293 cells expressing 5-HT₃R-EGFP resulted within a few minutes in the formation of tubular protrusions, detaching from the plasma membrane to form native vesicles. The successive confocal images are reflecting the fluorescence emitted by the EGFP label. Scale bar represents 2 μm.

(B) Agitation of cytochalasin-treated cells led to the release of about 50 native vesicles/cell, 80% of which have a diameter of 0.5-1 μm. The insert shows a vesicle emanating from cells transiently co-expressing cytosolic GFP (green) and the 5HT₃R, and subsequently incubated with 5nM of the fluorescent ligand GR-Rho (red). The fluorescence intensity profile at the indicated line across this vesicle shows clearly the GFP inside the lumen of the vesicle (green), and the ligand GR-Rho on the enveloping membrane (red).

Monitoring 5HT₃R-agonist induced calcium influx into single vesicles

Agonist induced activation of recombinant 5HT₃R in HEK293 cells increases intracellular calcium ion concentration resulting from calcium influx across the cell membrane [17]. Based on this finding, we measured agonist-activated calcium responses in individual native vesicles prepared from mammalian HEK293 cells stably expressing the 5-HT₃R-EGFP.

Changes of calcium ion concentration in individual cells and native vesicles were investigated using the indicator Fura-Red, which upon binding Ca²⁺ decreases its fluorescence emission at 650 nm. Transient calcium signaling was observed after the addition of the 5HT₃R-specific agonist 1-(*m*-chlorophenyl)-biguanide (mCPBG). Addition of 500 nM mCPBG to either live cells or native vesicles derived from these cells induced an immediate increase of intracellular calcium ion concentration, followed by a slower restoration (15-20 s) of resting concentration (Figure I.3.2). The preservation of the kinetics of the transient cellular calcium response in native vesicles in turn proves an unaltered function of the 5HT₃Rs and of ion pumps, which restore initial transmembrane calcium ion gradients.

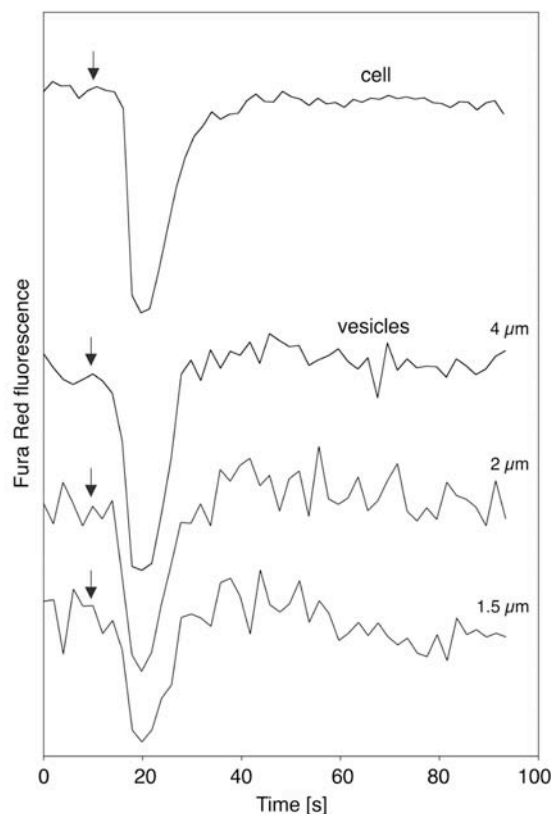


Figure I.3.2 Transient Ca²⁺ signaling in mammalian cells expressing 5HT₃R-EGFP (top trace) and in native vesicles produced from these cells (lower traces). Changes of the Ca²⁺ concentration inside cells and vesicles in response to receptor activation by addition (arrow) of the 5HT₃R-specific agonist mCPBG (500 nM) were recorded with laser scanning confocal microscopy using Fura Red (Ex 488/ Em 650) as a fluorescent Ca²⁺-indicator. Decrease of the fluorescence signal corresponds to increase of the Ca²⁺ concentration.

I.3.5 Discussion

We have developed an efficient protocol to produce native cell membrane vesicles using cytochalasin B, which is known as an active agent destabilizing cytoskeleton-membrane interactions [18]. Vesicle sizes varied from about 0.1 to a few micrometers in diameter depending on the shear forces during vesicle production. Mechanical shear forces released vesicles from the cell surface whereas the remaining cell bodies were removed by differential centrifugation or filtration. In contrast to previous work [19], the controlled vesiculation process induced by cytochalasin B did not involve any cell homogenizing steps, which would release cytoplasmic proteins and change membrane protein orientation.

Orientation and functional activity of cell surface receptors as well as the presence of cytosolic proteins are preserved in native vesicles. These vesicles can be immobilized as functional active containers on solid supports and therefore offer a number of interesting possibilities for investigating the function of receptor mediated cellular signaling by surface sensitive techniques. We provided evidence that native vesicles are the smallest functional units capable of performing transmembrane signaling at fractions of cellular dimensions. Activation of 5-HT₃Rs expressed in HEK293 was shown to evoke increase in intracellular Ca²⁺ concentration resulting from calcium influx across the cellular membrane [17]. Increased cytosolic Ca²⁺ concentrations as a response of agonist binding to the 5HT₃R-EGFP in cells was also observed in native vesicles. This finding demonstrates that cellular signaling reactions can be monitored in native vesicles.

The native vesicle approach presented here is not limited to cultured mammalian cells. All eukaryotic cell types are amenable to cytochalasin B treatment since they possess an actin cytoskeleton [20]. Of importance would be the use of native vesicles from primary cells for functional screening, thus providing central biological information at an early stage in drug discovery. So far such strategies were hampered by the limited availability of primary cells. Native vesicles allow to perform multiple bioanalytical experiments and tests starting with single live cells (e.g. cancer cells, stem cells, neuronal cells obtained from living organisms) opening new possibilities in multiplexing functional single cell bioanalytics.

Because native vesicles can be prepared in large quantities, which can be frozen and stored for many weeks without losing ligand binding activity (data not shown), they could serve as miniaturized artificial cells of constant quality for functional assays replacing time consuming, expensive analytical procedures based on cell cultures of highly variable quality. Downscaling functional assays from large numbers and volumes to single native vesicles open the door to new dimensions of miniaturized bioanalytics.

I.3.6 References

1. Ashcraft, F.M. (2000) *Ion channels and disease*. Academic Press, New York.
2. Drews, J. (2000) Drug discovery: a historical perspective. *Science*, **287**, 1960-1964.
3. Croston, G.E. (2002) Functional cell-based uHTS in chemical genomic drug discovery. *Trends Biotechnol*, **20**, 110-115.
4. Burke, M.D. and Schreiber, S.L. (2004) A planning strategy for diversity-oriented synthesis. *Angew Chem Int Ed Engl*, **43**, 46-58.
5. Sundberg, S.A. (2000) High-throughput and ultra-high-throughput screening: solution- and cell-based approaches. *Curr Opin Biotechnol*, **11**, 47-53.
6. Gonzalez, J.E. and Maher, M.P. (2002) Cellular fluorescent indicators and voltage/ion probe reader (VIPR) tools for ion channel and receptor drug discovery. *Receptors Channels*, **8**, 283-295.
7. Owicki, J.C., Bousse, L.J., Hafeman, D.G., Kirk, G.L., Olson, J.D., Wada, H.G. and Parce, J.W. (1994) The light-addressable potentiometric sensor: principles and biological applications. *Annu Rev Biophys Biomol Struct*, **23**, 87-113.
8. Kröger, D., Hucho, F. and Vogel, H. (1999) Ligand binding to nicotinic acetylcholine receptor investigated by surface plasmon resonance. *Analytical Chemistry*, **71**, 3157-3165.
9. Lowe, C.R. (2000) Nanobiotechnology: the fabrication and applications of chemical and biological nanostructures. *Curr Opin Struct Biol*, **10**, 428-434.
10. Schmidt, C., Mayer, M. and Vogel, H. (2000) A Chip-Based Biosensor for the Functional Analysis of Single Ion Channels. *Angew Chem Int Ed Engl*, **39**, 3137-3140.
11. Fritz, J., Baller, M.K., Lang, H.P., Rothuizen, H., Vettiger, P., Meyer, E., Guntherodt, H., Gerber, C. and Gimzewski, J.K. (2000) Translating biomolecular recognition into nanomechanics. *Science*, **288**, 316-318.
12. Müller, D.J., Heymann, J.B., Oesterhelt, F., Moller, C., Gaub, H., Buldt, G. and Engel, A. (2000) Atomic force microscopy of native purple membrane. *Biochim Biophys Acta*, **1460**, 27-38.
13. Levene, M.J., Korlach, J., Turner, S.W., Foquet, M., Craighead, H.G. and Webb, W.W. (2003) Zero-mode waveguides for single-molecule analysis at high concentrations. *Science*, **299**, 682-686.
14. Whitesides, G.M. (2003) The 'right' size in nanobiotechnology. *Nat Biotechnol*, **21**, 1161-1165.

15. Pick, H., Preuss, A.K., Mayer, M., Wohland, T., Hovius, R. and Vogel, H. (2003) Monitoring expression and clustering of the ionotropic 5HT₃ receptor in plasma membranes of live biological cells. *Biochemistry*, **42**, 877-884.
16. Tsien, R.Y. (1998) The green fluorescent protein. *Annu Rev Biochem*, **67**, 509-544.
17. Hargreaves, A.C., Lummis, S.C. and Taylor, C.W. (1994) Ca²⁺ permeability of cloned and native 5-hydroxytryptamine type 3 receptors. *Mol Pharmacol*, **46**, 1120-1128.
18. Haggmann, J., Burger, M.M. and Dagan, D. (1999) Regulation of plasma membrane blebbing by the cytoskeleton. *J Cell Biochem*, **73**, 488-499.
19. Klumpp, M., Scheel, A., Lopez-Calle, E., Busch, M., Murray, K.J. and Pope, A.J. (2001) Ligand binding to transmembrane receptors on intact cells or membrane vesicles measured in a homogeneous 1-microliter assay format. *J Biomol Screen*, **6**, 159-170.
20. Schoenenberger, C.A., Bischler, N., Fahrenkrog, B. and Aebi, U. (2002) Actin's propensity for dynamic filament patterning. *FEBS Lett*, **529**, 27-33.

Chapter I.4

GFPs at the intracellular side of the 5-HT₃ receptor sense transmembrane mediated conformational changes induced by extracellular binding of agonist

I.4 GFPs at the intracellular side of the 5-HT₃ receptor sense transmembrane mediated conformational changes induced by extracellular binding of agonist

I.4.1 Abstract

We inserted the enhanced green fluorescent protein (EGFP) into the predicted large intracellular loop of each subunit of the homopentameric 5-HT₃ receptor. FRET measurements between the receptor EGFPs and a rhodamine-labeled 5-HT₃ receptor-specific antagonist allowed for quantitative saturation binding studies on detergent solubilized receptors. Moreover, the close proximity of the five EGFPs in the assembled 5-HT₃ receptor lead to homo-FRET thus to a certain degree of fluorescence self-quenching. This effect was reversible by denaturing the receptor subunits by temperature increase. Binding of an agonist to the extracellular side of the 5-HT₃ receptor enhanced the receptor EGFPs fluorescence intensity reflecting conformational changes at the intracellular side of the receptor i.e. EGFPs sense transmembrane signaling. The thereof calculated EC₅₀ was identical to that obtained by electrophysiology on living cultured cells. These results point to a novel fluorescence-based strategy for sensing changes in receptor structure and open the way to a series of functional and structural investigations using the presented methodology.

I.4.2 Introduction

The family of cys-loop ionotropic receptors (IR) comprise structurally related pentameric membrane proteins like the nicotinic acetylcholine, 5-HT₃, GABA_A, and glycine receptors [1,2], which open an ion channel upon binding a particular neurotransmitter. This central transmembrane signaling event must be mediated by a yet undefined transmembrane conformational change within the receptor protein.

Electron microscopy provided a low resolution structural model of the nicotinic acetylcholine receptor (nAChR). In addition, from x-ray diffraction of the acetylcholine binding protein [3], detailed models of the ligand binding region of the nACh, the GABA and the 5-HT₃ receptors were published [4,5]. The question, how binding of a ligand finally leads to channel opening, i.e. transmembrane signaling, yet remains to be answered. Here we show for the first time for a ligand-gated ion channel, that agonist binding at the extracellular side of the receptor, which induces channel opening, finally transmits a conformational change at the intracellular side of the receptor. We investigated that for the case of the 5-HT₃R using optical detection.

To facilitate their study, ligand-gated receptors can be fused to the green fluorescent protein [6-10]. As a novel strategy we demonstrate the use of GFP tagging for sensing changes in receptor structure upon its activation.

The murine 5-HT₃ receptor, which is known to mediate fast signal transduction across synapses in the nervous system, consists of five identical subunits each comprising a large extracellular N-terminal ligand binding domain [5,11-15] followed by four transmembrane segments connected by three short loops, and a final large intracellular domain [16,17].

We have characterized the functional properties of a bioluminescent version of the 5-HT₃R, which was obtained by insertion of an enhanced green fluorescent protein into the large intracellular loop of each of its five subunits. The resulting receptor construct exhibited fully preserved functionality in terms of ligand binding and channel activity and its intrinsic autofluorescent labels allowed for FRET-based biophysical studies.

In that sense, it was possible to quantify saturation binding of a 5-HT₃R specific fluorescent antagonist. Furthermore, the direct integration of the EGFP labels into the intracellular part of the receptor allowed for monitoring conformational changes in its quaternary structure induced by agonist binding. Finally EGFP tagging and the use of specific fluorescent ligands enabled to determine molecular details of the 5-HT₃R structure by FRET analysis.

I.4.3 Experimental procedures

Materials

Synthetic oligonucleotides were purchased from MWG-Biotech AG (Ebersberg, Germany). Kits for plasmid and DNA-fragment purification were obtained from QIAGEN GmbH (Hilden, Germany). Restriction endonucleases (*Cla*I, *Hind*III and *Not*I) were provided by New England Biolabs (Massachusetts, USA). Purified rEGFP was purchased from Clontech (California, USA). The radioligand 3-(5-methyl-1H-imidazol-4-yl)-1-(1-[³H]methyl-1H-indol-3-yl)propanone ([³H]-GR65630; 85.5 Ci/ mmol) was from NEN-DuPont (Boston, MA); quipazine and 1-(m-chlorophenyl)biguanide (mCPBG) from Tocris-Cookson (Langford, UK), and granisetron from Apin Chemicals (Abingdon, UK).

All experimental data were treated using the software Igor Pro (Wavemetrics, Oregon, USA).

DNA constructs

All constructs are based on a vector containing the short splicing variant of the murine 5-hydroxytryptamine type 3A subunit cDNA preceded by the human cytomegalovirus gene promoter, as described before [18].

For purification purposes, a hexa-histidine tag was added at the N-terminus of the 5-HT₃ coding sequence, directly after the signal sequence. The p5HT₃R-N-His vector was obtained by site-directed mutagenesis (Quickchange kit, Stratagene, California, USA) using the oligonucleotides 5'-GCC GGA GGA GGG CCA CTA GTC ATC ACC ATC ACC ATC ACC AGG AGG ATA CCA CCC -3' and 5'-GGG TGG TAT CCT CCT GGT GAT GGT GAT GGT GAT GAC TAG TGG CCC TCC TCC GGC -3'. The plasmid construct was confirmed by restriction mapping and DNA sequencing.

The vector p5HT₃R-EGFP, containing the receptor fused to EGFP, was obtained as indicated in chapter I.3

Cell culture and transfections

Adherent mammalian cells (Human Embryonic Kidney, HEK293) were grown in DMEM/F12 (Dulbecco's modified Eagle medium; GIBCO BRL, Rockville, USA). The medium was supplemented with 2.2 % fetal calf serum (GIBCO BRL). The cultures were split regularly and kept at 37 °C in a humidified atmosphere with 5 % CO₂.

For electrophysiology, confocal microscopy measurements and membrane purification, cells were seeded in 35 mm cell culture dishes, six-well plates containing 22 mm-diameter glass cover slips and 150 cm² flasks at a density of 150'000 cells/ml and transfected using effectene reagent (Qiagen GmbH, Hilden, Germany). All experiments were performed 48 h after transfection.

Membrane solubilization

All following manipulations were performed on ice or at 4 °C, to avoid degradation of the receptor. An amount of 4 g of pelleted cells was used for the membrane solubilization. The cell pellets were resuspended in 10 ml of a solution containing 10 mM Hepes and 1 mM EDTA at pH 7.4, and homogenized for 90 seconds with an Ultra-Turrax T25 (IKA, Staufen, Germany). The membrane fraction was collected by centrifugation at 27'000 g for 40 minutes, and the membrane proteins were solubilized by resuspending and incubating the pellet in 20 ml of 50 mM NaPi (NaH₂PO₄–Na₂HPO₄), 300 mM NaCl and 50 cmc C₁₂E₉ (Anatrace, Maumee, USA) at pH 8.0. A final centrifugation at 100'000 g for 60 minutes served to remove the remaining membrane fraction, and the resulting supernatant was collected and stored at –80 °C until use.

Immobilized metal-ion chromatography purification

5ml of nickel nitrotriacetic acid agarose solution (Qiagen) was used for purification of the 5-HT₃R. The resin was washed 3 times with the membrane solubilization buffer, and incubated at 4 °C overnight with the solubilized 5-HT₃R-N-His solution. The resin was then packed into a column, and nonspecifically bound proteins were removed by washing with increasing concentrations of imidazole in 10 mM NaPi, 500 mM NaCl and 25cmc C₁₂E₉ at pH 7.4. Protein elution was followed by measuring the optical absorption at 280 nm, and the receptor was collected at a concentration of 250 mM imidazole.

The solution was desalted for further analysis of the protein by gel filtration on G-25 columns (NAP-10, Pharmacia Biotech, Uppsala, Sweden), using equilibration and elution buffers containing 1 mM Tris and 5 cmc C₁₂E₉ at pH 7.4.

Electrophysiology

We used the standard patch-clamp technique in whole-cell voltage-clamp, as described in chapter I.2.

Radioactive binding assays

Receptor concentrations as well as ligand affinities were measured by radioligand binding assay. 100µl of solubilized or purified receptor were incubated for 30 minutes at room temperature in solutions of 10mM Hepes pH7.4 with varying concentrations of the specific antagonist [³H]-GR65630 in a final volume of 1ml. A rapid filtration through Whatman GF/B filters (presoaked for 15 min in 0.5% (w/v) polyethylenimine) followed by two washes with 3 mL of ice-cold 10 mM HEPES at pH 7.4 terminated the incubation. Filters were then transferred into scintillation vials, and 4 mL of Ultima Gold (Packard, Meridan, CT) was added. The radioactivity was measured in a Tri-Carb 2200CA liquid scintillation counter (Packard). Nonspecific binding was determined in the presence of 1 µM quipazine. All experiments were performed in triplicate.

The dissociation constant K_d of [³H]-GR65630 and the Hill coefficient n were calculated by fitting the experimental data to the binding equation:

$$[GR65630]_{bound} = \frac{[5 - HT_3R]}{1 + (K_d / [GR65630]_{free})^n} \quad [I.4.1]$$

The binding constant of the rhodamine-labeled ligand GR-Rho[19] has been determined by competitive radioligand binding assay. The sample containing the receptor was incubated with a fixed concentration of radioactive [³H]-GR65630 (0.8nM) and increasing concentrations of GR-Rho. The resulting binding inhibition curve was fitted to:

$$y = \frac{y_0}{1 + (IC_{50} / [GR - Rho])^{-n}} \quad [I.4.2]$$

y and y_0 being respectively the fraction of bound [³H]-GR65630 in the presence and absence of the competitor GR-Rho. IC_{50} represents the concentration of GR-Rho that reduced y_0 by 50%. The dissociation constant of GR-Rho was then calculated referring to Cheng and Prusoff [20]:

$$K_d^{GR-Rho} = \frac{IC_{50}}{1 + [GR65630] / K_d^{GR65630}} \quad [I.4.3]$$

Circular dichroism

The CD spectra of purified 5-HT₃R-N-His receptors were obtained on a Model 62DS spectrometer (Aviv, Lakewood N.J., USA). The protein concentration was 10 nM in 5 cmc C₁₂E₉. The spectra were recorded each nm between 190 and 250 nm, using an averaging time of 10 seconds per wavelength increment.

For the temperature-dependence experiment, the cuvette chamber was heated at a rate of 1 °C per minute, and the sample was measured at 222 nm with an averaging time of 60 seconds. The ellipticity was recorded at intervals of 2 °C between 20 and 74 °C.

The evaluation of protein secondary structure from the CD spectra was performed as described elsewhere [21,22], based on the method of Hennessey and Johnson [23]. The experimental data were fitted to a set of 15 protein spectra of known secondary structures.

Fluorescence measurements

Fluorescence measurements on the solubilized 5-HT₃R-EGFP and on purified rEGFP (Clontech, California, USA) were performed on a SPEX Fluorolog II (Instruments S.A., Stanmore, U.K.), using 1.5 nm excitation and emission bandwidths. Purified rEGFP was dissolved using the same C₁₂E₉ buffer as used for solubilizing the receptor. Quartz cuvettes of 1x1 cm (Hellma, Müllheim, Germany) were placed in a temperature-controlled holder, and the sample solution was continuously stirred with a magnetic bar. All experiments were done at 20 °C, unless otherwise indicated.

For anisotropy measurements, Glan Taylor polarizers (Halbo Optics, Chelmsford, U.K.) were placed in the excitation and emission light paths to enable polarized excitation and emission detection. The excitation and emission wavelengths were 480nm and 512nm respectively, and the anisotropy r was estimated by

$$r \cdot (1 - K \cdot OD) = \left(I_{vv} - \frac{I_{hv} \cdot I_{vh}}{I_{hh}} \right) / \left(I_{vv} + \frac{2I_{hv} \cdot I_{vh}}{I_{hh}} \right) \quad \text{[I.4.4]}$$

where I_{vv} and I_{vh} are respectively the vertically and horizontally polarized fluorescence intensities measured upon vertical excitation and where I_{hv} and I_{hh} are the vertically and horizontally polarized fluorescence intensities, respectively, measured upon horizontal excitation. OD corresponds to the optical density of the sample, and the factor $(1-K \cdot OD)$ corrects the effect of light scattering due to turbidity [24,25]. The proportionality constant K was determined by the anisotropy measurement of different sample dilutions.

I.4.4 Results

The two 5-HT_{3A} receptor constructs used are depicted in Figure I.4.1. 5-HT_{3R}-N-His contains an N-terminal hexa-histidine sequence inserted at the 3' end of the membrane targeting cDNA sequence. We used this construct for receptor purification by affinity chromatography. In 5-HT_{3R}-EGFP the receptor sequence was modified by insertion of the enhanced GFP gene into the large cytoplasmic loop between the 3rd and 4th predicted membrane-spanning domains of each receptor subunit. After cellular expression the pentameric 5-HT_{3R}-EGFP receptor contains five green fluorescent proteins in the intracellular part of the receptor, one per subunit. Radioligand binding and electrophysiological channel measurement studies confirmed preserved functionality of both constructs. In the following, we first characterized the pharmacological and optical properties and then showed how to detect receptor activation by fluorescence.

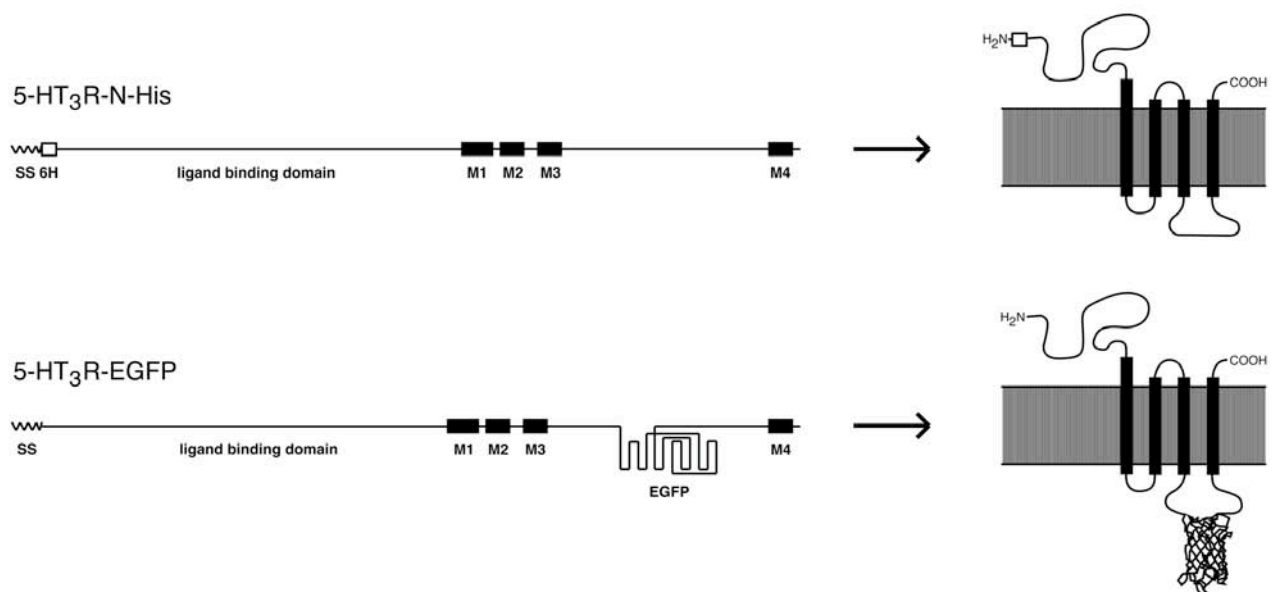


Figure I.4.1 Coding sequence scheme (left) and subunit topology (right) of the two mutated versions of the 5-HT₃ receptor used for this study. The 5-HT_{3R}-N-His construct contains a hexahistidine sequence (“6H”) between the membrane targeting signal sequence (SS) and the N-terminal extracellular ligand binding domain. Each subunit of the pentameric 5-HT_{3R}-EGFP mutant protein comprises one EGFP inserted into the receptor large intracellular loop. “M1”-“M4” are the 4 predicted transmembrane parts.

Hetero-FRET between the EGFP labels and the fluorescent antagonist GR-Rho

Incubation of solubilized 5-HT₃R-EGFP for 3 minutes with increasing concentrations of the rhodamine-labeled antagonist GR-Rho resulted in saturable quenching of EGFP fluorescence via FRET between EGFP and rhodamine moieties (Figure I.4.2). No quenching of the EGFP was observed when the receptor was pre-incubated with 1 μM quipazine, proving that the FRET observed before is due to specific binding of GR-Rho to the receptor. Evaluation of EGFP fluorescence intensity versus GR-Rho concentration data of Figure I.4.2 in the framework of a Langmuir binding equilibrium, yields a dissociation constant of $K_d \approx 1.4$ nM for GR-Rho, comparable to the K_d value obtained via competitive radioligand binding assay (Table I.4.1).

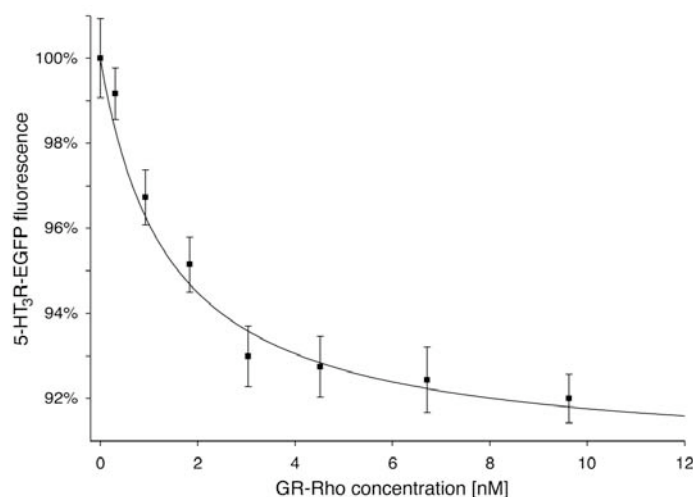


Figure I.4.2 Fluorescence resonance energy transfer between the EGFP label on solubilized 5-HT₃R-EGFP and the rhodamine-labeled antagonist GR-Rho: the EGFP fluorescence is measured after 3 minutes incubation in presence of increasing concentrations of the ligand.

	K_d [³ H]-GR65630 [nM]	EC_{50} GR-Rho [nM]	K_d GR-Rho [nM]
Radioactive binding assay	0.7 ± 0.2	42 ± 6	1.2 ± 0.5
FRET binding assay	–	–	1.4 ± 0.3

Table I.4.1 Determination of the dissociation constant of the ligand GR-Rho via radioactive and FRET binding assays. The GR-Rho EC_{50} value was obtained by competitive radioactive binding assay, and represents the concentration of GR-Rho necessary to reduce the binding of 0.8 nM [³H]-GR65630 by 50 % (see Materials and Methods).

Homo-FRET between EGFP-labeled subunits

The close distance between cytoplasmic EGFP labels in the 5-HT₃R-EGFP leads to a partial quenching of their fluorescence. In order to quantify the energy transfer between neighboring EGFP molecules in the homo-pentamer, we denatured the receptor by temperature increase. Unfolding of the receptor occurs at a temperature of 57.7 ± 0.3 °C, as measured by circular dichroism in a parallel experiment on the purified 5-HT₃R-N-His (Figure I.4.3A, Table I.4.2). Subsequent temperature decrease did not lead to the renaturation of the receptor. This denaturation temperature value will have no influence on the EGFP fluorescence since it is inferior to the EGFP fluorescence half-loss temperature of 78 °C [26,27]. Therefore, receptor unfolding can be monitored by following EGFP fluorescence properties.

The temperature dependence of the EGFP anisotropy was compared between the solubilized 5-HT₃R-EGFP construct and purified rEGFP dissolved into the same buffer containing an equivalent C₁₂E₉ concentration (Figure I.4.3B).

The relation between 5-HT₃R-EGFP and rEGFP volumes can be estimated using the Perrin equation

$$r = r_0 / [1 + (\tau / \phi)] \quad \text{[I.4.5]}$$

In this equation τ is the fluorescence lifetime and ϕ is the rotational correlation time, which can also be expressed as:

$$\phi = \frac{\eta V}{RT} \quad \text{[I.4.6]}$$

η being the viscosity of the sample, V the volume of the fluorescent protein, R the gas constant and T the absolute temperature. By fitting the anisotropy curves of rEGFP and 5-HT₃R-EGFP between 10 and 40 °C - temperature range in which the receptor was shown by circular dichroism to have a stable structure - using the water viscosity for η [28] and assuming same fluorescence lifetimes, we obtain a volume ratio of 1.0 ± 0.4 . However, by presuming a proportionality between volume and molecular weight, the expected volume of the 5-HT₃R-EGFP would be about 17 times superior to that of the EGFP alone. Indeed the 5-HT_{3A} receptor and each EGFP have molecular masses of approximately 320 kD [19] and 27 kD [29], respectively. This experimental divergence is due to the high “local” concentration of the EGFP fluorophores in the 5-HT₃R-EGFP that is reflected by a certain loss in polarization, as explained by Weber [30]. Above the temperature of 40 °C we can

observe differing tendencies of the two curves, as the 5-HT₃R-EGFP falls apart and its intramolecular energy transfer disappears.

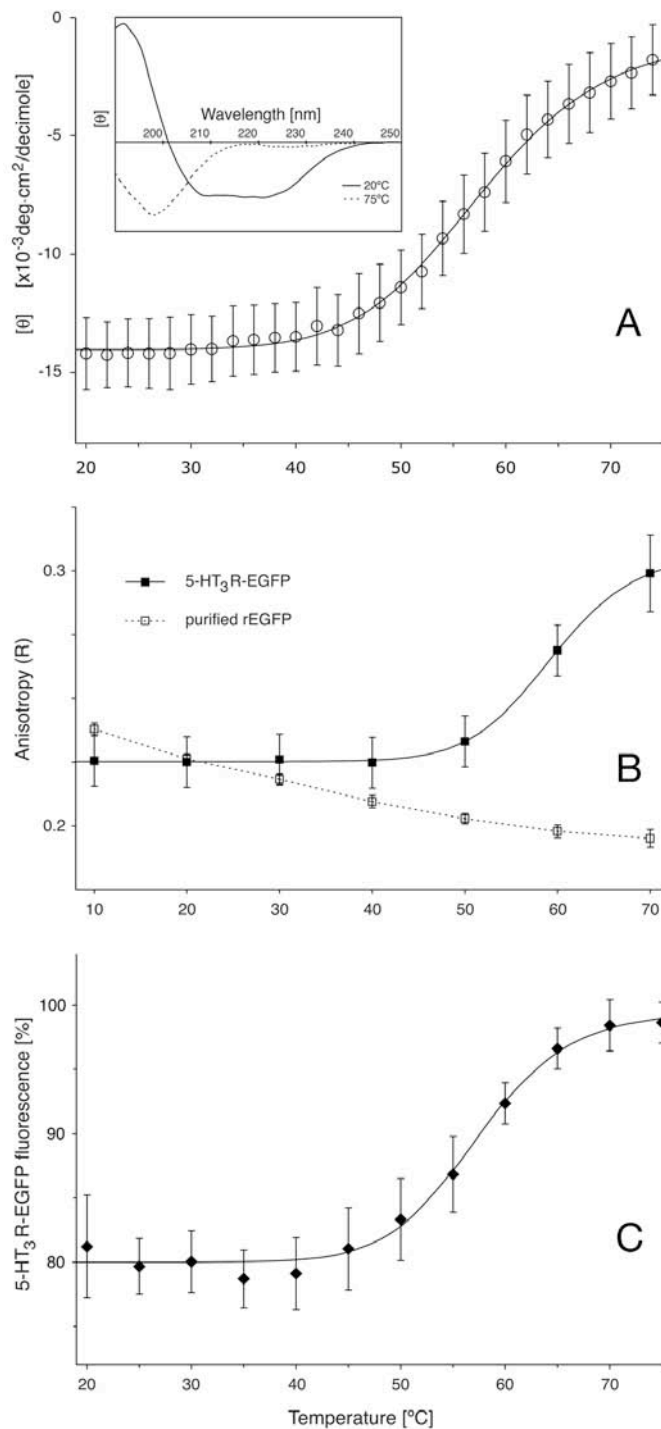


Figure I.4.3 Temperature dependence of the 5-HT₃ receptor structure. (A) Circular dichroism was measured on purified 5-HT₃R-N-His receptor at 222 nm with increasing temperatures. At high temperature the receptor secondary structure is altered, as shown by the CD spectra in inset. (B) Anisotropy of the solubilized 5-HT₃R-EGFP receptor (filled squares) and of purified rEGFP (empty squares), measured at excitation and emission wavelengths of 480 nm and 512 nm respectively. (C) Fluorescence intensity of the EGFP moiety in the solubilized 5-HT₃R-EGFP receptor.

	α -helix	β -sheet	β -turn	undefined
20 °C	51 %	24 %	17 %	8 %
75 °C	13 %	0 %	0 %	87 %

Table I.4.2 Secondary structure of the purified 5-HT₃R-N-His receptor at 20 °C and 75 °C, as determined by circular dichroism spectra analysis.

The fluorescence intensity was measured in function of the temperature, and the quenching of the fluorescent moieties in the 5-HT₃R-EGFP can be deduced by the fluorescence increase at a temperature corresponding to the denaturation of the receptors secondary structure (Figure I.4.3C). We measured a value of 80 ± 2 % of fluorescence intensity at low temperature in comparison to that obtained at temperatures higher than 70 °C. Quantification at room temperature by EGFP fluorescence intensity measurements using purified rEGFP at known concentrations for calibration revealed an apparent pentameric receptor concentration of 3.3 ± 0.1 nM. The radioligand binding assay on the same sample yielded a receptor concentration of 4.0 ± 0.2 nM, giving a similar ratio of 82 ± 7 %.

The transition temperatures measured by these three different methods are summarized in Table I.4.3 and indicate a reliable correlation between fluorescence measurements and secondary structure.

	Circular Dichroism	Anisotropy	Fluorescence
Transition temperature	57.7 ± 0.3 °C	59.5 ± 0.3 °C	57.3 ± 0.8 °C

Table I.4.3 Transition temperature of the 5-HT₃ receptor, measured by circular dichroism on purified 5-HT₃R-N-His, and by anisotropy and fluorescence measurements on solubilized 5-HT₃R-EGFP.

5-HT₃R activation by mCPBG

The solubilized 5-HT₃R-EGFP was submitted to different concentrations of the specific receptor agonist mCPBG [31] to assess any structural change via fluorescence intensity measurement. After 3 minutes incubation, the EGFP autofluorescence intensity of the receptor was recorded and a slight increase was quantified, reaching a plateau at saturated concentrations of the agonist (Figure I.4.4). When the solubilized receptor was pre-incubated with excess of the competing antagonist granisetron (1 μ M), the EGFP fluorescence did not increase in presence of mCPBG, proving the specificity of the fluorescence variation.

The calculated EC₅₀ of 0.5 ± 0.2 μ M was in perfect agreement with electrophysiology data, suggesting an EC₅₀ of 0.66 ± 0.08 μ M (Table I.4.4).

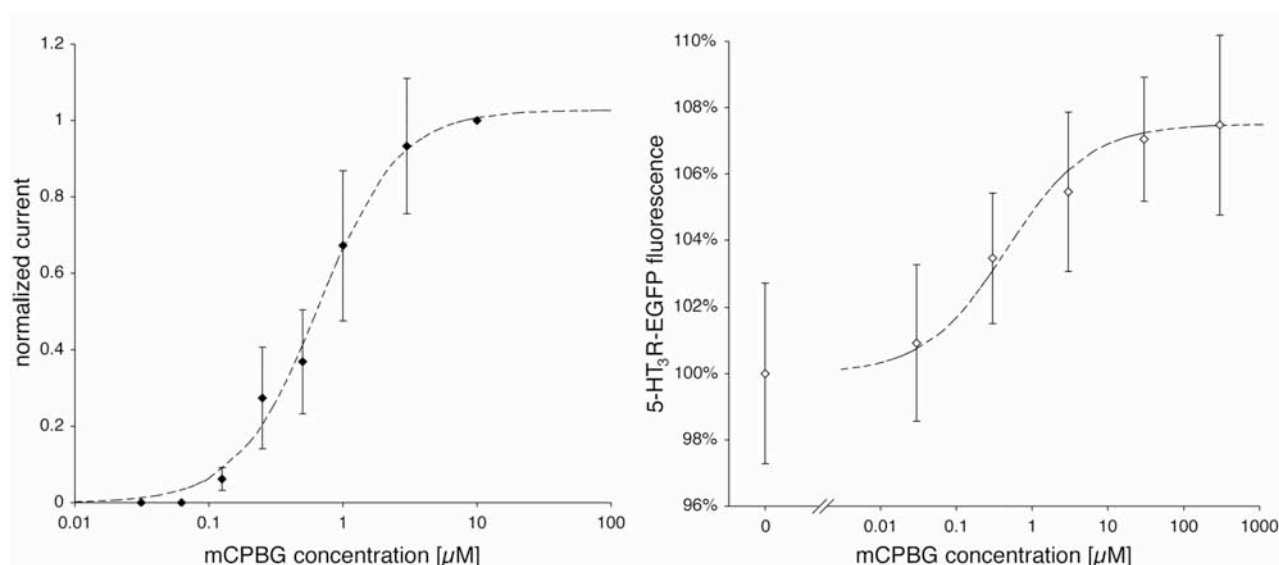


Figure I.4.4 Channel activity of the 5-HT₃R-EGFP as measured by conventional patch-clamp technique on whole cells (left) and by EGFP fluorescence of the solubilized receptor. Application of mCPBG to the receptor results in ion influx (left) and increased fluorescence intensity (right).

	EC ₅₀ [μ M]	Hill coefficient
Electrophysiology	0.66 ± 0.08	1.4 ± 0.2
EGFP fluorescence	0.5 ± 0.2	0.8 ± 0.3

Table I.4.4 Activation of the 5-HT₃R-EGFP mutant with the agonist mCPBG via electrophysiology and fluorescence quantification. Electrophysiology was performed on transiently transfected HEK293 cells, and the EGFP fluorescence measurement was recorded on solubilized labeled receptor.

Estimation of intramolecular distances in the 5-HT₃R-EGFP receptor

The fluorescence quantification in both hetero- and homo-FRET allows us to estimate intramolecular distances in our fusion receptor, using the relation

$$E = \frac{\sum_i (R_0/r_i)^6}{1 + \sum_i (R_0/r_i)^6} \quad \text{[I.4.7]}$$

where E is the energy transfer efficiency depending on the Förster distance R_0 and the intrachromophoric distances r_i [32,33].

In the present case, if we arbitrary assume the rhodamine label of the antagonist GR-Rho to be in the plane formed by one of the green fluorescent proteins and the receptor axis, the GFP cores can be classified in three groups – G_1 , G_2 , G_3 – corresponding to three different intrachromophoric distances due to symmetry (Figure I.4.5).

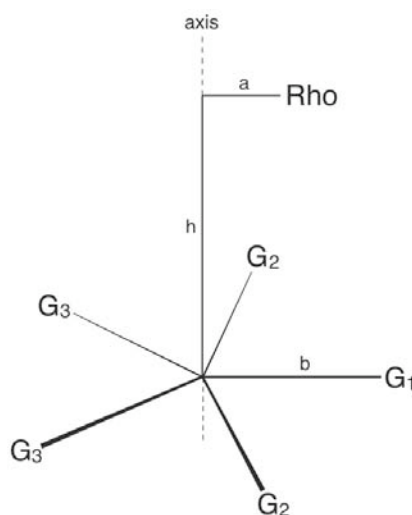


Figure I.4.5 Scheme of intramolecular distances. G_x represent the EGFP fluorescent cores, Rho the GR-Rho bound to the receptor, a and b represent the distance Rho~axis and G_x ~axis respectively, and h is the perpendicular distance between the EGFPs plane and GR-Rho. In our approximation, Rho~axis and G_1 ~axis are in the same plane. Distances in function of a, b and h:

$$\text{Rho} \sim G_1 = \sqrt{h^2 + (b - a)^2};$$

$$\text{Rho} \sim G_2 = \sqrt{h^2 + (b - (1 - 2 \sin(\pi/5))a)^2};$$

$$\text{Rho} \sim G_3 = \sqrt{h^2 + (b - (1 - 2 \sin(2\pi/5))a)^2};$$

$$G_1 \sim G_2 = 2b \sin(\pi/5);$$

$$G_1 \sim G_3 = 2b \sin(2\pi/5).$$

The energy transfer efficiency for the couple EGFP fluorophores/GR-Rho is then:

$$E_{EGFP \sim Rho} = \frac{\left(\frac{R_0^{EGFP \sim Rho}}{G_1 \sim Rho}\right)^6 + 2\left(\frac{R_0^{EGFP \sim Rho}}{G_2 \sim Rho}\right)^6 + 2\left(\frac{R_0^{EGFP \sim Rho}}{G_3 \sim Rho}\right)^6}{1 + \left(\frac{R_0^{EGFP \sim Rho}}{G_1 \sim Rho}\right)^6 + 2\left(\frac{R_0^{EGFP \sim Rho}}{G_2 \sim Rho}\right)^6 + 2\left(\frac{R_0^{EGFP \sim Rho}}{G_3 \sim Rho}\right)^6} \quad [\text{I.4.8}]$$

where $G_x \sim Rho$ are the distances between the GFP cores and the rhodamine label.

The relation between EGFP fluorescence and $E_{EGFP \sim Rho}$ is:

$$\frac{F_{bound_GRRho}}{F_{no_GRRho}} = 1 - E_{EGFP \sim Rho} \quad [\text{I.4.9}]$$

where F_{bound_GRRho} and F_{no_GRRho} are the fluorescence intensities of the receptor in presence of a saturating concentration of GR-Rho and in absence of fluorescent ligand, respectively.

The FRET efficiency between one EGFP fluorophore and its 4 neighbors is:

$$E_{EGFP \sim EGFP} = \frac{2\left(\frac{R_0^{EGFP \sim EGFP}}{G_1 \sim G_2}\right)^6 + 2\left(\frac{R_0^{EGFP \sim EGFP}}{G_1 \sim G_3}\right)^6}{1 + 2\left(\frac{R_0^{EGFP \sim EGFP}}{G_1 \sim G_2}\right)^6 + 2\left(\frac{R_0^{EGFP \sim EGFP}}{G_1 \sim G_3}\right)^6} \quad [\text{I.4.10}]$$

where $G_1 \sim G_x$ are the distances between the GFP donor and its neighboring acceptors.

Because the transferred energy is partially re-emitted by the acceptor, the observed EGFP fluorescence $F_{observed}$ is formulated:

$$\frac{F_{observed}}{F_{noFRET}} = (1 - E_{EGFP \sim EGFP}) \sum_{i=0}^{\infty} (\phi_{EGFP} \cdot E_{EGFP \sim EGFP})^i \quad [\text{I.4.11}]$$

where F_{noFRET} represents the EGFP fluorescence intensity in absence of homo-FRET and ϕ_{EGFP} is its quantum yield.

The different spectral overlaps (Figure I.4.6A) and Förster distances can be calculated using the equations:

$$J = \text{overlap integral} = \int F_D(\lambda)\varepsilon_A(\lambda)\lambda^4 d\lambda \quad [\text{I.4.12}]$$

and

$$R_0^6 = 8.785 \cdot 10^{-5} \frac{\kappa^2 \phi_D J}{n^4} \quad [\text{I.4.13}]$$

where $F_D(\lambda)$ is the peak-normalized fluorescence spectrum, $\varepsilon_A(\lambda)$ the molar absorption coefficient, κ^2 the orientation factor, ϕ_D the quantum yield of the donor in absence of acceptor and n the index of refraction. All wavelengths are expressed in cm.

While the refractive index of the medium between the donor and acceptor is not known precisely, it is assumed here to be equal to that of water.

Using quenching values of 20 ± 2 % due to homo-FRET, 9 ± 1 % due to FRET between the EGFP moieties and the rhodamine label, and assuming a κ^2 of $2/3$ we could estimate 5-HT₃R-EGFP intramolecular distances (Figure I.4.6B, Table I.4.5). We calculated a distance of 78 ± 5 Å between the EGFP plane and the rhodamine label on the fluorescent antagonist, independently of the distance “a” between the axis and the rhodamine label, and distances of 40 ± 5 Å and 43 ± 6 Å between the EGFPs and the 5-HT₃R symmetry axis in respectively resting and desensitized states.

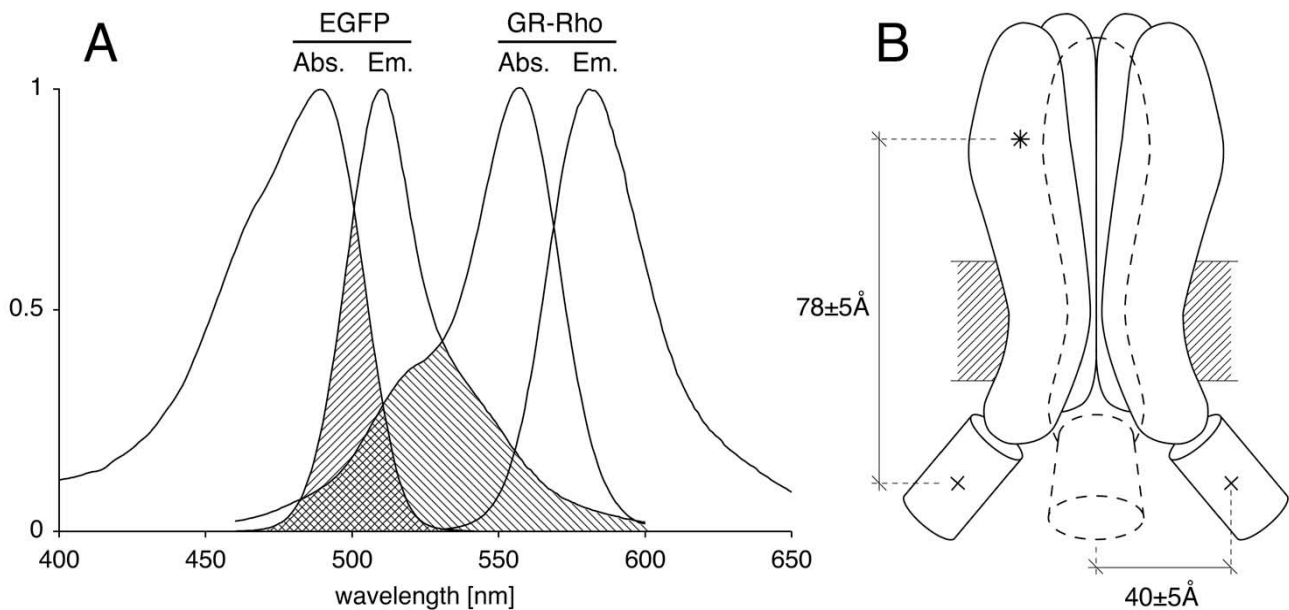


Figure I.4.6 Spectral overlaps of EGFP and GR-Rho absorbance and emission curves (A) and approximation of the distance between the rhodamine label and the EGFP plane and between each EGFP and the channel axis. The rhodamine label in the antagonist GR-Rho is represented by a star, and the EGFP cores are designated by crosses. One subunit is drawn with dashed lines for clarity purposes.

	R_0	GR-Rho~EGFP plane	EGFP~axis (closed state)	EGFP~axis (desensitized)
Hetero-FRET	47.7 Å	78 ± 5 Å	–	–
Homo-FRET	40.6 Å	–	40 ± 5 Å	43 ± 6 Å

Table I.4.5 Förster distance of the fluorescent couples EGFP-rhodamine (hetero-FRET) and EGFP-EGFP (homo-FRET), and estimation of inter-molecular distances. The distances were calculated assuming an orientation factor κ^2 of 2/3.

I.4.5 Discussion

We generated a bioluminescent version of the murine 5-HT_{3A} receptor by inserting the coding sequence of the enhanced green fluorescent protein (EGFP) into its large cytoplasmic loop. This construct exhibited preserved ligand binding and channel properties. The particular position of the EGFP label – between the 3rd and 4th predicted membrane-spanning domains in each of the five subunits – allowed for two different types of fluorescence energy transfer measurements. In a first case, we demonstrated the ability to on-line measure saturation ligand binding on detergent solubilized receptors by following the EGFP fluorescence diminishment in presence of increasing concentrations of a 5-HT_{3R} specific antagonist labeled with the acceptor rhodamine. With these FRET measurements we obtained a binding constant, which was virtually identical to the one obtained by competitive radioactive binding assay.

The relative proximity of the five EGFP labels in the assembled pentameric receptor causes specific fluorescence properties, which were shown to be sensitive to changes in the receptor structure. In the functionally active, detergent-solubilized 5-HT_{3R} the EGFPs are self-quenched due to homo-FRET. This was demonstrated by changes in both fluorescence intensity and fluorescence anisotropy denaturing the 5-HT_{3R}-EGFP at higher temperatures. The increase of EGFP fluorescence intensity after temperature-induced denaturation can be explained by a structural change mediated separation of the EGFP-labeled subunits. In a parallel experiment, unfolding of the 5-HT_{3R} was monitored by circular dichroism. The transition temperature T_t at which 50 % of the receptors were denatured corresponded to T_t observed by fluorescence anisotropy and fluorescence intensity measurements. Because the transition temperature for receptor unfolding at $T_t \sim 58$ °C is distinctly below the cloud point at 88 °C of the detergent C₁₂E₉ [34,35], the fluorescence and CD experiments were not influenced by structural transitions of the used detergent.

Since changes of the intrinsic EGFP fluorescence intensity were indicative to changes in the receptor structure, we then considered the possibility of monitoring conformational changes upon receptor activation directly by fluorescence measurements. By applying increasing concentrations of a non-fluorescent agonist to the EGFP-labeled receptor we observed an increase in fluorescence intensity. That intensity reached a plateau at an agonist concentration saturating the receptors' binding sites. The calculated EC₅₀ was consistent with electrophysiology data on living cells expressing the EGFP tagged 5-HT₃ receptor, suggesting that agonist induced changes in the receptor conformation might be reflected by changes in the intrinsic EGFP fluorescence intensity. Moreover, incubation of the receptor with the non-fluorescent antagonist granisetron had no effect

on the emission intensity, demonstrating the high specificity of our measurements and confirming the observed effect of agonist binding on receptor conformation.

Studies on the structurally related acetylcholine receptor show that the majority of the receptor molecules adopt a desensitized structure in presence of an agonist [36,37]. In the case of the 5-HT₃R-EGFP the agonist-induced changes of the EGFP fluorescence are measured under conditions where the 5-HT₃R is supposed to adopt a desensitized state as well. Structural modifications after receptor activation would then not be restricted to the second transmembrane domain lining the pore [38] but also to the more distant large intracellular loop between the 3rd and 4th transmembrane domains as demonstrated in the present study.

FRET measurements allowed us also to estimate the distance between the plane containing the EGFP moieties and the rhodamine label on the fluorescent antagonist, as well as between each EGFP and the axis of the receptor. The values obtained are in agreement with the cylindrical model of the 5-HT₃ receptor having a length of 11 nm and a radius of 4 nm [39]. Additionally, the distance of 78 ± 5 Å between the rhodamine label on the GR-Rho and the EGFP plane suggests that each EGFP is spatially localized at about 1 nm below the cell membrane. Indeed, the distance between the ligand binding site and the micellar plane replacing the original lipid bilayer [40,41] in solubilized 5-HT₃ receptors was shown to be in the order of 5.4 ± 0.9 nm [42], and the membrane thickness of 3 nm [43].

While it is impossible at this stage to know the exact value of the orientation factor κ^2 , we used an approximate value of $2/3$, corresponding to fluorophores isotropically distributed. This assumption is probably worthwhile in the case of the FRET couple EGFP-rhodamine, since it has been shown by fluorescence anisotropy measurements on the similar fluorescent ligand GR-flu that its fluoresceine label was highly mobile [44]. However in the case of homo-FRET between subunits, and due to the high polarization of the EGFP [45], the orientation factor could differ substantially hence providing a slightly diverging value for the distance between the EGFPs and the central symmetry axis. Figure I.4.7 provides a relation between the orientation factor κ^2 and the calculated average distances between the EGFPs. We see in that sense that the conformational change in the desensitized state can either be an opening of approximately 3 Å, an orientation change of the EGFPs, or a combination of both. Indeed, in the structurally related GABA and acetylcholine receptors opening of the channel gate was shown to be induced by the rotation of the second transmembrane domain, meaning that the activated state of the receptor does not necessarily implicate a dramatic enlargement of its structure, but possibly only twisting of its subunits [46-49]. More precise structural and functional informations might be obtained by analogous experiments based on the FRET but using smaller fluorophores. While EGFP labeling of the receptor is

somehow restricted to certain domains due to the sterical hindrance resulting from the fluorophore size, techniques such as site-specific incorporation of fluorescent unnatural amino acids [50-52] by nonsense codon suppression would permit a wide variation in the choice of labeling position thus the possibility to obtain a detailed structural map of the receptor. The suppression methodology is especially promising for such integral membrane proteins, which are not yet generally amenable to the methods of high resolution structure determination (e.g., NMR, x-ray crystallography) and could be a valuable alternative to tedious techniques such as electron microscopy, which is moreover restricted to fixed incontrovertible conformational states [48,53]. Fluorescent amino acid incorporation in, or near the 5-HT₃ receptor central pore would lead to precious enlightenments regarding the gating mechanism and spatial modifications over time upon activation by an agonist. In addition to structural studies the FRET methodology could have another potential application in drug screening. Using multiarray plates it might be possible to monitor at once and in real time both ligand binding and channel activation of a wide variety of agonists and antagonists via fluorescence measurements based on hetero-FRET with a competing fluorescent acceptor ligand and inter-subunit homo-FRET respectively.

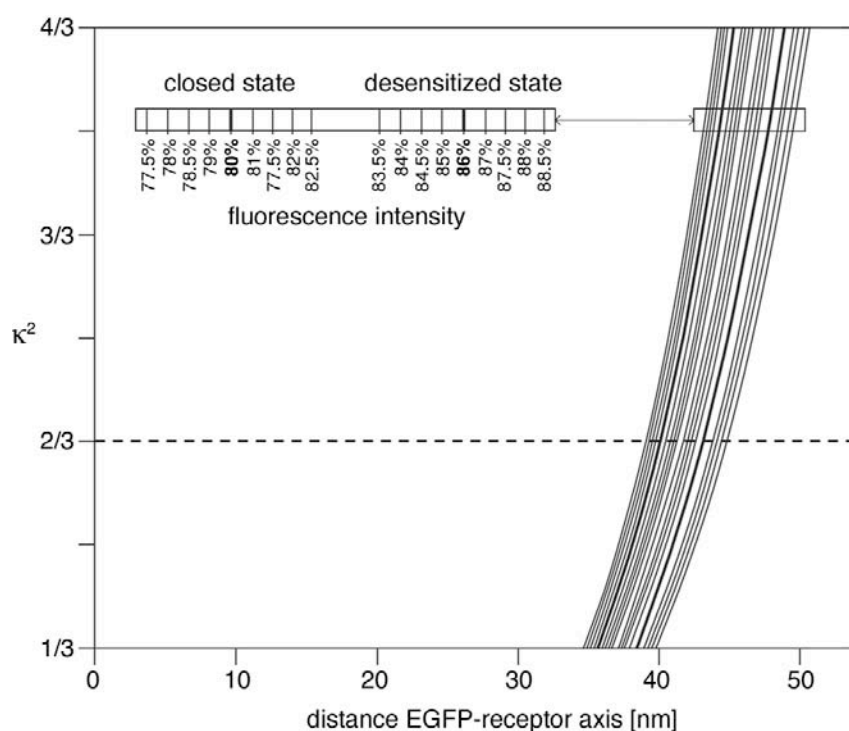


Figure I.4.7 Calculated distance between the EGFP label on one subunit and the channel axis, in relation to the orientation factor κ^2 . The two thick lines are representing the position of the EGFP in absence of any ligand and with a bound agonist (mCPBG). The corresponding fluorescence intensities are expressed in percentage of the fluorescence of completely separated subunits.

I.4.6 References

1. Betz, H. (1990) Ligand-gated ion channels in the brain: the amino acid receptor superfamily. *Neuron*, **5**, 383-392.
2. Barnard, E.A. (1992) Receptor classes and the transmitter-gated ion channels. *Trends Biochem Sci*, **17**, 368-374.
3. Brejc, K., van Dijk, W.J., Klaassen, R.V., Schuurmans, M., van Der Oost, J., Smit, A.B. and Sixma, T.K. (2001) Crystal structure of an ACh-binding protein reveals the ligand-binding domain of nicotinic receptors. *Nature*, **411**, 269-276.
4. Cromer, B.A., Morton, C.J. and Parker, M.W. (2002) Anxiety over GABA(A) receptor structure relieved by AChBP. *Trends Biochem Sci*, **27**, 280-287.
5. Reeves, D.C., Sayed, M.F., Chau, P.L., Price, K.L. and Lummis, S.C. (2003) Prediction of 5-HT(3) Receptor Agonist-Binding Residues Using Homology Modeling. *Biophys J*, **84**, 2338-2334.
6. Marshall, J., Molloy, R., Moss, G.W., Howe, J.R. and Hughes, T.E. (1995) The jellyfish green fluorescent protein: a new tool for studying ion channel expression and function. *Neuron*, **14**, 211-215.
7. David-Watine, B., Shorte, S.L., Fucile, S., de Saint Jan, D., Korn, H. and Bregestovski, P. (1999) Functional integrity of green fluorescent protein conjugated glycine receptor channels. *Neuropharmacology*, **38**, 785-792.
8. Zuo, J., Treadaway, J., Buckner, T.W. and Fritsch, B. (1999) Visualization of alpha9 acetylcholine receptor expression in hair cells of transgenic mice containing a modified bacterial artificial chromosome. *Proc Natl Acad Sci U S A*, **96**, 14100-14105.
9. Martinez-Torres, A. and Miledi, R. (2001) Expression of gamma-aminobutyric acid rho 1 and rho 1 Delta 450 as gene fusions with the green fluorescent protein. *Proc Natl Acad Sci U S A*, **98**, 1947-1951.
10. Fucile, S., Palma, E., Martinez-Torres, A., Miledi, R. and Eusebi, F. (2002) The single-channel properties of human acetylcholine alpha 7 receptors are altered by fusing alpha 7 to the green fluorescent protein. *Proc Natl Acad Sci U S A*, **99**, 3956-3961.
11. Boess, F.G., Steward, L.J., Steele, J.A., Liu, D., Reid, J., Glencorse, T.A. and Martin, I.L. (1997) Analysis of the ligand binding site of the 5-HT3 receptor using site directed mutagenesis: importance of glutamate 106. *Neuropharmacology*, **36**, 637-647.
12. Deane, C.M. and Lummis, S.C. (2001) The role and predicted propensity of conserved proline residues in the 5-HT3 receptor. *J Biol Chem*, **276**, 37962-37966.

13. Venkataraman, P., Venkatachalan, S.P., Joshi, P.R., Muthalagi, M. and Schulte, M.K. (2002) Identification of critical residues in loop E in the 5-HT₃ASR binding site. *BMC Biochem*, **3**, 15.
14. Hu, X.Q., Zhang, L., Stewart, R.R. and Weight, F.F. (2003) Arginine 222 in the Pre-transmembrane Domain 1 of 5-HT₃A Receptors Links Agonist Binding to Channel Gating. *J Biol Chem*, **278**, 46583-46589.
15. Schreiter, C., Hovius, R., Costioli, M., Pick, H., Kellenberger, S., Schild, L. and Vogel, H. (2003) Characterization of the Ligand-binding Site of the Serotonin 5-HT₃ Receptor: THE ROLE OF GLUTAMATE RESIDUES 97, 224, AND 235. *J Biol Chem*, **278**, 22709-22716.
16. Mukerji, J., Haghghi, A. and Seguela, P. (1996) Immunological characterization and transmembrane topology of 5- hydroxytryptamine₃ receptors by functional epitope tagging. *J Neurochem*, **66**, 1027-1032.
17. Spier, A.D. and Lummis, S.C. (2002) Immunological characterization of 5-HT₃ receptor transmembrane topology. *J Mol Neurosci*, **18**, 169-178.
18. Pick, H., Preuss, A.K., Mayer, M., Wohland, T., Hovius, R. and Vogel, H. (2003) Monitoring expression and clustering of the ionotropic 5HT₃ receptor in plasma membranes of live biological cells. *Biochemistry*, **42**, 877-884.
19. Wohland, T., Friedrich, K., Hovius, R. and Vogel, H. (1999) Study of ligand-receptor interactions by fluorescence correlation spectroscopy with different fluorophores: evidence that the homopentameric 5-hydroxytryptamine type 3As receptor binds only one ligand. *Biochemistry*, **38**, 8671-8681.
20. Cheng, Y. and Prusoff, W.H. (1973) Relationship between the inhibition constant (K₁) and the concentration of inhibitor which causes 50 per cent inhibition (I₅₀) of an enzymatic reaction. *Biochem Pharmacol*, **22**, 3099-3108.
21. Vogel, H. and Gartner, W. (1987) The secondary structure of bacteriorhodopsin determined by Raman and circular dichroism spectroscopy. *J Biol Chem*, **262**, 11464-11469.
22. Vogel, H. (1987) Comparison of the conformation and orientation of alamethicin and melittin in lipid membranes. *Biochemistry*, **26**, 4562-4572.
23. Hennessey, J.P., Jr. and Johnson, W.C., Jr. (1981) Information content in the circular dichroism of proteins. *Biochemistry*, **20**, 1085-1094.
24. Teale, F.W. (1969) Fluorescence depolarization by light-scattering in turbid solutions. *Photochem Photobiol*, **10**, 363-374.
25. Lentz, B.R., Moore, B.M. and Barrow, D.A. (1979) Light-scattering effects in the measurement of membrane microviscosity with diphenylhexatriene. *Biophys J*, **25**, 489-494.

26. Ward, W.W. (1981) In DeLuca, M. M., W. D. (ed.), *Bioluminescence and Chemiluminescence: Basic Chemistry and Analytical Applications*. Academic Press, Inc., NY, pp. 235-242.
27. Bokman, S.H. and Ward, W.W. (1981) Renaturation of *Aequorea* green-fluorescent protein. *Biochem Biophys Res Commun*, **101**, 1372-1380.
28. Cho, C.H., Urquidi, J. and Wilse Robinson, G. (1999) Molecular-level description of temperature and pressure effects on the viscosity of water. *Journal of Chemical Physics*, **111**, 10171-10176.
29. Shimomura, O. (1979) Structure of the chromophore of *Aequorea* green fluorescent protein. *FEBS Lett*, **104**, 220-222.
30. Weber, G. (1954) Dependence of the polarization of the fluorescence on the concentration. *Trans. Faraday Soc.*, **50**, 552-555.
31. Hargreaves, A.C., Lummis, S.C. and Taylor, C.W. (1994) Ca²⁺ permeability of cloned and native 5-hydroxytryptamine type 3 receptors. *Mol Pharmacol*, **46**, 1120-1128.
32. Forster, T. (1946) Energiewanderung Und Fluoreszenz. *Naturwissenschaften*, **33**, 166-175.
33. Forster, T. (1948) Zwischenmolekulare Energiewanderung Und Fluoreszenz. *Annalen Der Physik*, **2**, 55-75.
34. Huibers, P.D.T., Shah, D.O. and Katritzky, A.R. (1997) Predicting Surfactant Cloud Point from Molecular Structure. *J Colloid Interface Sci*, **193**, 132-136.
35. Inoue, T., Ohmura, H. and Murata, D. (2003) Cloud point temperature of polyoxyethylene-type nonionic surfactants and their mixtures. *J Colloid Interface Sci*, **258**, 374-382.
36. Auerbach, A. and Akk, G. (1998) Desensitization of mouse nicotinic acetylcholine receptor channels. A two-gate mechanism. *J Gen Physiol*, **112**, 181-197.
37. Grosman, C. and Auerbach, A. (2001) The dissociation of acetylcholine from open nicotinic receptor channels. *Proc Natl Acad Sci U S A*, **98**, 14102-14107.
38. Panicker, S., Cruz, H., Arrabit, C. and Slesinger, P.A. (2002) Evidence for a centrally located gate in the pore of a serotonin-gated ion channel. *J Neurosci*, **22**, 1629-1639.
39. Boess, F.G., Beroukhim, R. and Martin, I.L. (1995) Ultrastructure of the 5-hydroxytryptamine₃ receptor. *J Neurochem*, **64**, 1401-1405.
40. Le Maire, M., Kwee, S., Andersen, J.P. and Moller, J.V. (1983) Mode of interaction of polyoxyethyleneglycol detergents with membrane proteins. *Eur J Biochem*, **129**, 525-532.
41. Moller, J.V. and le Maire, M. (1993) Detergent binding as a measure of hydrophobic surface area of integral membrane proteins. *J Biol Chem*, **268**, 18659-18672.

42. Vallotton, P., Tairi, A.P., Wohland, T., Friedrich-Benet, K., Pick, H., Hovius, R. and Vogel, H. (2001) Mapping the antagonist binding site of the serotonin type 3 receptor by fluorescence resonance energy transfer. *Biochemistry*, **40**, 12237-12242.
43. Unwin, N. (1993) Nicotinic acetylcholine receptor at 9 Å resolution. *J Mol Biol*, **229**, 1101-1124.
44. Tairi, A.P., Hovius, R., Pick, H., Blasey, H., Bernard, A., Surprenant, A., Lundstrom, K. and Vogel, H. (1998) Ligand binding to the serotonin 5HT₃ receptor studied with a novel fluorescent ligand. *Biochemistry*, **37**, 15850-15864.
45. Inoue, S., Shimomura, O., Goda, M., Shribak, M. and Tran, P.T. (2002) Fluorescence polarization of green fluorescence protein. *Proc Natl Acad Sci U S A*, **99**, 4272-4277.
46. Horenstein, J., Wagner, D.A., Czajkowski, C. and Akabas, M.H. (2001) Protein mobility and GABA-induced conformational changes in GABA(A) receptor pore-lining M2 segment. *Nat Neurosci*, **4**, 477-485.
47. Unwin, N., Miyazawa, A., Li, J. and Fujiyoshi, Y. (2002) Activation of the nicotinic acetylcholine receptor involves a switch in conformation of the alpha subunits. *J Mol Biol*, **319**, 1165-1176.
48. Unwin, N. (2003) Structure and action of the nicotinic acetylcholine receptor explored by electron microscopy. *FEBS Lett*, **555**, 91-95.
49. Miyazawa, A., Fujiyoshi, Y. and Unwin, N. (2003) Structure and gating mechanism of the acetylcholine receptor pore. *Nature*, **424**, 949-955.
50. Turcatti, G., Nemeth, K., Edgerton, M.D., Meseth, U., Talabot, F., Peitsch, M., Knowles, J., Vogel, H. and Chollet, A. (1996) Probing the structure and function of the tachykinin neurokinin-2 receptor through biosynthetic incorporation of fluorescent amino acids at specific sites. *J Biol Chem*, **271**, 19991-19998.
51. Turcatti, G., Nemeth, K., Edgerton, M.D., Knowles, J., Vogel, H. and Chollet, A. (1997) Fluorescent labeling of NK2 receptor at specific sites in vivo and fluorescence energy transfer analysis of NK2 ligand-receptor complexes. *Receptors Channels*, **5**, 201-207.
52. Anderson, R.D., 3rd, Zhou, J. and Hecht, S.M. (2002) Fluorescence resonance energy transfer between unnatural amino acids in a structurally modified dihydrofolate reductase. *J Am Chem Soc*, **124**, 9674-9675.
53. Unwin, N., Toyoshima, C. and Kubalek, E. (1988) Arrangement of the acetylcholine receptor subunits in the resting and desensitized states, determined by cryoelectron microscopy of crystallized Torpedo postsynaptic membranes. *J Cell Biol*, **107**, 1123-1138.

Chapter II.1

Part II: protein labeling using mis-acylated suppressor tRNA technology

Part II - Protein labeling using mis-acylated suppressor tRNA technology

II.1.1 Introduction

A relatively new technique, pioneered by the group of P.G. Schultz [1], permits the covalent labeling of proteins using probes much smaller than reporter proteins such as the green fluorescent protein [2] or the human alkylguanine transferase (hAGT) [3]. Based on the site-specific biosynthetic incorporation of artificial amino acids, this approach exhibits minimal interference with the protein structure and function. Introduction of fluorescent unnatural amino acids is of special interest for energy transfer measurements that could lead to precise informations regarding topology, structure and function of membrane proteins. It has already been used with success in the laboratory of professor Horst Vogel for structural analysis of the tachykinin neurokinin-2 receptor [4,5]. Indeed, whereas classical site-directed mutagenesis allows for the study of molecular interactions between ligand molecules and specific amino acids in a receptor protein [6-8], the suppressor tRNA technology can be used to introduce fluorescent or other chemical groups for structural investigations as well as for monitoring conformational or functional changes inside a given protein induced by extremely fine modifications on the atomic level [9,10].

The original strategy was based on the synthesis of a messenger RNA containing an amber codon (UAG) at the incorporation position, to which an artificial transfer RNA carrying the artificial amino acid and containing the complementary anti-codon sequence is targeted during *in vivo* protein synthesis (Figure II.1.1).

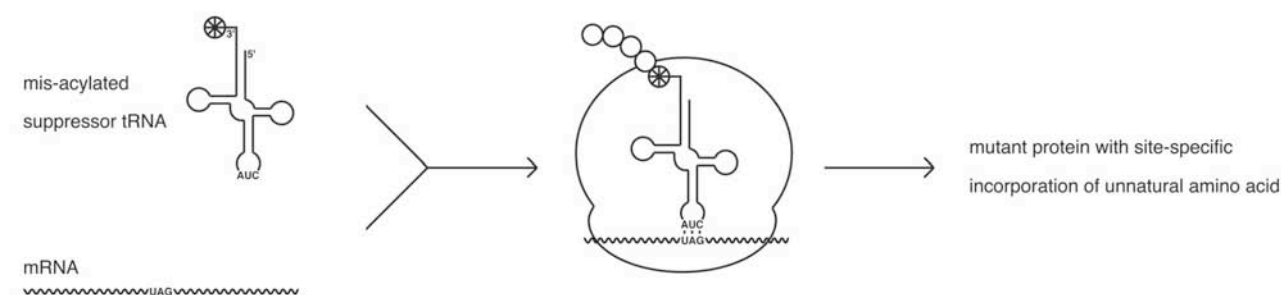


Figure II.1.1: General scheme of the site-specific incorporation of unnatural amino acids in proteins: a mis-acylated suppressor tRNA and a mRNA containing an amber stop codon at the incorporation position are applied to the translational machinery, integrating the artificial amino acid in the nascent protein emerging from the ribosome. Plain circle = natural amino acid, circled star = unnatural amino acid.

Acylation of the suppressor tRNA can either be carried out *in vitro*, by enzymatic ligation of a chemically acylated synthetic short nucleotide together with an *in vitro* transcribed RNA strand [11-14], or *in vivo*, by genetic modification of the host cell [15-24].

In most of the published experiments involving mis-acylated tRNA, the codon/anticodon triplets were chosen to be one of the three natural stop codons, amber (UAG), ochre (UAA) or opal (UGA), because none of them is coding for a specific natural amino acid (see Figure II.1.2 left). Preventing a non-desired incorporation of a competing natural amino acid, this choice of triplet has however the drawback of being recognized by the prokaryotic or eukaryotic release factors, triggering the termination of the protein synthesis [25,26]. This obstacle results in a low yield of unnatural amino acid incorporation. In an attempt to circumvent this impeding competition between the release factors and the mis-acylated suppressor tRNA, research has been focused to find codons not recognized by any endogenous tRNA nor the release factors, but still accepted by the ribosome. An extension of the genetic code would additionally permit in principle the site-specific incorporation of several different unnatural amino acids in the same protein, allowing for instance intramolecular fluorescence energy transfer measurements [27].

Such efforts lead to the synthesis of codons and anticodons containing artificial nucleotide analogues [28-31], necessitating complicated chemistry on both mRNA and tRNA levels. Unfortunately, the specificity of base pairing using such unnatural nucleotides is at this time not sufficient for a reliable incorporation of synthetic amino acids.

In parallel, research initiated by the group of M. Sisido focused on 4- and 5-bases codons [27,32-40]. By creating a novel tRNA based on a corresponding codon rarely used in the host cell system and having one or two supplementary bases in the anticodon, they succeeded in obtaining frame-shift suppression. The fact that the starting triplet is almost not used in the host cell allows for a minimal competition, whereas the additional base(s) permits the specific incorporation of several different unnatural amino acids. However, the triplet of choice is highly depending on the species used for translation, needing a specific customization that is maybe not possible in every case. This special codon/anticodon pair has also to be sufficiently specific: since the discovery of the genetic code degeneracy [41], it has been shown that unlike the first two base pairs, the third base pair between codon and anticodon is not closely monitored by the ribosome, as demonstrated later by x-ray crystallography [42]. The strongest codon-anticodon interaction is thus required in this “wobble” position [43-45] to allow for the fourth (and fifth) base to have an adequate specificity.

Apart from that, a disadvantage of this latter technique is the possible incorporation of natural amino acids at the position of interest by the natural frameshifting that can occur when the ribosome is stalled, once the artificial suppressor tRNA is “used-up”. Also, it is potentially possible that the artificial tRNA can incorporate unnatural amino acids at non-desired positions, using 3 instead of 4-5 bases.

Even though not universally exploitable, this frameshift suppression technique has already been applied with success using *Escherichia coli in vitro* translation systems [27].

For any of these suppressor codons, the rest of the tRNA sequence has also to be considered. While many tRNAs are recognized by aminoacyl RNA synthetases (AARS) by their anticodon [46,47], most of them are recognized by other nucleotides [48-53] (see Figure II.1.2 right). The consequence is that, although the anticodon is designed not to be present in any other tRNA, the suppressor tRNA could anyway be aminoacylated by endogenous AARS targeting natural tRNAs, leading to the incorporation of natural amino acids in the protein position of interest. Since the lifetime of an uncharged tRNA is relatively important as compared to the mis-acylated one [54], this could result in a large quantity of the unmodified form of the protein under investigation. An adequate tRNA sequence has hence to be engineered specifically for each cell type utilized.

		Second Position					
		U	C	A	G		
First Position (5' end)	U	UUU Phe UUC UUA Leu UUG	UCU Ser UCC UCA UCG	UAU Tyr UAC UAA Stop UAG	UGU Cys UGC UGA Stop UGG Trp	U C A G	Third Position (3' end)
	C	CUU Leu CUC CUA CUG	CCU Pro CCC CCA CCG	CAU His CAC CAA Gln CAG	CGU Arg CGC CGA CGG	U C A G	
	A	AUU Ile AUC AUA Met AUG	ACU Thr ACC ACA ACG	AAU Asn AAC AAA Lys AAG	AGU Ser AGC AGA Arg AGG	U C A G	
	G	GUU Val GUC GUA GUG	GCU Ala GCC GCA GCG	GAU Asp GAC GAA Glu GAG	GGU Gly GGC GGA GGG	U C A G	

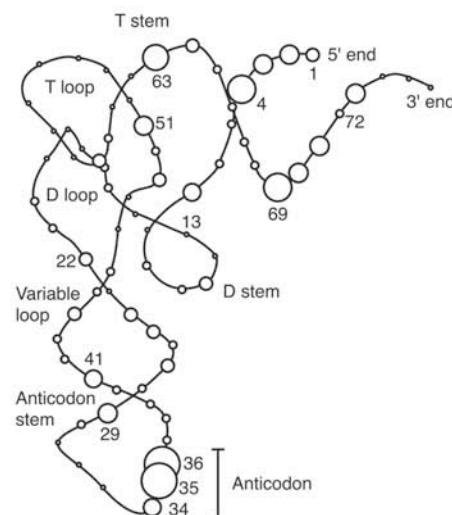


Figure II.1.2: (left) Codon table (adapted from F.H. Crick [55]). (right) Schematic representation of the three-dimensional structure of tRNA. Circles indicate the position of nucleotides, the size of which is proportional to the recognition frequency by AARSs. The acceptor stem is the helical structure formed by base pairing of bases 1 to 7 with bases 72 to 66. (Figure adapted from McClain & Nicholas [56])

The second part of the present thesis aims at the extension of this mis-acylated suppressor tRNA technology to cultured mammalian cells, generally more suitable for structural and functional studies of membrane proteins such as the 5-HT₃ neurotransmitter receptor. Indeed, this technique has been originally developed as an *in vitro* method [33,57-61], and later applied *in vivo* to *Xenopus oocytes* [4,5,9,62,63] and *Escherichia coli* [16,17,20,21], either unsuited to specific protein localization and folding or requiring purification to avoid their strong endogenous cellular autofluorescence when measuring specific fluorescence emitted by unnatural amino acids. An extension to mammalian cells would permit FRET measurements directly in living cells, circumventing a possible functional or structural change that can occur during purification.

Firstly, in chapter II.2, I study lipofection as a general tool to guide RNA molecules into cells and investigate the suitability of this technique for various RNA species through kinetic measurements of cellular uptake.

In the following chapter, I quantitatively measure specific amino acid incorporation efficiency using mis-acylated suppressor tRNA in adherent mammalian cells, and propose a general strategy to assay the adaptability of tRNA sequences to this suppressor technology in any cultured mammalian cell line.

Using any codon/anticodon pair, a natural suppression can lead to the incorporation of a natural amino acid in place of the desired unnatural one. This naturally occurring event [64-68] is depending on the codon sequence [69] and is varying among the cell lines under study. I propose in chapter II.4 an approach to measure the suitability of different cell lines and of the suppressor codon sequence, regarding the natural suppression aspect.

Finally, I study in the last chapter the effect of the eRF1 cellular concentration on the artificial suppression using stop codons, and investigate the possibility to improve incorporation efficiency.

II.1.2 References

1. Noren, C.J., Anthony-Cahill, S.J., Griffith, M.C. and Schultz, P.G. (1989) A general method for site-specific incorporation of unnatural amino acids into proteins. *Science*, **244**, 182-188.
2. Heim, R. and Tsien, R.Y. (1996) Engineering green fluorescent protein for improved brightness, longer wavelengths and fluorescence resonance energy transfer. *Curr Biol*, **6**, 178-182.
3. Keppler, A., Gendreizig, S., Gronemeyer, T., Pick, H., Vogel, H. and Johnsson, K. (2003) A general method for the covalent labeling of fusion proteins with small molecules in vivo. *Nat Biotechnol*, **21**, 86-89.
4. Turcatti, G., Nemeth, K., Edgerton, M.D., Meseth, U., Talabot, F., Peitsch, M., Knowles, J., Vogel, H. and Chollet, A. (1996) Probing the structure and function of the tachykinin neurokinin-2 receptor through biosynthetic incorporation of fluorescent amino acids at specific sites. *J Biol Chem*, **271**, 19991-19998.
5. Turcatti, G., Nemeth, K., Edgerton, M.D., Knowles, J., Vogel, H. and Chollet, A. (1997) Fluorescent labeling of NK2 receptor at specific sites in vivo and fluorescence energy transfer analysis of NK2 ligand-receptor complexes. *Receptors Channels*, **5**, 201-207.
6. Boess, F.G., Steward, L.J., Steele, J.A., Liu, D., Reid, J., Glencorse, T.A. and Martin, I.L. (1997) Analysis of the ligand binding site of the 5-HT₃ receptor using site directed mutagenesis: importance of glutamate 106. *Neuropharmacology*, **36**, 637-647.
7. Hu, X.Q., Zhang, L., Stewart, R.R. and Weight, F.F. (2003) Arginine 222 in the Pre-transmembrane Domain 1 of 5-HT_{3A} Receptors Links Agonist Binding to Channel Gating. *J Biol Chem*, **278**, 46583-46589.
8. Schreiter, C., Hovius, R., Costioli, M., Pick, H., Kellenberger, S., Schild, L. and Vogel, H. (2003) Characterization of the Ligand-binding Site of the Serotonin 5-HT₃ Receptor: THE ROLE OF GLUTAMATE RESIDUES 97, 224, AND 235. *J Biol Chem*, **278**, 22709-22716.
9. Beene, D.L., Brandt, G.S., Zhong, W., Zacharias, N.M., Lester, H.A. and Dougherty, D.A. (2002) Cation- π Interactions in Ligand Recognition by Serotonergic (5-HT_{3A}) and Nicotinic Acetylcholine Receptors: The Anomalous Binding Properties of Nicotine. *Biochemistry*, **41**, 10262-10269.
10. Beene, D.L., Dougherty, D.A. and Lester, H.A. (2003) Unnatural amino acid mutagenesis in mapping ion channel function. *Curr Opin Neurobiol*, **13**, 264-270.
11. Hecht, S.M., Alford, B.L., Kuroda, Y. and Kitano, S. (1978) "Chemical aminoacylation" of tRNA's. *J Biol Chem*, **253**, 4517-4520.

12. Heckler, T.G., Chang, L.H., Zama, Y., Naka, T., Chorghade, M.S. and Hecht, S.M. (1984) T4 RNA ligase mediated preparation of novel "chemically misacylated" tRNAPheS. *Biochemistry*, **23**, 1468-1473.
13. Baldini, G., Martoglio, B., Schachenmann, A., Zugliani, C. and Brunner, J. (1988) Mischarging Escherichia coli tRNAPhe with L-4'-[3-(trifluoromethyl)-3H-diazirin-3-yl]phenylalanine, a photoactivatable analogue of phenylalanine. *Biochemistry*, **27**, 7951-7959.
14. Robertson, S.A., Noren, C.J., Anthony-Cahill, S.J., Griffith, M.C. and Schultz, P.G. (1989) The use of 5'-phospho-2 deoxyribocytidylylriboadenosine as a facile route to chemical aminoacylation of tRNA. *Nucleic Acids Res*, **17**, 9649-9660.
15. Wang, L., Zhang, Z., Brock, A. and Schultz, P.G. (2003) Addition of the keto functional group to the genetic code of Escherichia coli. *Proc Natl Acad Sci U S A*, **100**, 56-61.
16. Wang, L., Brock, A. and Schultz, P.G. (2002) Adding L-3-(2-Naphthyl)alanine to the genetic code of E. coli. *J Am Chem Soc*, **124**, 1836-1837.
17. Wang, L., Brock, A., Herberich, B. and Schultz, P.G. (2001) Expanding the genetic code of Escherichia coli. *Science*, **292**, 498-500.
18. Pastrnak, M. and Schultz, P.G. (2001) Phage selection for site-specific incorporation of unnatural amino acids into proteins in vivo. *Bioorg Med Chem*, **9**, 2373-2379.
19. Mehl, R.A., Anderson, J.C., Santoro, S.W., Wang, L., Martin, A.B., King, D.S., Horn, D.M. and Schultz, P.G. (2003) Generation of a bacterium with a 21 amino Acid genetic code. *J Am Chem Soc*, **125**, 935-939.
20. Liu, D.R. and Schultz, P.G. (1999) Progress toward the evolution of an organism with an expanded genetic code. *Proc Natl Acad Sci U S A*, **96**, 4780-4785.
21. Liu, D.R., Magliery, T.J., Pastrnak, M. and Schultz, P.G. (1997) Engineering a tRNA and aminoacyl-tRNA synthetase for the site-specific incorporation of unnatural amino acids into proteins in vivo. *Proc Natl Acad Sci U S A*, **94**, 10092-10097.
22. Kiga, D., Sakamoto, K., Kodama, K., Kigawa, T., Matsuda, T., Yabuki, T., Shirouzu, M., Harada, Y., Nakayama, H., Takio, K. *et al.* (2002) An engineered Escherichia coli tyrosyl-tRNA synthetase for site-specific incorporation of an unnatural amino acid into proteins in eukaryotic translation and its application in a wheat germ cell-free system. *Proc Natl Acad Sci U S A*, **99**, 9715-9720.
23. Chin, J.W., Santoro, S.W., Martin, A.B., King, D.S., Wang, L. and Schultz, P.G. (2002) Addition of p-azido-L-phenylalanine to the genetic code of Escherichia coli. *J Am Chem Soc*, **124**, 9026-9027.

24. Chin, J.W., Martin, A.B., King, D.S., Wang, L. and Schultz, P.G. (2002) Addition of a photocrosslinking amino acid to the genetic code of *Escherichia coli*. *Proc Natl Acad Sci U S A*, **99**, 11020-11024.
25. Bertram, G., Bell, H.A., Ritchie, D.W., Fullerton, G. and Stansfield, I. (2000) Terminating eukaryote translation: domain 1 of release factor eRF1 functions in stop codon recognition. *Rna*, **6**, 1236-1247.
26. Bertram, G., Innes, S., Minella, O., Richardson, J. and Stansfield, I. (2001) Endless possibilities: translation termination and stop codon recognition. *Microbiology*, **147**, 255-269.
27. Taki, M., Hohsaka, T., Murakami, H., Taira, K. and Sisido, M. (2002) Position-specific incorporation of a fluorophore-quencher pair into a single streptavidin through orthogonal four-base codon/anticodon pairs. *J Am Chem Soc*, **124**, 14586-14590.
28. Hirao, I., Ohtsuki, T., Fujiwara, T., Mitsui, T., Yokogawa, T., Okuni, T., Nakayama, H., Takio, K., Yabuki, T., Kigawa, T. *et al.* (2002) An unnatural base pair for incorporating amino acid analogs into proteins. *Nat Biotechnol*, **20**, 177-182.
29. Hirao, I., Kimoto, M., Yamakage, S., Ishikawa, M., Kikuchi, J. and Yokoyama, S. (2002) A unique unnatural base pair between a C analogue, pseudoisocytosine, and an A analogue, 6-methoxypurine, in replication. *Bioorg Med Chem Lett*, **12**, 1391-1393.
30. Ohtsuki, T., Kimoto, M., Ishikawa, M., Mitsui, T., Hirao, I. and Yokoyama, S. (2001) Unnatural base pairs for specific transcription. *Proc Natl Acad Sci U S A*, **98**, 4922-4925.
31. Roberts, C., Bandaru, R. and Switzer, C. (1997) Theoretical and Experimental Study of Isoguanine and Isocytosine: Base Pairing in an Expanded Genetic System. *J Am Chem Soc*, **119**, 4640-4649.
32. Hohsaka, T., Ashizuka, Y., Murakami, H. and Sisido, M. (1996) Incorporation of Nonnatural Amino Acids into Streptavidin through In Vitro Frame-Shift Suppression. *J Am Chem Soc*, **118**, 9778-9779.
33. Hohsaka, T., Kajihara, D., Ashizuka, Y., Murakami, H. and Sisido, M. (1998) Efficient Incorporation of Nonnatural Amino Acids with Large Aromatic Groups into Streptavidin in In Vitro Protein Synthesizing Systems. *J Am Chem Soc*, **121**, 34-40.
34. Hohsaka, T., Ashizuka, Y. and Sisido, M. (1999) Incorporation of two nonnatural amino acids into proteins through extension of the genetic code. *Nucleic Acids Symp Ser*, **42**, 79-80.

35. Sisido, M. and Hohsaka, T. (2001) Introduction of specialty functions by the position-specific incorporation of nonnatural amino acids into proteins through four-base codon/anticodon pairs. *Appl Microbiol Biotechnol*, **57**, 274-281.
36. Hohsaka, T., Ashizuka, Y., Taira, H., Murakami, H. and Sisido, M. (2001) Incorporation of nonnatural amino acids into proteins by using various four-base codons in an *Escherichia coli* in vitro translation system. *Biochemistry*, **40**, 11060-11064.
37. Hohsaka, T., Ashizuka, Y., Murakami, H. and Sisido, M. (2001) Five-base codons for incorporation of nonnatural amino acids into proteins. *Nucleic Acids Res*, **29**, 3646-3651.
38. Moore, B., Persson, B.C., Nelson, C.C., Gesteland, R.F. and Atkins, J.F. (2000) Quadruplet codons: implications for code expansion and the specification of translation step size. *J Mol Biol*, **298**, 195-209.
39. Magliery, T.J., Anderson, J.C. and Schultz, P.G. (2001) Expanding the genetic code: selection of efficient suppressors of four- base codons and identification of "shifty" four-base codons with a library approach in *Escherichia coli*. *J Mol Biol*, **307**, 755-769.
40. Anderson, J.C., Magliery, T.J. and Schultz, P.G. (2002) Exploring the limits of codon and anticodon size. *Chem Biol*, **9**, 237-244.
41. Crick, F.H., Barnett, L., Brenner, S. and Watts-Tobin, R.J. (1961) General nature of the genetic code for proteins. *Nauchni Tr Vissh Med Inst Sofiia*, **192**, 1227-1232.
42. Ogle, J.M., Brodersen, D.E., Clemons, W.M., Jr., Tarry, M.J., Carter, A.P. and Ramakrishnan, V. (2001) Recognition of cognate transfer RNA by the 30S ribosomal subunit. *Science*, **292**, 897-902.
43. Crick, F.H. (1966) Codon--anticodon pairing: the wobble hypothesis. *J Mol Biol*, **19**, 548-555.
44. Topal, M.D. and Fresco, J.R. (1976) Base pairing and fidelity in codon-anticodon interaction. *Nature*, **263**, 289-293.
45. Jukes, T.H. (1977) How many anticodons? *Science*, **198**, 319-320.
46. Kiselev, L.L. and Frolova, L. (1989) [The tRNA anticodon is recognized by aminoacyl-tRNA-synthetase]. *Mol Biol (Mosk)*, **23**, 1603-1610.
47. Pallanck, L. and Schulman, L.H. (1991) Anticodon-dependent aminoacylation of a noncognate tRNA with isoleucine, valine, and phenylalanine in vivo. *Proc Natl Acad Sci U S A*, **88**, 3872-3876.
48. Schimmel, P.R. (1979) Recent results on how aminoacyl transfer RNA synthetases recognize specific transfer RNAs. *Mol Cell Biochem*, **25**, 3-14.

49. Hou, Y.M., Francklyn, C. and Schimmel, P. (1989) Molecular dissection of a transfer RNA and the basis for its identity. *Trends Biochem Sci*, **14**, 233-237.
50. Hou, Y.M. and Schimmel, P. (1988) A simple structural feature is a major determinant of the identity of a transfer RNA. *Nature*, **333**, 140-145.
51. Horowitz, J., Chu, W.C., Derrick, W.B., Liu, J.C., Liu, M. and Yue, D. (1999) Synthetase recognition determinants of E. coli valine transfer RNA. *Biochemistry*, **38**, 7737-7746.
52. Breitschopf, K., Achsel, T., Busch, K. and Gross, H.J. (1995) Identity elements of human tRNA(Leu): structural requirements for converting human tRNA(Ser) into a leucine acceptor in vitro. *Nucleic Acids Res*, **23**, 3633-3637.
53. Tocchini-Valentini, G., Saks, M.E. and Abelson, J. (2000) tRNA leucine identity and recognition sets. *J Mol Biol*, **298**, 779-793.
54. Schlegel, R.A., Iversen, P. and Rechsteiner, M. (1978) The turnover of tRNAs microinjected into animal cells. *Nucleic Acids Res*, **5**, 3715-3729.
55. Crick, F.H. (1966) The genetic code. 3. *Sci Am*, **215**, 55-60 passim.
56. McClain, W.H. and Nicholas, H.B., Jr. (1987) Differences between transfer RNA molecules. *J Mol Biol*, **194**, 635-642.
57. Cload, S.T., Liu, D.R., Froland, W.A. and Schultz, P.G. (1996) Development of improved tRNAs for in vitro biosynthesis of proteins containing unnatural amino acids. *Chem Biol*, **3**, 1033-1038.
58. Noren, C.J., Anthony-Cahill, S.J., Suich, D.J., Noren, K.A., Griffith, M.C. and Schultz, P.G. (1990) In vitro suppression of an amber mutation by a chemically aminoacylated transfer RNA prepared by runoff transcription. *Nucleic Acids Res*, **18**, 83-88.
59. Karginov, V.A., Mamaev, S.V. and Hecht, S.M. (1997) In vitro suppression as a tool for the investigation of translation initiation. *Nucleic Acids Res*, **25**, 3912-3916.
60. Kurzchalia, T.V., Wiedmann, M., Breter, H., Zimmermann, W., Bauschke, E. and Rapoport, T.A. (1988) tRNA-mediated labelling of proteins with biotin. A nonradioactive method for the detection of cell-free translation products. *Eur J Biochem*, **172**, 663-668.
61. Short, G.F., 3rd, Golovine, S.Y. and Hecht, S.M. (1999) Effects of release factor 1 on in vitro protein translation and the elaboration of proteins containing unnatural amino acids. *Biochemistry*, **38**, 8808-8819.
62. Chollet, A., Turcatti, G., Nemeth, K. and Vogel, H. (1998) In Slavik, J. (ed.), *Fluorescence Microscopy and Fluorescent Probes*. Plenum Press, New York, Vol. 2, pp. 87-92.

-
63. Cohen, B.E., McAnaney, T.B., Park, E.S., Jan, Y.N., Boxer, S.G. and Jan, L.Y. (2002) Probing protein electrostatics with a synthetic fluorescent amino acid. *Science*, **296**, 1700-1703.
 64. Berteaux, V., Rousset, J.P. and Cassan, M. (1991) UAG readthrough is not increased in vivo by Moloney murine leukemia virus infection. *Biochimie*, **73**, 1291-1293.
 65. Burke, J.F. and Mogg, A.E. (1985) Suppression of a nonsense mutation in mammalian cells in vivo by the aminoglycoside antibiotics G-418 and paromomycin. *Nucleic Acids Res*, **13**, 6265-6272.
 66. Sedivy, J.M., Capone, J.P., RajBhandary, U.L. and Sharp, P.A. (1987) An inducible mammalian amber suppressor: propagation of a poliovirus mutant. *Cell*, **50**, 379-389.
 67. Capone, J.P., Sedivy, J.M., Sharp, P.A. and RajBhandary, U.L. (1986) Introduction of UAG, UAA, and UGA nonsense mutations at a specific site in the Escherichia coli chloramphenicol acetyltransferase gene: use in measurement of amber, ochre, and opal suppression in mammalian cells. *Mol Cell Biol*, **6**, 3059-3067.
 68. Cassan, M., Berteaux, V., Angrand, P.O. and Rousset, J.P. (1990) Expression vectors for quantitating in vivo translational ambiguity: their potential use to analyse frameshifting at the HIV gag-pol junction. *Res Virol*, **141**, 597-610.
 69. Sogaard, T.M., Jakobsen, C.G. and Justesen, J. (1999) A sensitive assay of translational fidelity (readthrough and termination) in eukaryotic cells. *Biochemistry (Mosc)*, **64**, 1408-1417.

Chapter II.2

mRNA transfection as a mean to achieve homogeneous protein expression: uptake and expression profiles

II.2 mRNA transfection as a mean to achieve homogeneous protein expression: uptake and expression profiles

II.2.1 Abstract

The delivery of nucleic acids is a primordial step in most experiments based on cultured mammalian cells, permitting among others functional or structural studies of recombinant proteins. Transfections of populations of adherent cells generally involve the nuclear delivery of plasmid DNA using various techniques such as calcium-phosphate, lipofection, or electroporation. These methods show day-to-day variations in protein expression, notably because the plasmid DNA has to enter the cell nucleus and is therefore depending on the cell cycle. Furthermore, this fact is reflected by a lack of homogeneity regarding the protein expression level, impeding proper cell-to-cell comparisons.

The present chapter deals with the study of mRNA delivery using EGFP as a reporter gene. We compare protein expression levels between individual cells in cell populations, showing day-to-day and cell-to-cell homogeneities on the expression level contrarily to plasmid DNA transfection. The nucleic acid uptake kinetic using lipofection was additionally monitored to discuss the suitability of this transfection technique for the cellular delivery of degradable molecules such as RNAs.

II.2.2 Introduction

Biological and medical research is exploiting different transfection techniques for the delivery of genetic material to a wide variety of cell types. The methods used are either targeting single cells by microinjection [1,2], or cell population in culture by calcium-phosphate precipitation [3], DEAE-dextran [4], viral transfection [5], electroporation [6,7] or lipofection [8-10] to mention the most commonly exploited techniques.

In most cases, the genetic material is transferred to the cell as circular DNA because of its stability, high levels of expression obtained, and the possibility to generate stably expressing cell lines. This “nuclear transfection” – because the DNA needs to enter the nucleus in order to express the desired protein – is however not suitable for experiments depending on reproducibility and on a homogeneous yield of expression level among individual cells. Indeed it has been shown that transfections based on nuclear targeted DNA requires mitotic activity, as proven by experiments based on cell cycle synchronization [11,12]. Therefore non-synchronized cells having individual differing cell cycles exhibit cell-to-cell variations in levels of protein expression.

In the present study, we investigate transfection efficiencies and protein expression yields on the single cell level by comparing delivery of DNA and mRNA encoding the enhanced green fluorescent protein (EGFP) as a reporter. We use DOTAP lipofection [13] for the transfection of adherent mammalian cells. We also evaluate the lipid-nucleotide complex cellular uptake time to study the suitability of cytoplasmic lipofection to highly degradation-sensitive molecules such as mRNA, tRNA or siRNA, taking into account that cationic lipids have protecting properties [14].

II.2.3 Experimental procedures

Materials

Synthetic oligonucleotides were purchased from MWG-Biotech AG (Ebersberg, Germany). Kits for plasmid and DNA-fragment purification were obtained from QIAGEN GmbH (Hilden, Germany). The restriction endonuclease *NotI* was provided by New England Biolabs (Massachusetts, USA). Chemicals were purchased from Sigma-Aldrich (Missouri, USA). The MEGAscript kit for *in vitro* transcription and the cap analog m⁷G(5')ppp(5')G were from Ambion (Texas, USA). Purified rEGFP was purchased from Clontech (California, USA), and DOTAP liposomal reagent was obtained from Boehringer (Mannheim, Germany).

EGFP mRNA transcription

Capped mRNA coding for the EGFP was synthesized from the DNA template pT7PEGFP as described in details in Chapter II.3, using the MEGAscript kit (Ambion, Texas, USA) and the cap analog m⁷G(5')ppp(5')G (Ambion).

Cell lines and transfection

HEK293 cells were grown in DMEM/F12 (Dulbecco's modified Eagle medium; GIBCO BRL, Rockville, USA) at a density of 150'000 cells/ml. The medium was supplemented with 2.2 % fetal calf serum (GIBCO BRL). The cultures were split regularly prior to transfection and kept at 37 °C in a humidified atmosphere with 5 % CO₂. The transfection was performed as follows, per milliliter of cell culture: a mixture containing 2.5 µg of mRNA or DNA and 3.75 µl DOTAP diluted in 50 µl of 10 mM HEPES buffer at pH 7.4 was incubated for 10 minutes at room temperature, and applied dropwise to the cell medium. Experiments involving the use of the fluorescently labeled oligonucleotide were done by replacing 10 % (mass) of the reporter EGFP mRNA with a Cy5-labeled primer (random sequence: 5'-GTC GTC GTC GTC TGA CCT GGA TGA TCT GTC GTC GTC GTC-3'). All fluorescent measurements were performed 20 hours after transfection.

EGFP and Cy5 quantification using a fluorescence plate reader

We used 6-well plates (TPP, Trasadingen, Switzerland) for fluorescence intensity quantifications in a plate reader. The growth medium was removed and the adherent cells were homogenized for 10 minutes at 37 °C in 270 µl PBS containing 10 % Triton-X100 (Fluka, Buchs, Switzerland). The measurements were performed with an Analyst plate reader (LJL Biosystems, California, USA) using 200 µl per sample in 96-well plates (Greiner, Frickenhausen, Germany).

FACS analysis

Cells were transfected in 25 cm² flasks 20 hours before analysis, detached using Trypsin-EDTA and resuspended in PBS. FACS analysis was performed on a PAS III flow cytometer (Partec GmbH, Münster, Germany), using a 488 nm laser excitation and a 520-560 nm detection filter. Each experiment was based on the analysis of approximately 30'000 cells per sample at a rate of 100-200 cells/s.

Laser scanning confocal microscopy

The cells were seeded on glass coverslips and imaged using a Zeiss LSM510 (Carl Zeiss AG) confocal microscope. Detection and distinction of the fluorescence signals of EGFP (excitation at 488 nm) and Cy5 (excitation at 633 nm) was achieved by appropriate filter sets.

II.2.4 Results

We present here a comparison study between two different transfection pathways by lipofection in adherent mammalian cells, as depicted in Figure II.2.1.

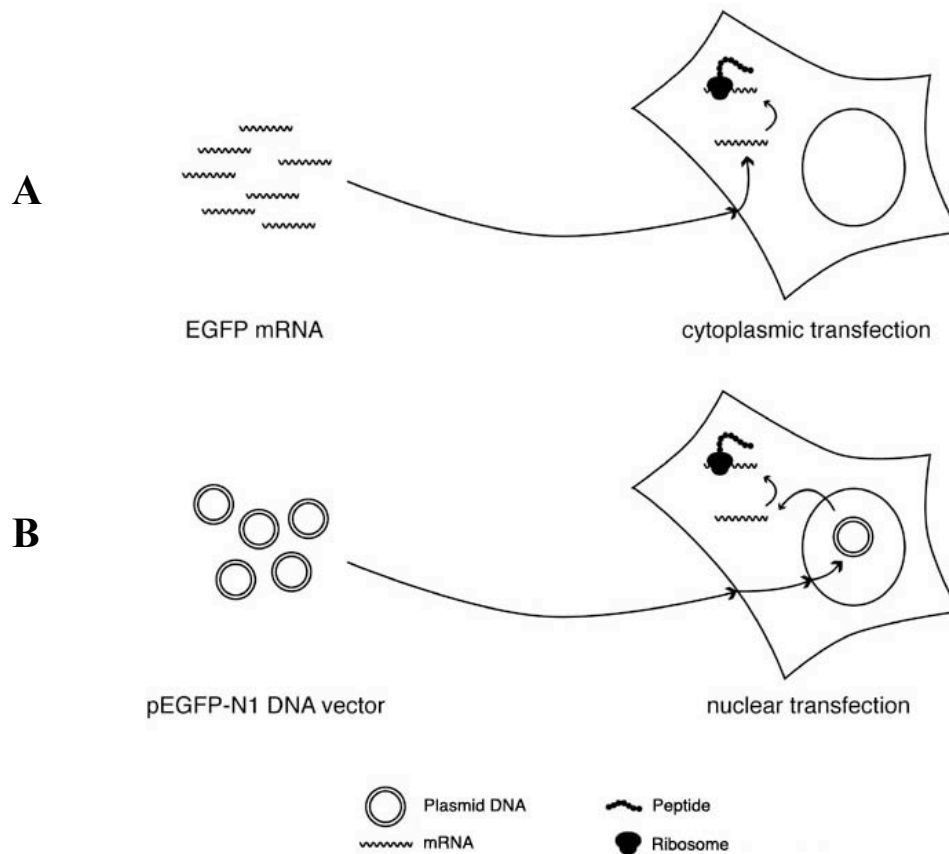


Figure II.2.1 Comparison of transfection pathways: whereas transfection with mRNA (A) only needs to traverse the cell plasma membrane for successful expression of the protein of interest, the transfection with DNA vectors targeting nuclear polymerases (B) additionally requires to pass through the nuclear membrane. In the present study, the expression level is quantified by the use of nucleotides coding for the EGFP, which is finally measured by its fluorescence.

Transfections of adherent mammalian cell cultures are generally performed using DNA vectors containing a eukaryotic promoter (Figure II.2.1B). A successful expression of the gene of interest requires the vector to pass the plasma membrane, cytoplasm and nuclear membrane to be recognized and processed by nuclear transcription factors. Direct transfection of *in vitro*-transcribed mRNA represents the shortest way between gene and protein by bypassing the need to cross the nuclear barrier in order to obtain a translation (Figure II.2.1A).

In order to quantify the expression levels we performed transfections of templates coding for the enhanced version of the green fluorescent protein (EGFP).

Cells were split 16 hours prior to transfection, and the fluorescence intensities were measured on the single cell level 24 hours after transfection by FACS analysis (Figure II.2.2). The fluorescence of blank cells was identical with or without application of the transfection reagent DOTAP (not shown).

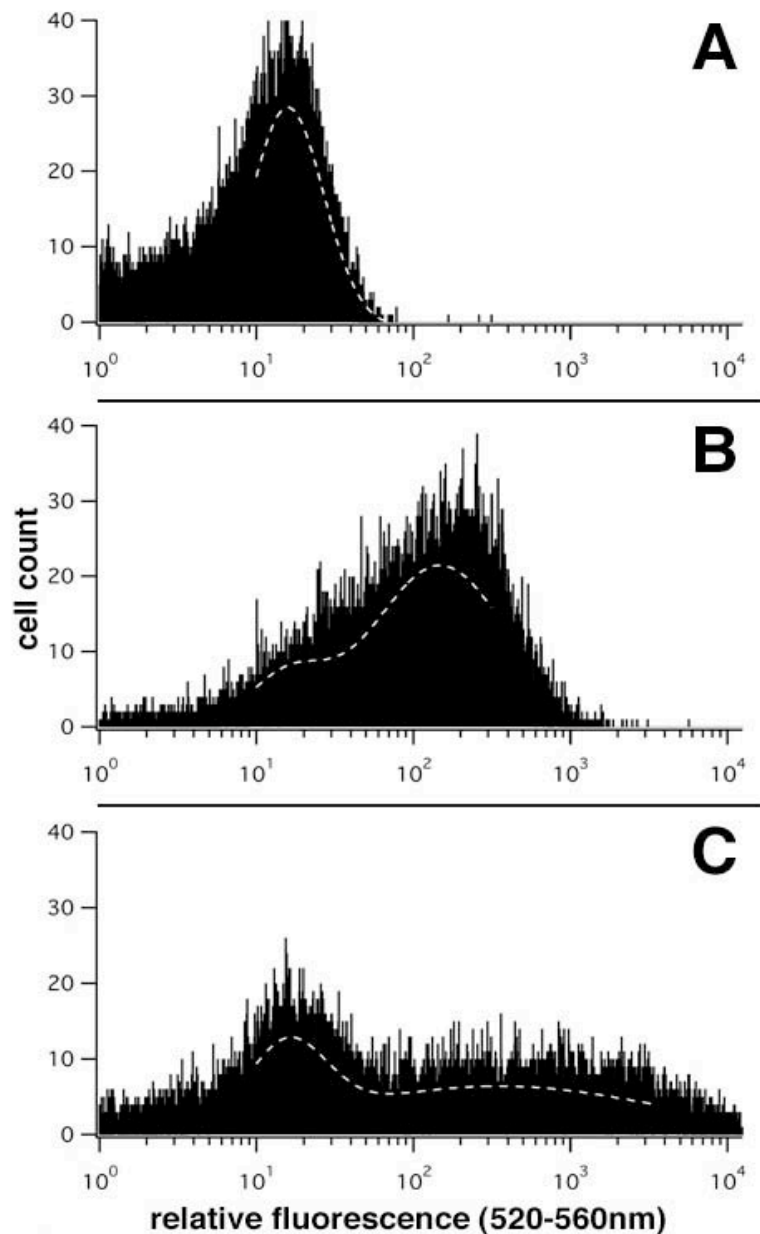


Figure II.2.2 Analysis by flow cytometry of the EGFP fluorescence on individual HEK293 cells, 20 hours after transfection. (A) non-transfected cells, (B) EGFP coding mRNA-transfected cells, and (C) cells transfected with pEGFP-N1 plasmid.

As depicted by the dotted lines, the contribution of non-transfected cells to the expression level histogram is relatively low in the mRNA transfection case ($15 \pm 3 \%$), contrarily to the plasmid DNA transfection ($30 \pm 15 \%$). Furthermore homogeneity in fluorescence levels was observed after transfection of mRNA coding for the EGFP, whereas plasmid DNA transfection exhibited extremely various expression levels.

Focusing on the mRNA transfection, we examined whether the average expression level was depending on the cell cycle by transfecting at different time points after cell splitting. 20 hours after transfection, the cells were lysed and the EGFP fluorescence was measured using a plate reader. The results are exposed in Figure II.2.3, showing a transfection efficiency almost unchanged three days after cell splitting.

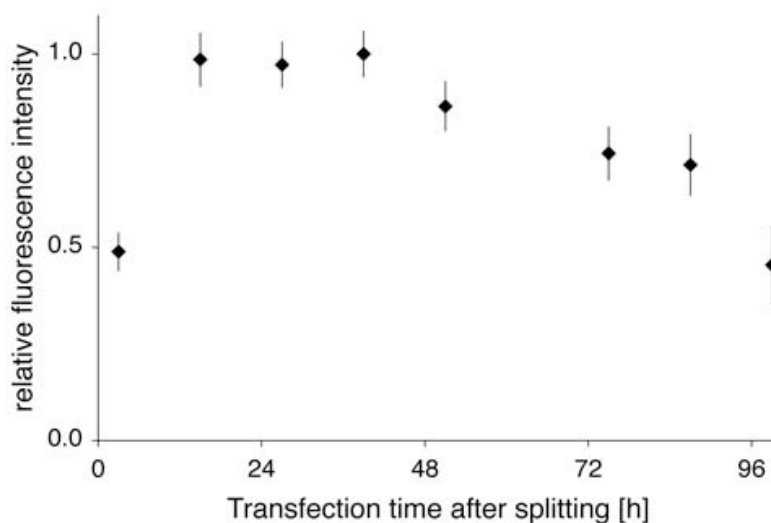


Figure II.2.3

EGFP fluorescence emitted 24 hours after mRNA transfection in HEK293 cells. The transfection was performed at different time points after splitting.

By co-transfecting HEK293 cells with EGFP mRNA and a random Cy5-labeled oligonucleotide at a ratio of 9:1, we investigated the cellular uptake kinetics of nucleic acids. At various times after transfection, the medium was exchanged to remove the lipofection reagent, allowing to monitor the uptake that took place during various incubation times. The cells were kept in the incubator for 20 hours after transfection, and lysed for fluorescence measurement (Figure II.2.4) using a plate reader. The uptake kinetics were similar for both Cy5 and EGFP, with a half-uptake time of about 45-50 minutes (see Table II.2.1). By measuring the Cy5 fluorescence remaining in the growth medium we estimated the uptake efficiency as $20 \pm 2 \%$ of the original nucleic acid content.

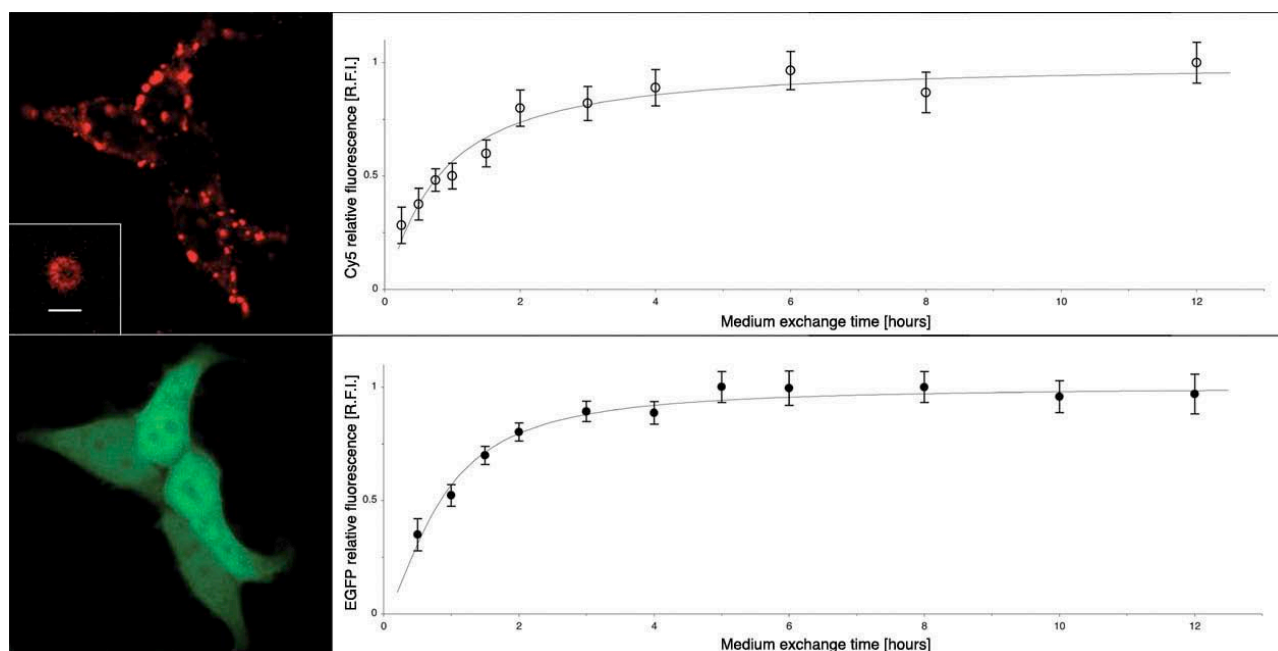


Figure II.2.4 Monitoring mRNA uptake by liposome-mediated transfection: a complex made of EGFP mRNA, Cy5-labeled synthetic oligonucleotides and DOTAP lipids was applied to HEK293 cells, and the uptake efficiency was estimated by changing the medium at several time points after transfection and measuring both Cy5 fluorescence and EGFP fluorescence 20 hours later. The Cy5 fluorescence reflects the oligonucleotide uptake kinetics (A), the EGFP fluorescence shows the non-degraded mRNA uptake kinetics (B). The confocal image shows typical fluorescence emerging from cells 20 hours after transfection for Cy5 (A) and for EGFP (B). The insert of the Cy5 image shows a typical vesicular form of the lipid-nucleic acid complex, imaged during in the first minutes after transfection (size bar = 2 μm).

Transfection kinetics	Rate	Half-time [hours]	Uptake percentage
Cy5 uptake	1.1 ± 0.1	0.79 ± 0.07	$20 \pm 2 \%$
EGFP expression	1.4 ± 0.2	0.84 ± 0.05	-

Table II.2.1

Study of cellular uptake kinetics by lipofection of a 9:1 mixture containing EGFP mRNA and a Cy5-labeled oligonucleotide on HEK293 cells. The curves are fitted to the Hill equation $f(\text{time})=1/[1+(\text{HalfTime}/\text{time})^{\text{rate}}]$. The uptake percentage is based on the Cy5 fluorescence measurement in the cells compared to the fluorescence in the growth medium after an incubation of 24 hours.

II.2.5 Discussion

The cell delivery of a messenger RNA encoding the enhanced green fluorescent protein (EGFP) resulted in a protein expression of remarkable homogeneity among individual cells, as measured by flow cytometry. Without any cell cycle synchronization we could achieve similar EGFP fluorescence intensities throughout cell populations. This demonstrates that cytoplasmic translation process is not cell cycle dependent, whereas the evident heterogeneity of fluorescence levels in non-synchronized DNA-transfected cells likely reflects differences in nuclear DNA uptake due to cell-to-cell variations in cell cycle stages. The transfection efficiency, meaning the number of transfected cells versus the total cell number, was also notably higher than in the case when the coding DNA had to enter the nucleus.

We measured the uptake kinetics of mRNA-lipid complexes by cotransfecting EGFP mRNA together with a Cy5-labeled oligonucleotide. The fluorescence of both Cy5 and expressed EGFP was quantified over time by incubating populations of cells with the lipid complexes for increasing periods of time. By fitting the obtained curve to a Hill equation, we obtained a half-time for uptake of about 45-50 minutes, at a slightly higher rate for EGFP mRNA than for the Cy5-labeled oligonucleotide. This can be explained by the fact that the EGFP mRNA is degrading over time, while the Cy5 label remains stable.

These results lead us to the conclusion that mRNA transfection is apparently independent of cell cycle processes and can lead to homogeneous protein expression in cell populations, ideal for cell-to-cell comparison on a large scale. Despite a relatively long uptake time, this technique allows for mRNA and siRNA transfection, partly relieved by a certain RNA stabilization in lipoplexes [14]. Unfortunately, the very short half-life of an acylated tRNA makes lipofection a non-perfectly suited technique for experiments such as incorporation of non-natural amino acids in proteins using misacylated suppressor tRNA, where microinjection would be more appropriate.

II.2.6 References

1. Ansorge, W. (1982) Improved system for capillary microinjection into living cells. *Exp Cell Res*, **140**, 31-37.
2. Ansorge, W. and Pepperkok, R. (1988) Performance of an automated system for capillary microinjection into living cells. *J Biochem Biophys Methods*, **16**, 283-292.
3. Batard, P., Jordan, M. and Wurm, F. (2001) Transfer of high copy number plasmid into mammalian cells by calcium phosphate transfection. *Gene*, **270**, 61-68.
4. Schenborn, E.T. and Goiffon, V. (2000) DEAE-dextran transfection of mammalian cultured cells. *Methods Mol Biol*, **130**, 147-153.
5. Lundstrom, K. (2003) Semliki Forest virus vectors for rapid and high-level expression of integral membrane proteins. *Biochim Biophys Acta*, **1610**, 90-96.
6. Weaver, J.C. (1993) Electroporation: a general phenomenon for manipulating cells and tissues. *J Cell Biochem*, **51**, 426-435.
7. Neumann, E., Kakorin, S. and Toensing, K. (1999) Fundamentals of electroporative delivery of drugs and genes. *Bioelectrochem Bioenerg*, **48**, 3-16.
8. Chesnoy, S. and Huang, L. (2000) Structure and function of lipid-DNA complexes for gene delivery. *Annu Rev Biophys Biomol Struct*, **29**, 27-47.
9. Schenborn, E.T. and Oler, J. (2000) Liposome-mediated transfection of mammalian cells. *Methods Mol Biol*, **130**, 155-164.
10. Templeton, N. (2002) Liposomal delivery of nucleic acids in vivo. *DNA Cell Biol*, **21**, 857-867.
11. Mortimer, I., Tam, P., MacLachlan, I., Graham, R.W., Saravolac, E.G. and Joshi, P.B. (1999) Cationic lipid-mediated transfection of cells in culture requires mitotic activity. *Gene Ther*, **6**, 403-411.
12. Grosjean, F., Batard, P., Jordan, M. and Wurm, F.M. (2002) S-phase synchronized CHO cells show elevated transfection efficiency and expression using CaPi. *Cytotechnology*, **38**, 57-62.
13. Haukenes, G., Szilvay, A.M., Brokstad, K.A., Kanestrom, A. and Kalland, K.H. (1997) Labeling of RNA transcripts of eukaryotic cells in culture with BrUTP using a liposome transfection reagent (DOTAP). *Biotechniques*, **22**, 308-312.
14. El Ouahabi, A., Pector, V., Fuks, R., Vandenbranden, M. and Ruyschaert, J.M. (1996) Double long-chain amidine liposome-mediated self replicating RNA transfection. *FEBS Lett*, **380**, 108-112.

Chapter II.3

Monitoring mis-acylated tRNA suppression efficiency in mammalian cells via EGFP fluorescence recovery

II.3 Monitoring mis-acylated tRNA suppression efficiency in mammalian cells via EGFP fluorescence recovery

II.3.1 Abstract

A reporter assay was developed to detect and quantify nonsense codon suppression by chemically aminoacylated tRNAs in mammalian cells. It is based on the cellular expression of the enhanced green fluorescent protein (EGFP) as a reporter for the site-specific amino acid incorporation in its sequence using an orthogonal suppressor tRNA derived from *E.coli*. Suppression of an engineered amber codon at position 64 in the EGFP run-off transcript could be achieved by the incorporation of a leucine via an *in vitro* aminoacylated suppressor tRNA. Microinjection of defined amounts of mutagenized EGFP mRNA and suppressor tRNA into individual cells allowed us to accurately determine suppression efficiencies by measuring the EGFP fluorescence intensity in individual cells using laser scanning confocal microscopy. Control experiments showed the absence of natural suppression or aminoacylation of the synthetic tRNA by endogenous aminoacyl-tRNA synthetases. This reporter assay opens the way for the optimization of essential experimental parameters for expanding the scope of the suppressor tRNA technology to different cell types.

The results of this chapter have been published in :

Ilegems, E., Pick, H.M. and Vogel, H. (2002) Monitoring mis-acylated tRNA suppression efficiency in mammalian cells via EGFP fluorescence recovery. *Nucleic Acids Res*, **30**, e128.

II.3.2 Introduction

The site-specific incorporation of unnatural amino acids into proteins in living cells is of importance to analyze *in vivo* protein structure and function as well as cellular processes using amino acid analogues comprising probes which are photo-activatable, fluorescent or chemically reactive [1-6]. This emerging technology relies on the suppression of nonsense codon mutations by chemically acylated tRNAs and has been originally developed as an *in vitro* method [7-12]. Meanwhile several reports for its *in vivo* application in *Xenopus oocytes* [4-6,13,14], *Escherichia coli* [15-18] and COS1 cells [19] appeared in literature. An expansion of this technology to other cell lines would demand a reporter system permitting the definition of optimal parameters for the site-specific incorporation of amino acid analogues into proteins.

Here, suppressor tRNA technology was applied to Chinese hamster ovary (CHO) cells which, like other mammalian cell types, are generally more suitable for structural and functional studies of human derived proteins if specific post-translational modifications are important. In addition, certain proteins such as neuro-receptors are optimally expressed only in particular cell lines. We focused on the enhanced green fluorescent protein (EGFP) as a reporter to assess the efficiency of nonsense codon suppression directly in living cells. An amber stop codon mutation was site-specifically introduced in the core position of the EGFP, removing an amino acid essential for the formation of the fluorophore. The transfer of that mutagenized *in vitro* transcript into CHO cells was followed by the expression of an incomplete, non-fluorescent protein. After co-transfer with a cognate synthetic suppressor tRNA, we could monitor the successful re-incorporation of the missing amino acid by recovery of the EGFP fluorescence signal, which could be quantified by using laser scanning confocal microscopy on living cells.

Unlike other fluorescent reporters such as luciferase or β -galactosidase, EGFP does not require the addition of substrate or cofactors nor cell lysis or fixation. Furthermore, it is stable over a period of several days and, due to its strong fluorescence allows an accurate and sensitive determination of suppression efficiencies in individual cells. This strategy could be used to find proper conditions for an efficient suppression in a number of different mammalian cell lines.

II.3.3 Experimental procedures

Materials

Synthetic oligonucleotides were purchased from MWG-Biotech AG (Ebersberg, Germany). Kits for plasmid and DNA-fragment purification were obtained from QIAGEN GmbH (Hilden, Germany). Restriction endonucleases (*Bsa*I, *Eco*RI and *Not*I) were provided by New England Biolabs (Massachusetts, USA). The MEGAscript kit for *in vitro* transcription and the cap analog m⁷G(5')ppp(5')G were from Ambion (Texas, USA). Purified rEGFP was purchased from Clontech (California, USA). Octadecyl rhodamine B (R18) and Alexa Fluor 546 C₅ maleimide were obtained from Molecular Probes (Oregon, USA). Other chemicals were purchased from Sigma-Aldrich (Missouri, USA).

Transcription of reporter gene

The coding sequence of the enhanced green fluorescent protein (pEGFP-N1, Clontech) was modified by the addition of a T7 promoter site and a poly(A) tail using PCR amplification with synthetic oligonucleotides (Figure II.3.1). The resulting 814 bp fragment was ligated into the pCR2.1 vector using the TA cloning kit (Invitrogen, California, USA) to obtain the plasmid pT7PEGFP.

The pT7PEGFPam64L is a mutated version of the pT7PEGFP plasmid. The CTG codon at position 64 of the EGFP coding sequence was mutated to a nonsense amber (TAG) codon by site-directed mutagenesis using the Quickchange kit (Stratagene, California, USA). All plasmid constructs were controlled by restriction mapping and DNA sequencing.

After linearization of the wild type and mutated plasmids by *Not*I, *in vitro* transcription was performed with T7 RNA polymerase using the MEGAscript kit (Ambion, Texas, USA). Capping of mRNA was achieved during transcription by replacing 80 % of the GTP level with the cap analog m⁷G(5')ppp(5')G (Ambion). After removing the DNA template by *DNase*I treatment, the resulting mRNAs were purified by successive phenol:chloroform:isoamyl alcohol (25:24:1) and chloroform:isoamyl alcohol (24:1) extractions, precipitation with an equal volume of isopropanol for 1 hour at -20 °C, followed by centrifugation at 0 °C / 20'800 g for 15 minutes. The mRNA pellet was dried and redissolved in sterile H₂O treated with diethyl pyrocarbonate (DEPC). The integrity and size of the mRNAs were assayed by agarose gel electrophoresis under denaturing conditions, and the concentration was determined by measuring the optical density at 260 nm.

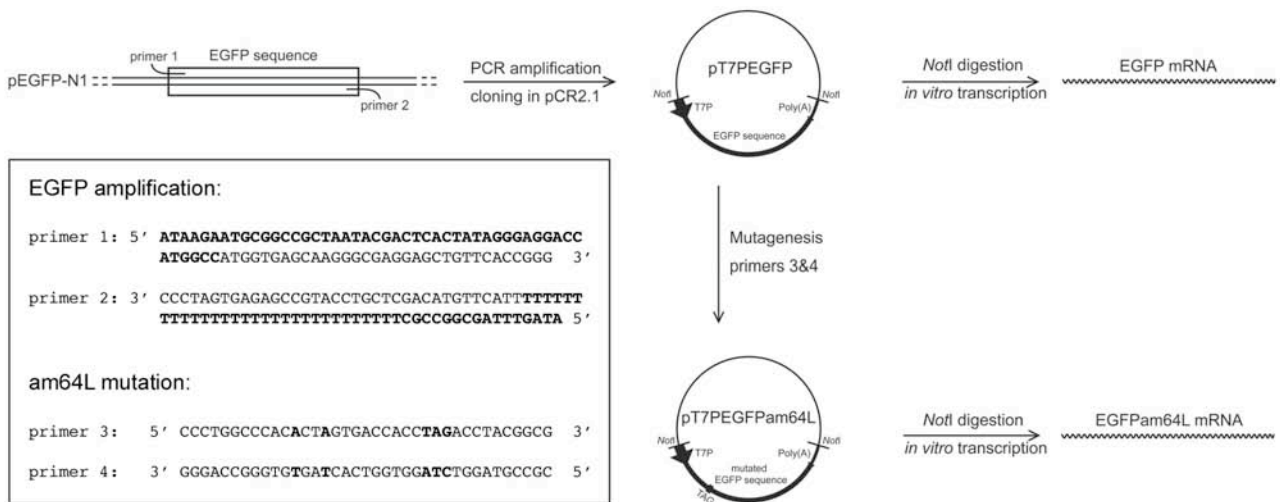


Figure II.3.1 Scheme of the cloning steps for the wild type (pT7PEGFP) and mutant EGFP (pT7PEGFPam64L) encoding plasmids used for the *in vitro* transcription. PCR amplification with primers 1 and 2 was performed to add a T7 promoter to the 5' end and a poly(A) tail to the 3' end of the EGFP coding sequence. Primers 3 and 4 were used for replacing the leucine 64 codon by TAG, and providing silent mutations for clonal selection. All nucleotide sequence modifications are shown in bold letters.

Transcription of suppressor tRNA gene

A 105bp synthetic template fragment encoding the *E.coli* suppressor tRNA^{Ala}_{CUA} was prepared by reannealing and ligating two synthetic oligonucleotides containing the tRNA gene flanked by a T7 promoter (Figure II.3.2). This blunt-end DNA fragment was cloned into the pCR4 vector using the TOPO cloning Kit (Invitrogen), following the instructions of the manufacturer. The resulting plasmid pEcoliAlaCUA was checked by restriction mapping and sequencing.

Plasmid pEcoliAlaCUA was linearized by successive restriction endonuclease digests with *EcoRI* and *BsaI*. After agarose gel purification this DNA fragment was used for the run-off transcription with T7 RNA polymerase following the protocol of the MegaScript Kit (Ambion). After removing the template DNA by *DNaseI* treatment the tRNA was purified by following the protocol described above for mRNA. The integrity and purity of the tRNA was assayed by polyacrylamide gel electrophoresis, and the concentration was determined by measuring the optical density at 260 nm.

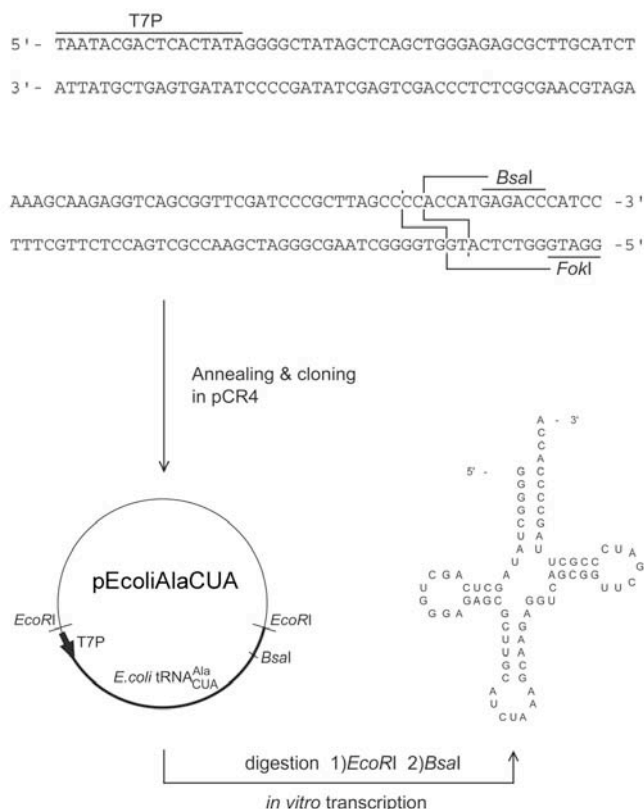


Figure II.3.2 Scheme for the *in vitro* synthesis of the suppressor tRNA from a synthetic DNA template by T7 run-off transcription. Two synthetic complementary oligonucleotides encoding the *E. coli* derived suppressor tRNA^{Ala}_{CUA} were annealed and cloned into the pCR4 vector, leading to pEcoliAlaCUA. T7 RNA polymerase run-off transcription was performed on the purified *EcoRI* and *BsaI* fragment giving rise to a 76-mer suppressor tRNA.

Deprotection of N-(4-Pentenoyl)-S-leucyl-tRNA

Pentenoyl-protected aminoacylated tRNA^{Ala}_{CUA} was customly synthesized at Cruachem Ltd (Glasgow, Scotland). 10 µg of lyophilized protected tRNA were resuspended in 10 µl H₂O. Deprotection was accomplished by adding 2.5 µl of 25 mM I₂ in 1:1 THF-H₂O and incubating the mixture for 10 min at 25 °C. The leucyl-tRNA was precipitated by successive additions of 1.25 µl of 3 M NaOAc pH 5.3 and 31.25 µl of cold ethanol. After centrifugation at 0 °C / 20'800 g for 15 minutes the pellet was washed once with 70 % cold ethanol, dried and dissolved in H₂O to a final concentration of 4 µg/µl.

Cell lines and cell culture

Adherent mammalian cells (Chinese hamster ovary, CHO) were grown in DMEM/F12 (Dulbecco's modified Eagle medium; GIBCO BRL, Rockville, USA). The medium was supplemented with 2.2 % fetal calf serum (GIBCO BRL). The cultures were split, distributed in 35 mm Nunc dishes at a density of 50'000 cells/ml 1 day prior to injection, and kept at 37 °C in a humidified atmosphere with 5 % CO₂.

Injections

Microinjections of CHO cells with mRNA and tRNA mixtures diluted in sterile DEPC-treated H₂O were performed using an InjectMan controller and a Transjector 5246 system (both from Eppendorf, Hamburg, Germany) mounted on an Axiovert S100TV inverted microscope (Carl Zeiss AG, Oberkochen, Germany). FemtotipsII capillaries (Eppendorf) were used for all injections.

Laser scanning confocal microscopy

Laser scanning confocal microscopy was performed using a Zeiss LSM510 (Carl Zeiss AG). Detection and distinction of the fluorescence signals of EGFP (excitation 488 nm / emission 505-530 nm), Alexa546 and R18 (excitation 543 nm / emission > 560 nm) was achieved by appropriate filter sets using a multitracking mode. Scanning speed and laser intensity were adjusted to avoid photobleaching of the fluorophores.

II.3.4 Results

The general scheme used for *in vivo* visualization of mis-acylated tRNA suppression is presented in Figure II.3.3A. The suppression efficiency was determined by measuring the appearance of EGFP fluorescence in living cells. The EGFP coding sequence was mutated at position 64 by replacing the CTG (leucine) codon with an amber stop codon in the core of the reporter gene, giving rise to the EGFPam64L *in vitro* transcript. A successful suppression by co-injection of this mutated mRNA with a suppressor tRNA carrying the “removed” amino acid would lead to the completion of the EGFP translation. Twenty hours after co-injection of suppressor leucyl-tRNA with EGFPam64L mRNA, we observed the recovery of the EGFP fluorescence in CHO cells by laser scanning confocal microscopy (see Figure II.3.3B), whereas the co-injection of the mutated mRNA together with the non-aminoacylated tRNA did not lead to any detectable fluorescence within the cells (data not shown).

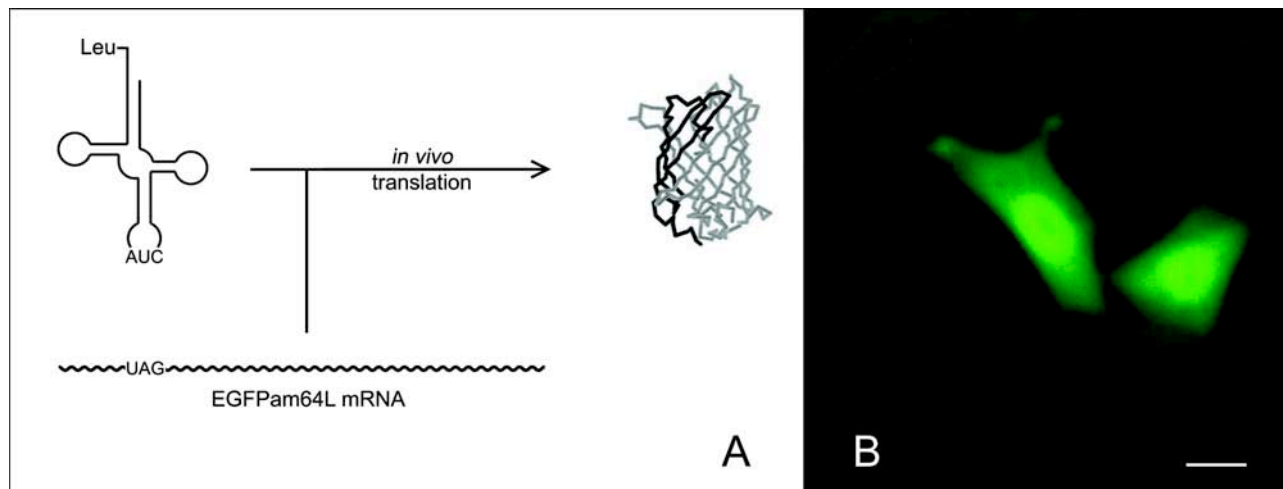


Figure II.3.3 *In vivo* suppression visualized by EGFP fluorescence recovery:

(A) Schematic view of the assay for the amber suppressor tRNA function: co-injection of a mutated EGFP mRNA containing an amber codon at position 64 with an amber suppressor leucyl-tRNA. A successful suppression leads to complete translation of the mRNA transcript thus to the appearance of the EGFP molecule.

(B) Laser scanning confocal micrograph of CHO cells visualizing EGFP fluorescence 20 hours after co-injection of the mutated EGFP-mRNA with the amber suppressor tRNA. Size bar is 10 μm .

Because the injected volume may slightly vary between cells, mostly depending on their intrinsic viscosity, it was necessary to quantify this parameter in order to validate further comparisons between different experiments. Therefore, the injections of mRNA and tRNA were performed together with a known concentration of Alexa546. This dye is non-toxic for the cell and its excitation and emission wavelengths are well distinguishable from those of EGFP.

Correlation between the fluorescence of the co-loaded dye and the injected volume was obtained by measuring its dilution in the cell and by calculating individual cell volumes. We first elaborated a fluorescence intensity calibration curve by measurements on droplets containing known concentrations of the Alexa546 dye using laser scanning confocal microscopy. A linear relation between fluorescence intensity versus dye concentration was found. Fluorescence intensity measurements of the co-injected Alexa546 dye on living cells permitted the determination of the dye concentration within the cells on the basis of this calibration curve.

The injection volume of the Alexa dye together with mRNA and tRNA mixtures can then be determined by calculating the cell volume. We therefore detached the adherent cells by addition of 1 mM EDTA and incubation at 37 °C for 10 minutes. Under these conditions the cells became spherical. They were then membrane-stained with R18 (5 μ M / 10 minutes incubation at 37 °C) to measure their diameter by laser scanning confocal microscopy, leading to a volume of 1.2 ± 0.1 pl. The number of EGFP molecules which were expressed during *in vivo* translation in individual cells can be estimated by comparison of cell-derived EGFP fluorescence intensities with EGFP fluorescence intensities measured on droplets of known concentrations of purified rEGFP (Figure II.3.4).

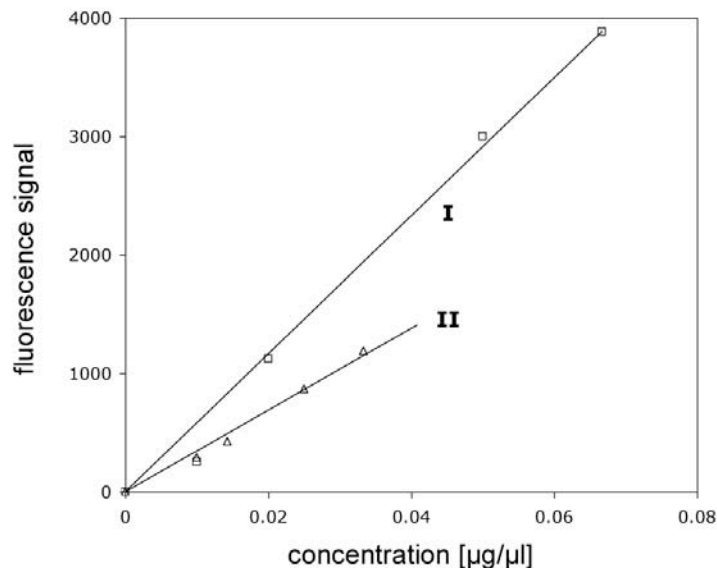


Figure II.3.4 Confocal calibration curve established by measurement of signal intensities emerging from droplets containing known concentrations of rEGFP (I) and Alexa546 (II).

To validate the precision of our injections and concentration calibrations, we also co-injected variable volumes of a solution containing 500 ng/ μl rEGFP and 250 ng/ μl Alexa546 in CHO cells. As seen in Figure II.3.5, there is a linear correlation between injected volume, given by the Alexa546 fluorescence signal, and the number of EGFP molecules per cell.

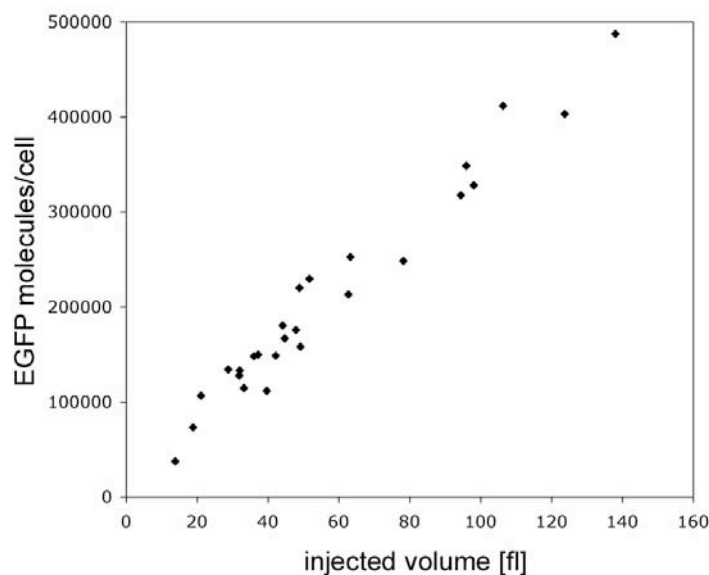


Figure II.3.5 Correlation between injection volume and number of EGFP molecules per cell by microinjection of variable volumes of a solution containing 500 ng/ μl rEGFP and 250 ng/ μl Alexa546 in CHO cells. The injected volume is calculated on the basis of the known cell volume (see text for detailed description) and the final concentration of Alexa546 dye measured directly in the cell (based the calibration curve in Figure II.3.5).

On the basis of the presented control experiments we performed all following measurements using concentrations of 250 ng/ μ l Alexa546, 2 μ g/ μ l mRNA, and 2 μ g/ μ l leucyl-tRNA^{Ala}_{CUA}. These concentrations gave best suppression efficiencies, (i) permitting the highest number of RNA molecules delivery without capillary blocking due to the resulting high solution viscosity, and (ii) favoring the suppression against competing endogenous termination factors at an excess of 10:1 of tRNA:mRNA molecules.

The EGFP fluorescence resulting from *in vivo* suppression was stable between 12 and 24 hours post-injection. The injected cells were easily identified under the microscope via fluorescence of the co-injected dye. Thereby we could confirm that every injected cell turned green and could be re-identified even after 24 h incubation at 37 °C. Using the EGFP and Alexa546 fluorescence intensity calibration curves, we calculated the number of translated EGFP molecules by confocal microscopy 20 hours after microinjection. Because the variation between injection volumes was 0.05 ± 0.01 pl, we corrected the number of translated EGFP molecules by extrapolation to an average injection volume of 0.05 pl (Table II.3.1). We obtained suppression efficiencies of 15 ± 3 % by comparing EGFP fluorescence signals resulting from *in vivo* suppression with fluorescence signals derived from the injection of the identical amounts of non-mutated EGFP mRNA.

0.05pl injection	mRNA x10 ³ molecules/cell	tRNA x10 ³ molecules/cell	EGFP x10 ³ molecules/cell
EGFPam64L mRNA + tRNA _{CUA}	250 \pm 20	2500 \pm 200	ND
EGFPam64L mRNA + leucyl-tRNA _{CUA}	250 \pm 20	2500 \pm 200	270 \pm 30
EGFP mRNA	250 \pm 20	-	1800 \pm 200

Table II.3.1 Number of mRNA and tRNA molecules per cell directly calculated after microinjection by comparison of the co-injected Alexa dye with the confocal calibration curve on droplets. Expression of EGFP molecules per cell determined on 50 individual cells, 20 hours after injection of RNA. The values are corrected for a standard injection volume of 0.05 pl. Co-injections were all processed using concentrations of 2 μ g/ μ l mRNA, 2 μ g/ μ l tRNA and 250 ng/ μ l Alexa546. ND = not detectable.

II.3.5 Discussion

A novel assay has been developed using EGFP as a reporter for direct quantification of termination codon suppression efficiencies in living mammalian cells. We have shown by fluorescence recovery that an aminoacylated tRNA derived from *E.coli* can suppress an amber mutation at codon 64 of the EGFP mRNA by *in vivo* translation in CHO cells, whereas the non-aminoacylated form of the same tRNA cannot. EGFP fluorescence intensities measured in individual cells by laser-scanning confocal microscopy allowed us to quantify suppression efficiencies. Kohrer *et al.* [19] have used a different approach to insert amino acid analogues into the chloramphenicol acetyltransferase (CAT) by importing a suppressor Tyr-tRNA in COS1 cells using lipofection. These authors measured CAT activities in cell extracts to determine average levels of termination codon suppression efficiencies in cell samples, but not in individual cells.

The use of EGFP as a suppression reporter offers advantages compared to other detection techniques such as those based on luciferase, β -galactosidase or CAT. In contrast to these destructive methods, EGFP suppression can be followed *in vivo* in a single cell without further chemical or enzymatic treatment, due to the sufficiently high quantum yield of this protein.

To improve the suppression-specific fluorescent signal, we increased the signal-to-noise ratio by lowering the background signal resulting from possible natural suppressor tRNAs. This was fulfilled by choosing an amino acid in the protein sequence which plays an important role for the fluorescence properties of the EGFP. As a consequence, a cell line which comprises a natural suppressor tRNA aminoacylated with a different amino acid would provide a background signal reduced to an undetectable value. We selected the leucine at position 64 for its importance in the fluorescence properties of the EGFP, particularly because it highly improves correct protein folding [20,21]. Furthermore, due to the fact that it is neither a charged nor a polar amino acid, it is more quickly accepted and processed by the ribosome, thus better competes with the undesirable effect of termination factors which could prevent the completion of the full-length protein [22-26].

To determine the contribution of unnatural suppression under investigation, the suppressor tRNA should also not be recognized by any endogeneous aminoacyl-tRNA synthetases. This natural aminoacylation of the suppressor tRNA can be minimized by choosing a tRNA from another organism. In our present study, the tRNA sequence was based on that of *E.coli* tRNA^{Ala}_{GGC} [27] mutated to CUA at the anticodon site and modified by two other mutations: A38U improves amber suppression efficiency [28-30], and C70U, renders the non-aminoacylated tRNA a poor substrate for *E.coli* alanyl-tRNA synthetase [31]. This tRNA sequence has been shown by Karginov *et al.* [9] to have good suppression properties in *in vitro* translation systems.

Our experiments to determine suppression efficiencies by measuring EGFP fluorescence intensities in cells and to estimate amounts of injected mRNA and tRNA molecules were based on laser scanning confocal microscopy measurements. Microinjection of defined amounts of fluorescent dyes in CHO cells demonstrated the suitability of this transfection technique to incorporate in a controlled way quantifiable molecule amounts, in contrast to saponin permeabilization [32], electroporation [33] or lipofection [19] of mammalian cells. Furthermore, unlike these other techniques, control of the transfected amount does not depend on cell type or density, admitting a more accurate comparison between different cell types. Finally, microinjection requires only low amounts of material, and prevents the RNA degradation that can take place during delivery in other transfection techniques.

We were able to observe amber suppression of an amber mutated EGFP mRNA using mis-acylated tRNA in CHO cells, obtaining 15 ± 3 % of the fluorescence signal obtained by injection of the same amount of non-mutated EGFP mRNA. After estimation of the RNA molecules and EGFP protein numbers, we obtained approximately one suppressed translation by mRNA (see Table II.3.1). Referring to a typical injection volume in CHO cells of 0.05 pl, the number of proteins resulting from unnatural suppression was in the range of $270'000 \pm 30'000$.

The general applicability of the presented EGFP-based reporter assay will allow us to extend the suppressor tRNA technique for many other cell types, and hence permit the selection of suitable suppressor tRNAs for the site-directed modification of proteins.

In particular interest for applying suppressor tRNA technology are investigations of selective molecular interactions in live biological cells by fluorescence techniques with high time, spatial and single molecule resolution to elucidate the complex cellular biochemical networks [34,35].

II.3.6 References

1. Gallivan, J.P., Lester, H.A. and Dougherty, D.A. (1997) Site-specific incorporation of biotinylated amino acids to identify surface-exposed residues in integral membrane proteins. *Chem Biol*, **4**, 739-749.
2. Mamaev, S.V., Laikhter, A.L., Arslan, T. and Hecht, S.M. (1996) Firefly Luciferase: Alteration of the Color of Emitted Light Resulting from Substitutions at Position 286. *J Am Chem Soc*, **118**, 7243-7244.
3. Mendel, D., Cornish, V.W. and Schultz, P.G. (1995) Site-directed mutagenesis with an expanded genetic code. *Annu Rev Biophys Biomol Struct*, **24**, 435-462.
4. Turcatti, G., Nemeth, K., Edgerton, M.D., Meseth, U., Talabot, F., Peitsch, M., Knowles, J., Vogel, H. and Chollet, A. (1996) Probing the structure and function of the tachykinin neurokinin-2 receptor through biosynthetic incorporation of fluorescent amino acids at specific sites. *J Biol Chem*, **271**, 19991-19998.
5. Cohen, B.E., McAnaney, T.B., Park, E.S., Jan, Y.N., Boxer, S.G. and Jan, L.Y. (2002) Probing protein electrostatics with a synthetic fluorescent amino acid. *Science*, **296**, 1700-1703.
6. Beene, D.L., Brandt, G.S., Zhong, W., Zacharias, N.M., Lester, H.A. and Dougherty, D.A. (2002) Cation- π Interactions in Ligand Recognition by Serotonergic (5-HT(3A)) and Nicotinic Acetylcholine Receptors: The Anomalous Binding Properties of Nicotine. *Biochemistry*, **41**, 10262-10269.
7. Cload, S.T., Liu, D.R., Froland, W.A. and Schultz, P.G. (1996) Development of improved tRNAs for in vitro biosynthesis of proteins containing unnatural amino acids. *Chem Biol*, **3**, 1033-1038.
8. Noren, C.J., Anthony-Cahill, S.J., Suich, D.J., Noren, K.A., Griffith, M.C. and Schultz, P.G. (1990) In vitro suppression of an amber mutation by a chemically aminoacylated transfer RNA prepared by runoff transcription. *Nucleic Acids Res*, **18**, 83-88.
9. Karginov, V.A., Mamaev, S.V. and Hecht, S.M. (1997) In vitro suppression as a tool for the investigation of translation initiation. *Nucleic Acids Res*, **25**, 3912-3916.
10. Kurzchalia, T.V., Wiedmann, M., Breter, H., Zimmermann, W., Bauschke, E. and Rapoport, T.A. (1988) tRNA-mediated labelling of proteins with biotin. A nonradioactive method for the detection of cell-free translation products. *Eur J Biochem*, **172**, 663-668.

11. Hohsaka, T., Kajihara, D., Ashizuka, Y., Murakami, H. and Sisido, M. (1998) Efficient Incorporation of Nonnatural Amino Acids with Large Aromatic Groups into Streptavidin in In Vitro Protein Synthesizing Systems. *J Am Chem Soc*, **121**, 34-40.
12. Short, G.F., 3rd, Golovine, S.Y. and Hecht, S.M. (1999) Effects of release factor 1 on in vitro protein translation and the elaboration of proteins containing unnatural amino acids. *Biochemistry*, **38**, 8808-8819.
13. Turcatti, G., Nemeth, K., Edgerton, M.D., Knowles, J., Vogel, H. and Chollet, A. (1997) Fluorescent labeling of NK2 receptor at specific sites in vivo and fluorescence energy transfer analysis of NK2 ligand-receptor complexes. *Receptors Channels*, **5**, 201-207.
14. Chollet, A., Turcatti, G., Nemeth, K. and Vogel, H. (1998) In Slavik, J. (ed.), *Fluorescence Microscopy and Fluorescent Probes*. Plenum Press, New York, Vol. 2, pp. 87-92.
15. Liu, D.R. and Schultz, P.G. (1999) Progress toward the evolution of an organism with an expanded genetic code. *Proc Natl Acad Sci U S A*, **96**, 4780-4785.
16. Wang, L., Brock, A., Herberich, B. and Schultz, P.G. (2001) Expanding the genetic code of Escherichia coli. *Science*, **292**, 498-500.
17. Wang, L., Brock, A. and Schultz, P.G. (2002) Adding L-3-(2-Naphthyl)alanine to the genetic code of E. coli. *J Am Chem Soc*, **124**, 1836-1837.
18. Liu, D.R., Magliery, T.J., Pastnak, M. and Schultz, P.G. (1997) Engineering a tRNA and aminoacyl-tRNA synthetase for the site-specific incorporation of unnatural amino acids into proteins in vivo. *Proc Natl Acad Sci U S A*, **94**, 10092-10097.
19. Kohrer, C., Xie, L., Kellerer, S., Varshney, U. and RajBhandary, U.L. (2001) Import of amber and ochre suppressor tRNAs into mammalian cells: a general approach to site-specific insertion of amino acid analogues into proteins. *Proc Natl Acad Sci U S A*, **98**, 14310-14315.
20. Cormack, B.P., Valdivia, R.H. and Falkow, S. (1996) FACS-optimized mutants of the green fluorescent protein (GFP). *Gene*, **173**(1), 33-38.
21. Palm, G.J., Zdanov, A., Gaitanaris, G.A., Stauber, R., Pavlakis, G.N. and Wlodawer, A. (1997) The structural basis for spectral variations in green fluorescent protein. *Nat Struct Biol*, **4**, 361-365.
22. Drugeon, G., Jean-Jean, O., Frolova, L., Le Goff, X., Philippe, M., Kisselev, L. and Haenni, A.L. (1997) Eukaryotic release factor 1 (eRF1) abolishes readthrough and competes with suppressor tRNAs at all three termination codons in messenger RNA. *Nucleic Acids Res*, **25**, 2254-2258.

23. Le Goff, X., Philippe, M. and Jean-Jean, O. (1997) Overexpression of human release factor 1 alone has an antisuppressor effect in human cells. *Mol Cell Biol*, **17**, 3164-3172.
24. Cornish, V.W., Mendel, D. and Schultz, P.G. (1995) Probing Protein Structure and Function with an Expanded Genetic Code. *Angewandte Chemie-International Edition in English*, **34**, 621-633.
25. Karginov, V.A., Mamaev, S.V., An, H., Van Cleve, M., Hecht, S.M., Komatsoulis, G. and Abelson, J. (1997) Probing the Role of an Active Site Aspartic Acid in Dihydrofolate Reductase. *J Am Chem Soc*, **119**, 8166-8176.
26. Cornish, V.W., Benson, D.R., Altenbach, C.A., Hideg, K., Hubbell, W.L. and Schultz, P.G. (1994) Site-specific incorporation of biophysical probes into proteins. *Proc Natl Acad Sci U S A*, **91**, 2910.
27. Mims, B.H., Prather, N.E. and Murgola, E.J. (1985) Isolation and nucleotide sequence analysis of tRNA^{Ala}GGC from *Escherichia coli* K-12. *J Bacteriol*, **162**, 837-839.
28. Raftery, L.A. and Yarus, M. (1987) Systematic alterations in the anticodon arm make tRNA(Glu)-Suoc a more efficient suppressor. *Embo J*, **6**, 1499-1506.
29. Bruce, A.G., Atkins, J.F., Wills, N., Uhlenbeck, O. and Gesteland, R.F. (1982) Replacement of anticodon loop nucleotides to produce functional tRNAs: amber suppressors derived from yeast tRNA^{Phe}. *Proc Natl Acad Sci U S A*, **79**, 7127-7131.
30. Kleina, L.G., Masson, J.M., Normanly, J., Abelson, J. and Miller, J.H. (1990) Construction of *Escherichia coli* amber suppressor tRNA genes. II. Synthesis of additional tRNA genes and improvement of suppressor efficiency. *J Mol Biol*, **213**, 705-717.
31. Hou, Y.M. and Schimmel, P. (1988) A simple structural feature is a major determinant of the identity of a transfer RNA. *Nature*, **333**, 140-145.
32. Negrutskii, B.S., Stapulionis, R. and Deutscher, M.P. (1994) Supramolecular organization of the mammalian translation system. *Proc Natl Acad Sci U S A*, **91**, 964-968.
33. Negrutskii, B.S. and Deutscher, M.P. (1991) Channeling of aminoacyl-tRNA for protein synthesis in vivo. *Proc Natl Acad Sci U S A*, **88**, 4991-4995.
34. Remy, I. and Michnick, S.W. (2001) Visualization of biochemical networks in living cells. *Proc Natl Acad Sci U S A*, **98**, 7678-7683.
35. Luker, G.D., Sharma, V., Pica, C.M., Dahlheimer, J.L., Li, W., Ochesky, J., Ryan, C.E., Piwnica-Worms, H. and Piwnica-Worms, D. (2002) Noninvasive imaging of protein-protein interactions in living animals. *Proc Natl Acad Sci U S A*, **99**, 6961-6966.

Chapter II.4

Quantification of natural nonsense codon suppression in mammalian cells using an EGFP reporter assay

II.4 Quantification of natural nonsense codon suppression in mammalian cells using an EGFP reporter assay

II.4.1 Abstract

A general method for the background detection and quantification of natural nonsense codon suppression in mammalian cell cultures was developed. It is based on the cellular expression of the enhanced green fluorescent protein (EGFP) as a reporter carrying engineered termination codons in the *in vitro* run-off transcript. Delivery of mutagenized EGFP mRNA into adherently growing cells was achieved by cationic DOTAP liposomes. EGFP fluorescence recovery allowed us to detect cell type specific differences in natural nonsense codon suppression efficiencies and quantitative data on cell populations were obtained by fluorescence measurements on cell lysates. This fluorescence-based reporter assay allows for the screening of cell types exhibiting low levels of natural nonsense codon suppression suitable for the suppressor tRNA technology as an emerging tool for *in vivo* protein engineering.

II.4.2 Introduction

Genetically engineered termination codons which interrupt a messenger RNA can be targeted by chemically acylated nonsense suppressor tRNAs to direct nonnatural amino acid residues to specified locations in a protein. This emerging technology is currently expanding into mammalian live cell applications [1-4] (see chapter II.3).

The development of this suppressor technology in various mammalian cell cultures requires cell type specific optimizations. Indeed, the choice of an optimal termination codon in a specific cellular background has to be considered, since natural nonsense-codon readthrough [5-9] is a well-described phenomenon, which potentially competes with the desired unnatural suppression event.

Most of the natural suppression in higher eukaryotic cells seems to involve misreading of termination codons by normal cytoplasmic aminoacyl-tRNAs by unusual or wobble base pairing [10], but part of it is also due to natural suppressor tRNAs complementary to one of the three stop codons carrying a common amino acid [11-15] or a selenocysteine [16-18]. These different types of natural suppression could also be more specific to one or the other of the three existing stop codons and its occurrence unequal among the studied organisms, because of a non-homogeneous stop codon usage in mammalian cells [19].

Depending on the investigated cell type, it has furthermore been shown that these unique interactions between codons and anticodons in ribosomes could also be affected by the structure of mRNAs surrounding the nonsense-codon [20-22]. As a matter of fact, these “neighboring” effects tend to be demonstrated by the natural non-randomness in the codon context in mRNAs [23], and as an example Phillips-Jones et al. have shown evidence that the codon context effect on UAG suppressor tRNA is different in *Escherichia coli* and human cells [24].

We propose here a reporter system based on mutants of the enhanced green fluorescent protein to assess the efficiency of nonsense codon suppression, in order to define optimal parameters for future site-specific incorporation of amino acid analogs into proteins in a number of different mammalian cell lines. The read-through of specifically engineered stop codons in mRNA leads to the completion of the EGFP translation, which fluorescence is quantified using a convenient plate reader. By measuring the protein function rather than its size by protein gel electrophoresis we enumerate only integer proteins completed by natural suppression, and not the random proteins translated after a frameshift at the stop codon position. As an example we study the suitability of the amber, ochre and opal stop codons to mis-acylated suppressor tRNA technique in the three cell lines CHO, HEK293 and N1E-115. In principle, this natural suppression reporter assay could be extended to other adherent mammalian cell lines, and specific codon contexts could be investigated.

II.4.3 Experimental procedures

Materials

Synthetic oligonucleotides were purchased from MWG-Biotech AG (Ebersberg, Germany). Kits for plasmid and DNA-fragment purification were obtained from QIAGEN GmbH (Hilden, Germany). Restriction endonucleases (*Bsa*I, *Eco*RI and *Not*I) were provided by New England Biolabs (Massachusetts, USA). Chemicals were purchased from Sigma-Aldrich (Missouri, USA). The MEGAscript kit for *in vitro* transcription and the cap analog m⁷G(5')ppp(5')G were from Ambion (Texas, USA). Purified rEGFP was purchased from Clontech (California, USA).

Transcription of EGFP reporter genes

The reporter genes are based on the vector pT7PEGFP, as described in Chapter II.3. This vector contains the coding sequence of the EGFP preceded by a T7 promoter for *in vitro* transcription purposes and ended by a poly(A) tail. The mutated versions comprising nonsense codons after the Kozak sequence were constructed by site-directed mutagenesis (Quickchange kit, Stratagene, California, USA) as schemed in Figure II.4.1. The resulting vectors pT7PamEGFP, pT7PocEGFP and pT7PopEGFP carry respectively the amber, ochre and opal non-sense codons. All plasmid constructs were controlled by restriction mapping and DNA sequencing.



Figure II.4.1 The synthesis of the mutated EGFP mRNAs was based on the vector pT7PEGFP, containing the EGFP sequence preceded by a T7 promoter and followed by a poly(A) tail. Amber, ochre and opal codons were inserted by site-directed mutagenesis right after the Kozak sequence to give rise to the plasmids pT7PamEGFP, pT7PocEGFP and pT7PopEGFP, respectively. After digestion of these vectors with the restriction enzyme *Not*I, purification of the template containing the EGFP sequence, and *in vitro* transcription based on a T7 RNA polymerase, we obtained the mRNAs amEGFP, ocEGFP and opEGFP.

After linearization of the wild type and mutated plasmids by *NotI*, *in vitro* transcription was performed with T7 RNA polymerase using the MEGAscript kit (Ambion, Texas, USA). Capping of mRNA was achieved during transcription by replacing 80 % of the GTP level with the cap analog m⁷G(5')ppp(5')G (Ambion). After removing the DNA template by *DNaseI* treatment, the resulting mRNAs were purified by successive phenol:chloroform:isoamyl alcohol (25:24:1) and chloroform:isoamyl alcohol (24:1) extractions, precipitation with an equal volume of isopropanol for 1 hour at -20 °C, followed by centrifugation at 0 °C / 20'800 g for 15 minutes. The mRNA pellet was dried and redissolved in sterile DEPC-treated H₂O. The integrity and size of the mRNAs were assayed by agarose gel electrophoresis under denaturing conditions, and the concentration was determined by measuring the optical density at 260 nm.

Transcription of the 5-HT₃R gene

The murine 5-HT₃R sequence (obtained from H.Pick [25]) was modified by addition of a T7 promoter site and a poly(A) tail using PCR amplification with the synthetic oligonucleotides 5'-ATA AGA ATG CCG CCG CTA ATA CGA CTC ACT ATA GGG AGG ACC ATG GCC ATG CCG CTC TGC ATC CCG CAG GTG CTG TTG GCC -3' and 5'-ATA GTT TAG CGG CCG CTT TTT TTT TTT TTT TTT TTT TTT TTT TTT TTC AAG AAT AAT GCC AAA TGG ACC AGA GAG TGA CCA G -3'. The resulting 1524 bp fragment was ligated into the pCR2.1 vector using the TA cloning kit (Invitrogen, California, USA) to obtain the plasmid pT7P5HT3R. The construct was controlled by restriction mapping and DNA sequencing, and the corresponding mRNA was transcribed as described for the EGFP mutants.

Cell lines and transfection

Adherent mammalian cells were grown in DMEM/F12 (Dulbecco's modified Eagle medium; GIBCO BRL, Rockville, USA) at 37 °C in a humidified atmosphere with 5 % CO₂. The medium was supplemented with 2.2 % fetal calf serum (GIBCO BRL) for HEK293 and CHO cells, and 10 % for N1E cells. The cultures were split and distributed in 12-well plates at a density of 150'000 cells/ml 12 hours prior to transfection.

Lipofection was performed as follows, per milliliter of cell culture: a mixture containing 2.5 µg of mRNA and 0.5-6.25 µl DOTAP diluted in 50 µl of 10 mM HEPES buffer at pH 7.4 was incubated for 10 minutes at room temperature, and applied dropwise to the cell medium. All fluorescence measurements were performed 20 hours after transfection.

EGFP quantification using a fluorescence plate reader

We used 6-well plates for the plate reader quantification. The growth medium was removed and the adherent cells were homogenized for 10 minutes at 37 °C in 270 µl PBS containing 10 % Triton-X100 (Fluka, Buchs, Switzerland). The measurements were performed with an Analyst plate reader (LJL Biosystems, California, USA) using 200 µl per sample in 96-well plates (Greiner, Frickenhausen, Germany).

Radioactive binding assay

The expression level of cells transfected with 5-HT₃R coding mRNA was assayed by binding assay using the radioactively-labeled specific ligand [³H]-GR65630 (NEN-DuPont, Boston, MA). All experiments were made in triplicate, using 300'000 cells per measurement. The receptor quantification was performed as described in chapters I.2, I.3 and I.4.

II.4.4 Results

In this present study, we use non-sense mutants of the EGFP mRNA to quantify natural suppression in adherent mammalian cells as depicted in Figure II.4.2. Transfection of the reporter mRNAs causes an expression level of EGFP proportional to the readthrough properties of the cell system under investigation. The non-mutated version of the EGFP mRNA serves as a positive reference, and the level of expression can be conveniently quantified by fluorescence measurements in a plate reader.

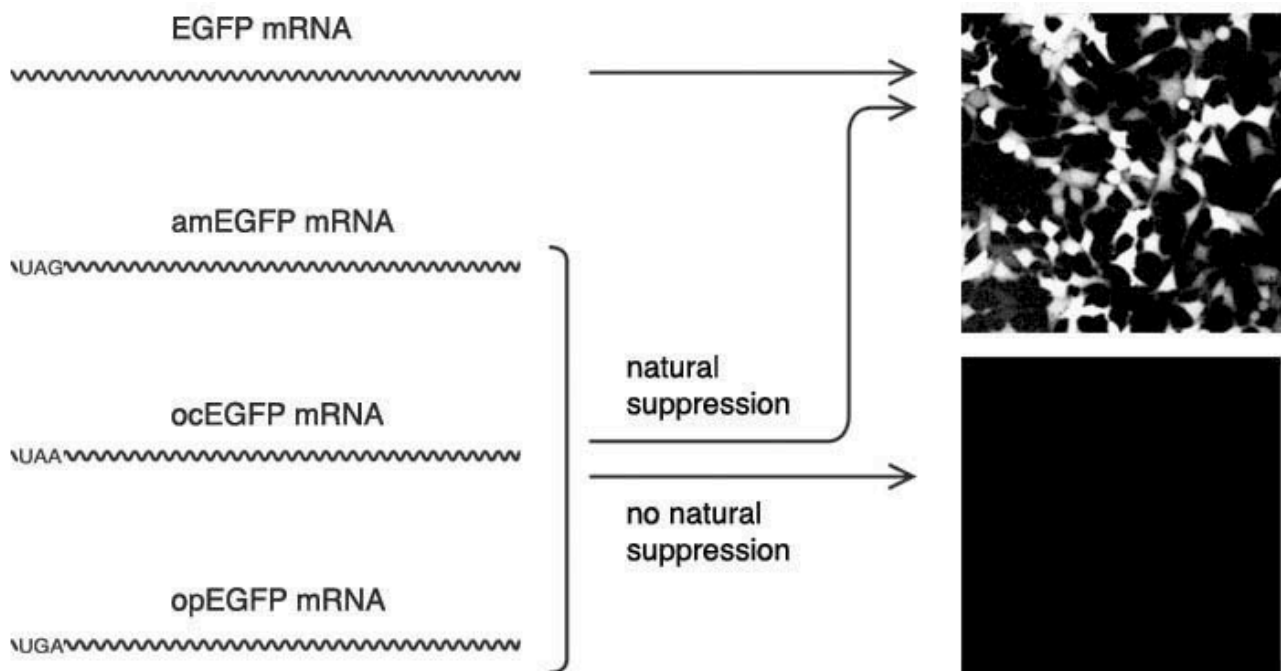


Figure II.4.2 Scheme for the natural suppression measurement in adherent mammalian cells. Transfection of the mRNA coding for the EGFP induces the expression of the fluorescent protein as shown by the confocal image, whereas transfection of the mutated EGFP mRNAs will only induce the translation of EGFP when natural suppression occurs. The intensity of EGFP is measured 20 hours after transfection, and reflects the natural suppression efficiency as compared to suppression-less translation.

To probe the validity of comparisons among cell lines and between mRNA constructs, we first examined the non-dependencies of cellular transfections.

In a first series of experiments, we transfected different cell lines with mRNA coding for the EGFP, and observed the expression level 20 hours later. By varying the ratio between mRNA and DOTAP liposomal reagent, we could observe that the same optimal ratio was universally perceived whatsoever the nature of the cell line (see Figure II.4.3).

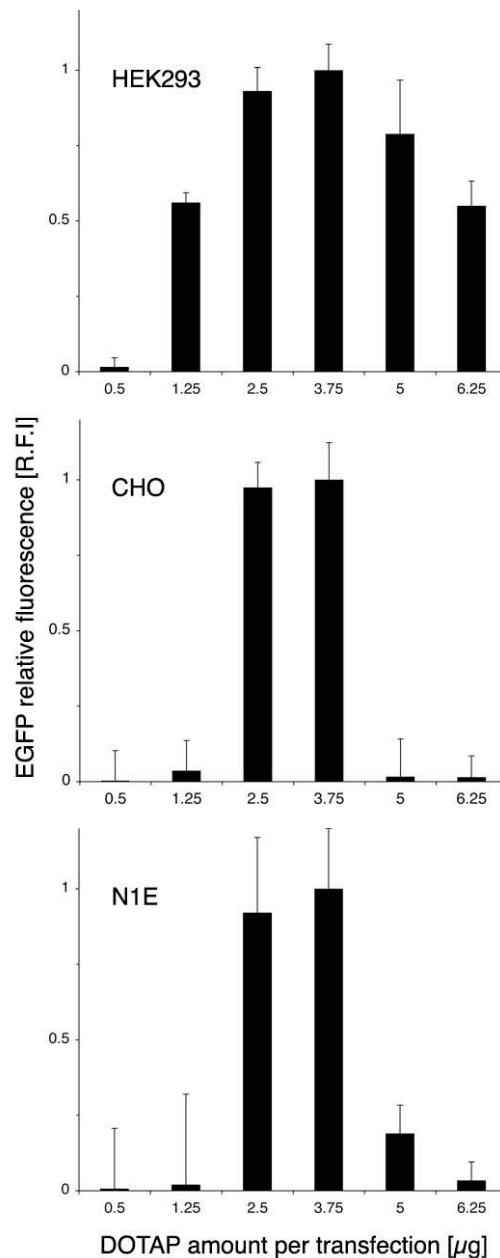


Figure II.4.3 Optimization of transfection parameters in three different cell lines, using EGFP mRNA as an expression reporter: the optimal ratio between mRNA and lipid quantities is independent of the studied cell line.

Secondly, HEK293 cells were transfected with mRNA coding for the 5-HT₃ receptor. This mRNA having a size double of that of the EGFP mRNA and a different nucleotide composition, it allows to demonstrate the full independence of the mRNA properties to the transfection optimizations. As seen in Figure II.4.4, the optimal ratio between mRNA and DOTAP lipid is unchanged compared to the same experiment using EGFP mRNA.

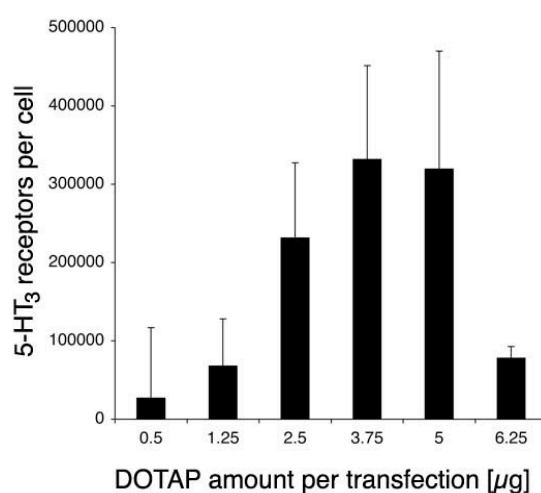


Figure II.4.4 Optimization of transfection parameters in HEK293 cells, using mRNA coding for the 5-HT₃ receptor as an expression reporter monitored via radioactive binding assay: the optimal ratio between mRNA and lipid quantities is shown to be identical to that obtained using EGFP mRNA as a reporter, thus revealing the optimization independency of the transfected mRNA.

The natural suppression was then measured in three different cell lines using the same optimized lipofection technique and the 4 reporter mRNAs. The mRNA-lipid complexes were applied to the adherent cells during 20 hours, the cells were lysed by Triton-X100 treatment and the EGFP fluorescence was recorded using a plate reader. Whereas HEK293 and N1E cell lines had low natural suppression levels, the CHO cells exhibited a fluorescence signal due to natural suppression in the order of 20 %, no matter which stop codon was used (Table II.4.1).

	Amber suppression (UAG)	Ochre suppression (UAA)	Opal suppression (UGA)
CHO	20 ± 8 %	17 ± 9 %	19 ± 8 %
HEK293	2 ± 2 %	4 ± 3 %	10 ± 5 %
N1E-115	5 ± 3 %	6 ± 4 %	5 ± 3 %

Table II.4.1 Natural suppression measurement in three different cell lines. All values are relative to the fluorescence obtained by transfection of the non-mutated EGFP mRNA. The cells were dissolved using Triton-X100 20 hours after transfection, and the fluorescence intensities were measured in a plate reader. Each experiment was made in triplicate, using 150'000 cells per sample.

II.4.5 Discussion

We elaborated a system permitting an easy measurement of natural suppression in living cells via lipofection of EGFP mutant mRNAs. The transfection allowed an equal uptake of each mRNA construct, permitting a proper comparison between nonsense mRNAs and EGFP mRNA. This was demonstrated by the non-dependence of the mRNA nature to the optimization of lipoplexes formation and uptake, a fact already established for plasmid DNA [26].

Furthermore, the transfection optimization was shown to be identical whatever the cell line used, allowing a possible extended use of this technique to several other adherent mammalian cell cultures.

We based our measures on the EGFP fluorescence: *in vitro* transcripts containing a stop codon between the Kozak sequence and the EGFP sequence were used to transfect batches of 150'000 cells per measurement, and the fluorescence emitted from cell lysates was recorded 20 hours later.

We could observe in a quantitative way the fluorescence emitted due to natural suppression. It was especially high in CHO cells independently on the stop codon triplet, and relatively low for HEK293 and N1E-115 cells. However, the opal suppression in HEK293 cells appeared stronger than the almost undetectable natural readthrough of amber and ochre codons. This could be explained by the discovery of opal suppressor tRNAs contained in human DNA library, however not proven to be transcribed [27]. Sogaard et al. have also shown via DNA transfections that UGA codons in HeLa and AMA (human epithelial amnion) cells are subject to readthrough [28], suggesting that this particular readthrough can be observed in all human cells. We based our measurements on the more direct RNA rather than DNA transfection because of the cell cycle independence of this method (chapter II.2). Additionally in the case of DNA transfection the number of mRNA copies leading to detectable proteins highly depends on the RNA polymerase activity, which could vary between cells depending on DNA quantity and possibly on the presence of nonsense codons.

In our system, the fluorescence observed is directly reflecting the percentage of incorporation of a natural amino acid at the nonsense codon position. Indeed, other phenomenons such as frameshift suppression [29-33], or bypassing of the Kozak sequence and translation start at the next AUG which is out of frame would both lead to a non-fluorescent protein, thus not detectable. Even if the translational mechanism skips the first AUG and moreover makes a frameshift at the second AUG, repositioning the ribosome in the EGFP sequence correct frame, the translated protein would not be fluorescent because the second AUG is situated at the amino acid position Nr 37, and it has been shown that amino acids Nr 7 to 229 are essential for the fluorescence of the EGFP [34].

We have shown in precedent experiments that CHO cells can in principle be used for the site-specific incorporation of unnatural amino acids in proteins, and we obtained an incorporation efficiency of about 15 % using amber codon suppression (chapter II.3). This relatively low efficiency is due in part to the natural suppression – as measured here – and we can foresee that this efficiency will most likely not vary dramatically using opal or ochre codons in place of amber because of the similar levels of natural suppression among the three stop codons. On the contrary, HEK293 and N1E cells are good candidates for mis-acylated tRNA suppression studies, especially if the presence of proteins translated without incorporation of the desired unnatural amino acids has to be avoided. Nevertheless the amber and ochre codons should be preferentially chosen for mis-acylated suppressor tRNA experiments in HEK293, due to the relatively higher natural opal suppression in this cell line.

Our present screening strategy can straightforwardly be extended to other cell lines, since mRNA transfection is generally applicable to a wide range of cells (chapter I.2). This system could help elucidating complex interactions between the mRNA and the various components of the translation termination machinery [35,36], and the study of codon context could furthermore be of great use for the optimization of *in vivo* unnatural amino acid incorporation technique.

II.4.6 References

1. Kohrer, C., Xie, L., Kellerer, S., Varshney, U. and RajBhandary, U.L. (2001) Import of amber and ochre suppressor tRNAs into mammalian cells: a general approach to site-specific insertion of amino acid analogues into proteins. *Proc Natl Acad Sci U S A*, **98**, 14310-14315.
2. Ilegems, E., Pick, H.M. and Vogel, H. (2002) Monitoring mis-acylated tRNA suppression efficiency in mammalian cells via EGFP fluorescence recovery. *Nucleic Acids Res*, **30**, e128.
3. Sakamoto, K., Hayashi, A., Sakamoto, A., Kiga, D., Nakayama, H., Soma, A., Kobayashi, T., Kitabatake, M., Takio, K., Saito, K. *et al.* (2002) Site-specific incorporation of an unnatural amino acid into proteins in mammalian cells. *Nucleic Acids Res*, **30**, 4692-4699.
4. Monahan, S.L., Lester, H.A. and Dougherty, D.A. (2003) Site-specific incorporation of unnatural amino acids into receptors expressed in Mammalian cells. *Chem Biol*, **10**, 573-580.
5. Berteaux, V., Rousset, J.P. and Cassan, M. (1991) UAG readthrough is not increased in vivo by Moloney murine leukemia virus infection. *Biochimie*, **73**, 1291-1293.
6. Burke, J.F. and Mogg, A.E. (1985) Suppression of a nonsense mutation in mammalian cells in vivo by the aminoglycoside antibiotics G-418 and paromomycin. *Nucleic Acids Res*, **13**, 6265-6272.
7. Sedivy, J.M., Capone, J.P., RajBhandary, U.L. and Sharp, P.A. (1987) An inducible mammalian amber suppressor: propagation of a poliovirus mutant. *Cell*, **50**, 379-389.
8. Capone, J.P., Sedivy, J.M., Sharp, P.A. and RajBhandary, U.L. (1986) Introduction of UAG, UAA, and UGA nonsense mutations at a specific site in the Escherichia coli chloramphenicol acetyltransferase gene: use in measurement of amber, ochre, and opal suppression in mammalian cells. *Mol Cell Biol*, **6**, 3059-3067.
9. Cassan, M., Berteaux, V., Angrand, P.O. and Rousset, J.P. (1990) Expression vectors for quantitating in vivo translational ambiguity: their potential use to analyse frameshifting at the HIV gag-pol junction. *Res Virol*, **141**, 597-610.
10. Hatfield, D. (1985) Suppression of termination codons in higher eukaryotes. *Trends Biochem Sci*, **10**, 201-204.
11. Hatfield, D., Diamond, A. and Dudock, B. (1982) Opal suppressor serine tRNAs from bovine liver form phosphoseryl-tRNA. *Proc Natl Acad Sci U S A*, **79**, 6215-6219.

12. Diamond, A., Dudock, B. and Hatfield, D. (1981) Structure and properties of a bovine liver UGA suppressor serine tRNA with a tryptophan anticodon. *Cell*, **25**, 497-506.
13. Valle, R.P., Morch, M.D. and Haenni, A.L. (1987) Novel amber suppressor tRNAs of mammalian origin. *Embo J*, **6**, 3049-3055.
14. Kuchino, Y., Beier, H., Akita, N. and Nishimura, S. (1987) Natural UAG suppressor glutamine tRNA is elevated in mouse cells infected with Moloney murine leukemia virus. *Proc Natl Acad Sci U S A*, **84**, 2668-2672.
15. Kuchino, Y., Beier, H., Hanyu, N. and Nishimura, S. (1987) In Inouye, M. and Dudock, B. (eds.), *Molecular biology of RNA: new perspectives*. Academic Press, San Diego, California, pp. 305-320.
16. Baron, C. and Bock, A. (1995) In Söll, D. and RajBhandary, U. L. (eds.), *tRNA: structure, biosynthesis, and function*. ASM Press, Washington, DC, pp. 529-544.
17. Atkins, J.F. and Gesteland, R. (2002) Biochemistry. The 22nd amino acid. *Science*, **296**, 1409-1410.
18. Commans, S. and Bock, A. (1999) Selenocysteine inserting tRNAs: an overview. *FEMS Microbiol Rev*, **23**, 335-351.
19. Tate, W.P., Dalphin, M.E., Pel, H.J. and Mannering, S.A. (1996) The stop signal controls the efficiency of release factor-mediated translational termination. *Genet Eng (N Y)*, **18**, 157-182.
20. Kuchino, Y. and Muramatsu, T. (1996) Nonsense suppression in mammalian cells. *Biochimie*, **78**, 1007-1015.
21. Martin, R. (1994) On the relationship between preferred termination codon contexts and nonsense suppression in human cells. *Nucleic Acids Res*, **22**, 15-19.
22. Phillips-Jones, M.K., Hill, L.S., Atkinson, J. and Martin, R. (1995) Context effects on misreading and suppression at UAG codons in human cells. *Mol Cell Biol*, **15**, 6593-6600.
23. Buckingham, R.H. (1990) Codon context. *Experientia*, **46**, 1126-1133.
24. Phillips-Jones, M.K., Watson, F.J. and Martin, R. (1993) The 3' codon context effect on UAG suppressor tRNA is different in Escherichia coli and human cells. *J Mol Biol*, **233**, 1-6.
25. Pick, H., Preuss, A.K., Mayer, M., Wohland, T., Hovius, R. and Vogel, H. (2003) Monitoring expression and clustering of the ionotropic 5HT3 receptor in plasma membranes of live biological cells. *Biochemistry*, **42**, 877-884.
26. Kreiss, P., Cameron, B., Rangara, R., Mailhe, P., Aguerre-Charriol, O., Airiau, M., Scherman, D., Crouzet, J. and Pitard, B. (1999) Plasmid DNA size does not affect the

- physicochemical properties of lipoplexes but modulates gene transfer efficiency. *Nucleic Acids Res*, **27**, 3792-3798.
27. O'Neill, V.A., Eden, F.C., Pratt, K. and Hatfield, D.L. (1985) A human opal suppressor tRNA gene and pseudogene. *J Biol Chem*, **260**, 2501-2508.
 28. Søgaaard, T.M., Jakobsen, C.G. and Justesen, J. (1999) A sensitive assay of translational fidelity (readthrough and termination) in eukaryotic cells. *Biochemistry (Mosc)*, **64**, 1408-1417.
 29. Tucker, S.D., Murgola, E.J. and Pagel, F.T. (1989) Missense and nonsense suppressors can correct frameshift mutations. *Biochimie*, **71**, 729-739.
 30. Gao, W., Jakubowski, H. and Goldman, E. (1995) Evidence that uncharged tRNA can inhibit a programmed translational frameshift in *Escherichia coli*. *J Mol Biol*, **251**, 210-216.
 31. Plant, E.P., Jacobs, K.L., Harger, J.W., Meskauskas, A., Jacobs, J.L., Baxter, J.L., Petrov, A.N. and Dinman, J.D. (2003) The 9-A solution: how mRNA pseudoknots promote efficient programmed -1 ribosomal frameshifting. *Rna*, **9**, 168-174.
 32. Urbonavicius, J., Stahl, G., Durand, J.M., Ben Salem, S.N., Qian, Q., Farabaugh, P.J. and Bjork, G.R. (2003) Transfer RNA modifications that alter +1 frameshifting in general fail to affect -1 frameshifting. *Rna*, **9**, 760-768.
 33. Wilson, G.M. and Brewer, G. (1999) Slip-sliding the frame: programmed -1 frameshifting on eukaryotic transcripts. *Genome Res*, **9**, 393-394.
 34. Li, X., Zhang, G., Ngo, N., Zhao, X., Kain, S.R. and Huang, C.C. (1997) Deletions of the *Aequorea victoria* green fluorescent protein define the minimal domain required for fluorescence. *J Biol Chem*, **272**, 28545-28549.
 35. Namy, O., Hatin, I. and Rousset, J.P. (2001) Impact of the six nucleotides downstream of the stop codon on translation termination. *EMBO Rep*, **2**, 787-793.
 36. Cassan, M. and Rousset, J.P. (2001) UAG readthrough in mammalian cells: effect of upstream and downstream stop codon contexts reveal different signals. *BMC Mol Biol*, **2**, 3.

Chapter II.5

**RNA interference targeting eRF1 in human cells
increases mis-acylated tRNA suppression efficiency**

II.5 RNA interference targeting eRF1 in human cells increases mis-acylated tRNA suppression efficiency

II.5.1 Abstract

The site-specific incorporation of non-natural amino acids into proteins by nonsense suppression has been widely used to investigate protein structure and function. Usually this technique exhibits low incorporation efficiencies of unnatural amino acids into proteins. We describe for the first time an approach for achieving an increased level of nonsense codon suppression with synthetic suppressor tRNAs in cultured human cells. We find that the intracellular concentration of the eukaryotic release factor 1 (eRF1) is a critical parameter influencing the efficiency of amino acid incorporation by nonsense suppression. Using RNA interference we were able to significantly lower eRF1 gene expression. We achieved a five times higher level of amino acid incorporation as compared to non-treated control cells, as demonstrated by EGFP fluorescence recovery after importing a mutated reporter mRNA together with an artificial amber suppressor tRNA.

The results of this chapter have been submitted for publication:

Ilegems, E., Pick, H.M. and Vogel, H.: RNA interference targeting eRF1 in human cells increases mis-acylated tRNA suppression efficiency.

II.5.2 Introduction

The site-specific incorporation of unnatural amino acids into proteins by nonsense suppression opens novel routes for protein engineering. For example individual proteins can be site-selectively equipped with fluorescent, photo-activatable or other reactive probes suitable for structural and functional investigations. Originally developed as an *in vitro* labeling technique [1-6], nonsense suppression has been progressively adapted to prokaryotic [7-10] and eukaryotic cells [11-15]. Recently the scope of this technique expanded to mammalian live cells [16,17] yielding levels of non-natural amino acids incorporation in the order of 15 - 18 % (see Chapter II.3). Here we report on strategies to increase substantially this level of nonsense suppression efficiency.

The intracellular concentration of the eukaryotic release factor eRF1 is a parameter, which is known to influence natural nonsense suppression efficiency [18]. Published data point to competitive actions between natural suppressor tRNAs and eRF1 for stop codon recognition based on their structural similarity [19-21]. Whereas a suppressor tRNA is required for incorporation of amino acids and ribosomal read-through, the eRF1 factor triggers the release of the nascent peptide resulting in termination of translation [18]. Overexpression of eRF1 was shown to increase termination efficiency [22] whereas a decreased eRF1 activity promoted stop codon read-through *in vitro* and in eukaryotic cells [6,18]. Furthermore, it has been shown in recent studies that mRNAs containing a premature stop codon spatially distant from the 3' end can be degraded by a Upf1 complex in which the eRF1 is involved [23,24]. These observations point to eRF1 as a factor which is potentially influencing nonsense codon suppression also in presence of artificial suppressor tRNAs.

Here we explore the feasibility of post-transcriptional gene silencing of eRF1 to achieve higher efficiencies of amino acid incorporation by nonsense suppression in HEK293 cells. The silencing property of short interfering RNAs [25-28] was used to target eRF1 messenger RNA. Changes in eRF1 gene expression were quantified by real-time RT-PCR. The effects of eRF1 silencing on nonsense suppression efficiency were investigated using an EGFP reporter transcript carrying an amber codon suppression site at an amino acid position, which is essential for fluorophore formation, as described in Chapter II.3. We found that only the co-injection of the mutated EGFP reporter messenger RNA together with an artificial suppressor tRNA, which can be amino-acylated *in vivo*, gave rise to detectable EGFP fluorescence signals inside HEK293 cells indicating site-specific nonsense suppression events. The level of EGFP fluorescence recovery reflected the suppression efficiency and could be quantified in eRF1 silenced cells compared to non-treated cells using laser-scanning confocal microscopy.

II.5.3 Experimental procedures

Materials

Synthetic oligonucleotides were purchased from MWG-Biotech AG (Ebersberg, Germany), kits for plasmid and DNA-fragment purification from QIAGEN GmbH (Hilden, Germany), restriction endonucleases (*Bsa*I, *Eco*RI and *Not*I) from New England Biolabs (Massachusetts, USA), MEGAscript and MEGAshortscript kits for *in vitro* transcription as well as the cap analog m⁷G(5')ppp(5')G from Ambion (Texas, USA), and purified rEGFP from Clontech (California, USA). All other chemicals were obtained from Sigma-Aldrich (Missouri, USA).

Cell culture

Adherent mammalian cells (Human Embryonic Kidney, HEK293) were grown in DMEM/F12 (Dulbecco's modified Eagle medium; GIBCO BRL, Rockville, USA). The medium was supplemented with 2.2 % fetal calf serum (GIBCO BRL). One day prior to injection cells were transferred to 35/12 mm WillCo-dishes (WPI, Herts, United Kingdom) at a density of 100'000 cells/ml, and kept at 37 °C in a humidified atmosphere with 5 % CO₂.

In vitro transcription of reporter genes

The coding sequence of the red fluorescent protein DsRedExpress (pDsRedExpress, Clontech) was modified by the addition of a T7 promoter site and a poly(A) tail using PCR amplification with synthetic oligonucleotides. The resulting fragment was ligated into the pCR2.1 vector using the TA cloning kit (Invitrogen, California, USA) to obtain the plasmid pT7PDsRedExpress, which was analysed by restriction mapping and DNA sequencing.

We used the plasmid pT7PEGFPam64L, described in Chapter II.3, as the second template. It contains the coding sequence of the EGFP (Clontech) with an amber mutation at an amino acid sequence position important for the correct folding of the fluorophore.

After linearization of the plasmids pT7DsRedExpress and pT7EGFPam64L by *Not*I, *in vitro* transcription was performed with T7 RNA polymerase using the MEGAscript kit. Capping of mRNA was achieved during transcription by replacing 80 % of the GTP level with the cap analog m⁷G(5')ppp(5')G. After removing the DNA template by *DNase*I treatment, the resulting mRNAs were purified by successive phenol:chloroform:isoamyl alcohol (25:24:1) and chloroform:isoamyl alcohol (24:1) extractions, precipitation with an equal volume of isopropanol for 1 hour at -20 °C, followed by centrifugation at 0 °C and 20'800 g for 15 minutes. The mRNA pellet was dried and redissolved in sterile DEPC-treated H₂O. The integrity and size of the mRNAs were analysed by

agarose gel electrophoresis under denaturing conditions, and the concentration was determined by measuring the optical density at 260 nm.

siRNA synthesis and transfection

The siRNA targeting the eRF1 mRNA was synthesized by annealing *in vitro* transcripts as depicted in Figure II.5.1A: for each RNA fragment, two synthetic DNA oligonucleotides were annealed to obtain templates flanked by a double-stranded T7 promoter [29]. *In vitro* transcriptions were performed using the MEGAscript kit (Ambion, Texas, USA). After removing the DNA templates by *DNase*I treatment, the resulting RNAs were purified by successive phenol:chloroform:isoamyl alcohol (25:24:1) and chloroform:isoamyl alcohol (24:1) extractions. RNA precipitation was achieved by adding an equal volume of isopropanol and by 1 hour incubation at $-20\text{ }^{\circ}\text{C}$, followed by centrifugation at $0\text{ }^{\circ}\text{C} / 20'800\text{ g}$ for 15 minutes. The RNA pellets were air dried at room temperature and redissolved in sterile DEPC-treated H_2O . RNA concentrations were determined by measuring the optical density at 260 nm. The two complementary RNA strands were annealed at an equimolar ratio and dissolved in DEPC-treated water to finally obtain the siRNA at a concentration of $20\text{ }\mu\text{M}$. The integrity and size of the siRNA was assayed by polyacrylamide gel electrophoresis under denaturing conditions.

HEK293 cells were transfected with siRNA using the TransMessenger Kit from Qiagen, following the manufacturer's instructions. Typically, for a 35 mm Nunc dish, $3.4\text{ }\mu\text{l}$ Enhancer-R, $6\text{ }\mu\text{l}$ siRNA ($20\text{ }\mu\text{M}$) and $8.5\text{ }\mu\text{l}$ TransMessenger were used. The medium was changed 4 hours after transfection.

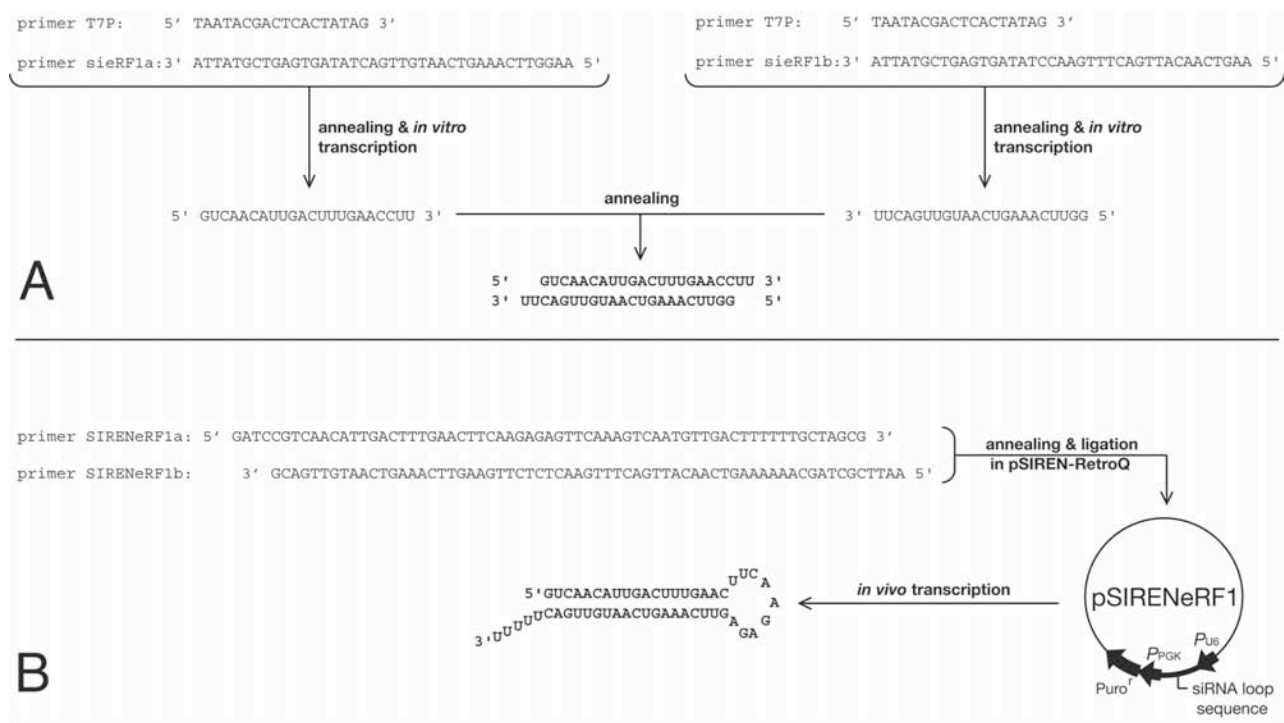


Figure II.5.1 Scheme of the synthesis of interfering RNAs targeting the eRF1 transcripts. (A) siRNA obtained by ligation of complementary RNA strands, both *in vitro*-transcribed from annealed synthetic DNA oligonucleotides. (B) Hairpin interfering RNA synthesized *in vivo* after transfection of the vector pSIRENeRF1. This vector was obtained by annealing and ligating two synthetic oligonucleotides in the vector pSIREN-RetroQ.

Generation of the stable cell line HEK-seRF1

Complementary DNA nucleotides were annealed and ligated into pSIREN-RetroQ (Clontech, California, USA), as shown in Figure II.5.1B, giving rise to the plasmid pSIRENeRF1. This vector leads to the expression of hairpin RNAs containing a 9 nucleotides loop, as described by Yu et al. [30]. After calcium phosphate transfection of HEK293 cells [31], the expression was maintained by supplementing 1 µg/ml of puromycin in the growth media. This selection was made during 3 weeks prior to real-time PCR experiments.

cDNA preparation and Real-Time PCR quantification

Total messenger RNA was extracted from approximately 2 million cells per sample using TRIZOL Reagent (Invitrogen, California, USA). The subsequent eRF1 reverse transcription was achieved using a TaqMan Gold RT-PCR Kit from Applied Biosystems (California, USA) and random hexamers. We used the SYBR® Green I kit (Eurogentec, Seraing, Belgium) for quantitative PCR, together with the eRF1-specific primers 5'- TCACAGACAAAGAGACCGGACA-3' and 5'- CGCAAGATACCTCCAATTCCAC-3'. Primers used for the internal reference gene glyceraldehyde-3-phosphate dehydrogenase (GAPDH) were supplied in the TaqMan Gold RT-PCR Kit (Applied Biosystems). The ABI Prism 7700 was used as a sequence detection system and data were treated with the software "Sequence Detection Systems 1.9.1", both from Applied Biosystems. The amplification specificities were controlled with dissociation measurements followed by treatment using "Dissociation Curves 1.0" software (Applied Biosystems). The efficiencies of the reactions were calculated using "LinRegPCR 7.4" [32], with a minimum of 5 data points for the determination of each amplification slope.

Injections

Microinjections of HEK293 cells with mRNA and tRNA mixtures diluted in sterile DEPC-treated H₂O were performed using an InjectMan controller and a Transjector 5246 system (both from Eppendorf, Hamburg, Germany) mounted on an Axiovert S100TV inverted microscope (Carl Zeiss AG, Oberkochen, Germany). FemtotipsII capillaries (Eppendorf) were used for all injections.

Laser scanning confocal microscopy and fluorescence measurements

Laser scanning confocal microscopy was performed using a Zeiss LSM510 (Carl Zeiss AG). Detection and distinction of the fluorescence signals of EGFP (excitation at 488 nm) and DsRedExpress (excitation at 543 nm) was achieved by appropriate filter sets using a multitracking mode. Scanning speed and laser intensity were adjusted to avoid photobleaching of the fluorophores and proper comparison between samples of variable fluorescence intensities.

II.5.4 Results

A schematic view of our strategy to improve mis-acylated tRNA suppression efficiency in human cells is presented in Figure II.5.3. In a first step the intracellular mRNA level of eRF1 is lowered via RNA interference and its effect on nonsense suppression is later evaluated by microinjection of reporter mRNAs. One of the transcripts gives rise to the suppression-dependent expression of a green fluorescent protein. The other non-mutated, red fluorescent reporter is used as an internal standard for the amount of injected molecules, allowing the comparison between individual cells.

Lowering of the intrinsic eRF1 messenger concentration has been approached in two different ways using either a transient siRNA transfection or a stable transcription of a hairpin RNA, both targeting eRF1 transcripts. The siRNA sequence was designed following Elbashir et al. [27,28] and the selection of a specific location on the target eRF1 mRNA was made such that both synthesized RNA strands begin with a guanine, as detailed by Donze et al. [33].

We studied alterations in eRF1 mRNA concentration by real-time PCR, using glyceraldehyde-3-phosphate dehydrogenase (GAPDH) as an independent reference gene (Figure II.5.4). Transfection of siRNA had substantial effect on the eRF1 mRNA concentration, which decreased to approximately 40 % of its initial value within two days after transfection. The cell line HEK-seRF1 stably expressing the eRF1 targeting hairpin RNA exhibited approximately 60 % of the eRF1 mRNA concentration of non-treated cells. No noticeable difference was observed in the eRF1 mRNA level between non-transfected cells and cells pre-transfected with a control (non-eRF1 targeting) siRNA.

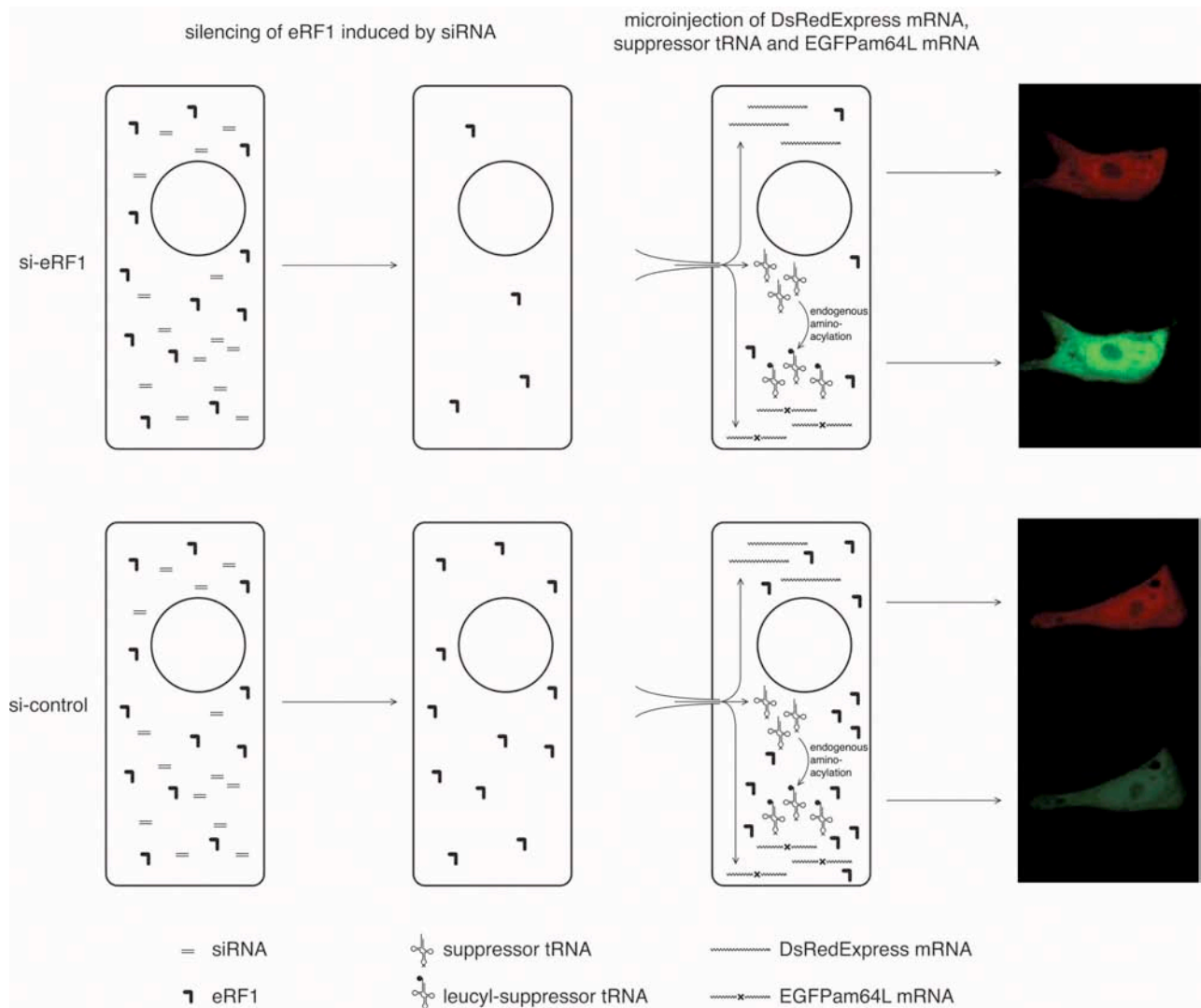


Figure II.5.3 General representation of the eRF1 silencing effect on the mis-acylated tRNA suppression efficiency.

Upper line: Interfering RNAs in the cell – obtained by either siRNA or pSIRENeRF1 transfection – lead to a lower intracellular concentration of eRF1. Subsequently, a solution containing DsRedExpress mRNA, suppressor tRNA and EGFPam64L mRNA is microinjected into the cell. The tRNA is aminoacylated by endogenous AARSs and the expression of EGFP reflects the suppression efficiency, whereas the DsRedExpress expression level serves as a standard for non-suppressed translation (shown by typical confocal images taken 20 hours after injection). Lower line: Control experiment using non-interfering siRNA, having no effect on the eRF1 level. In the confocal image on the right, the ratio between the EGFP and the DsRedExpress expression levels reflects an increase in the suppression efficiency after silencing of the eRF1.

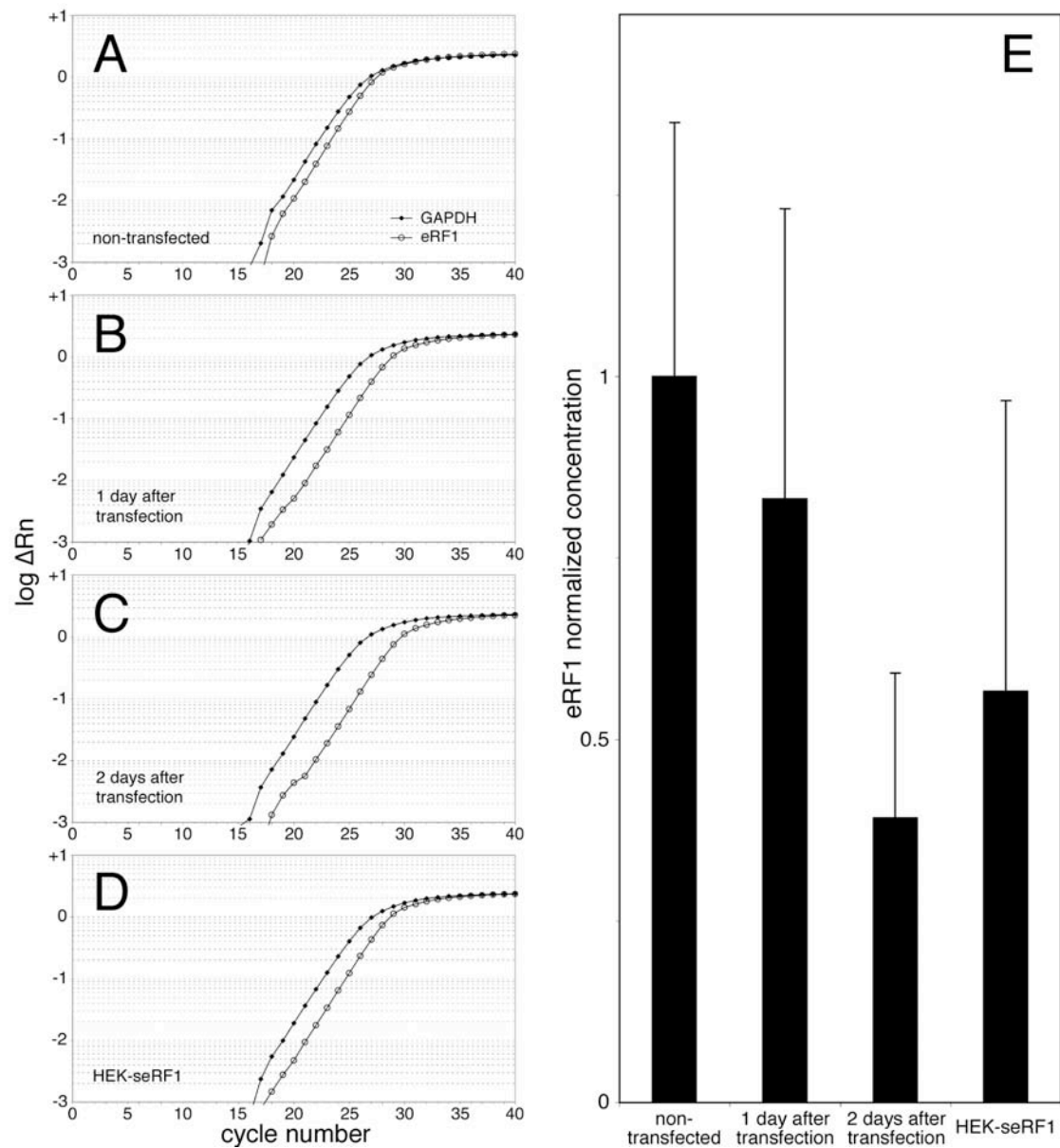


Figure II.5.4 Real-time PCR experiments.

(A)-(D): PCR profiles of the amplifications of eRF1 and GAPDH (used as an internal standard). The cDNAs were produced from (A) non-transfected cells or cells transfected with a non-interfering siRNA, (B) cells transfected with siRNA 1 day before, (C) cells transfected with siRNA 2 days before, and (D) HEK-seRF1 cells (HEK293 cells stably transfected with pSIRENeRF1).

(E): Comparison of the level of eRF1 mRNA in the different samples, using the GAPDH as an internal standard.

To study the correlation between eRF1 concentration and artificial suppression efficiency microinjection experiments were performed 2 days after siRNA transfection, which we observed resulted in more homogeneous eRF1 silencing among cells than via DNA transfection, thus permitting precise cell-to-cell comparisons (see also Chapter II.11). We co-injected DsRedExpress mRNA, human suppressor tRNA^{Leu}_{CUA}, and EGFPam64L mRNA at fixed ratios and controlled volumes of about 0.05 ± 0.01 pl (as described in Chapter II.3). About 20 hours later, the expression of both reporter proteins was monitored by laser-scanning confocal microscopy. Whereas the DsRed fluorescence intensity was shown to be proportional to the number of injected molecules, the EGFP fluorescence intensity mainly depended on the suppression efficiency. Indeed, the mutated EGFPam64L mRNA is only translated in a full-length fluorescent EGFP when its amber codon is suppressed by a specific suppressor tRNA charged with a leucine (for details, see Chapter II.3). Plotting the fluorescence intensity of the DsRedExpress versus that of EGFP revealed that the suppression efficiency of the siRNA-transfected cells is increased 5 fold as compared to the non-treated HEK293 cells (Figure II.5.5, Table II.5.1).

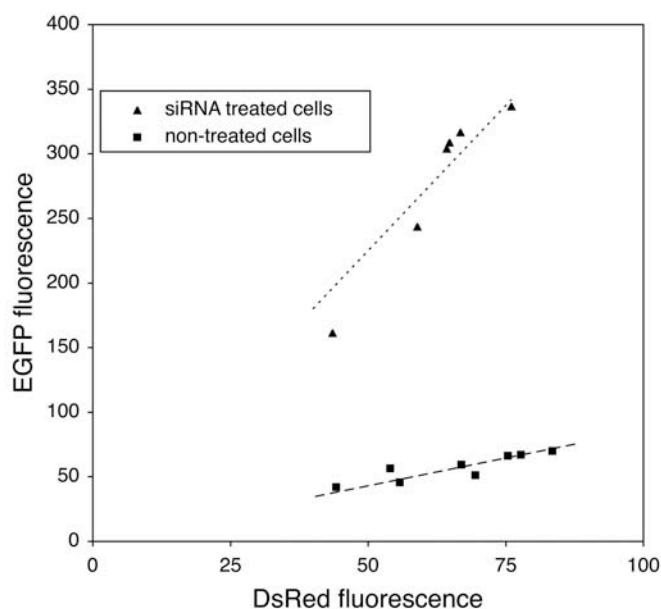


Figure II.5.5 Fluorescence intensities of DsRedExpress and EGFP 20 hours after co-injection of DsRedExpress mRNA, suppressor tRNA and EGFPam64L mRNA, as measured by confocal microscopy. Each data point represents a single cell (squares represent non-treated cells, triangles represent cells pre-transfected with siRNA targeting the eRF1).

	Intracellular eRF1 mRNA concentration	Mis-acylated tRNA suppression efficiency
Non-treated HEK293 cells	100 %	100 %
HEK transfected with siRNA: 1 day after transfection	83 ± 70 %	N.D.
HEK transfected with siRNA: 2 days after transfection	39 ± 33 %	500 ± 100 %
HEK-seRF1 cells	57 ± 60 %	N.D.

Table II.5.1 Concentration of eRF1 mRNA as determined by Real-Time PCR, and its effect on mis-acylated suppression efficiency as deduced from DsRedExpress/EGFP expression level ratios. All samples were microinjected using concentrations of 2 µg/µl DsRedExpress mRNA, 2 µg/µl EGFPam64L mRNA, 2 µg/µl tRNA, and imaged 20 hours later. All values are normalized to non-treated HEK293 cells. N.D. = not determined.

The expression level of the DsRedExpress was controlled to be independent of the siRNA transfection by co-injecting treated and non-treated cells with DsRedExpress mRNA together with purified rEGFP as an indicator for injection volume: the DsRedExpress expression level was identical regardless of the eRF1 concentration, and only depending on the injection volume reflected by the rEGFP fluorescence intensity (data not shown).

II.5.5 Discussion

We developed a strategy to enhance the yield of artificial nonsense codon suppression in cultured human cells. The eukaryotic release factor eRF1, which is known to compete with suppressor tRNAs for stop codon recognition [21] was down-regulated on the transcript level. Based on the silencing properties of interfering RNA a substantial decrease in eRF1 mRNA concentration was achieved. The silencing effect was followed by real-time PCR and increased over time to result in a two-fold reduction of eRF1 transcripts two days after transfection. A comparable degree of gene silencing was obtained by stable transfection of HEK293 cells with a vector capable of inducing *in vivo* transcription of a hairpin RNA for targeting eRF1 mRNAs.

The effect of eRF1 gene silencing on nonsense codon suppression efficiency was investigated in individual cells by co-injection of an artificial suppressor tRNA together with *in vitro* transcripts encoding two reporter proteins DsRedExpress and EGFPam64L. The suppressor tRNA was designed in order to obtain a natural aminoacylation by human cells, required for charging it with a leucine to recover the green fluorescence of the EGFPam64 reporter by amber codon suppression. The tRNA sequence used in this study was based on the human tRNA^{Leu}_{CAA} [34], which anticodon was mutated to CUA and which was modified by two other mutations A38G/A39U to improve amber suppression efficiency [35].

Only by co-injecting the amber codon containing EGFP transcript together with the cognate suppressor tRNA complete translation was achieved as indicated by EGFP fluorescence recovery. The injection of the EGFPam64L reporter alone did not result in detectable expression of fluorescent proteins as judged by laser-scanning confocal microscopy (see also Chapter II.3). DsRedExpress mRNA encoding a red fluorescent protein was co-injected as a standard reflecting the amount of injected molecules. Since the two reporter mRNAs were always injected at the same molar ratio the ratio between the resulting EGFP and the DsRedExpress fluorescence intensities could be used to compare suppression efficiencies in individual cells. Lowering the eRF1 mRNA concentration by a factor of two resulted in a five-fold increase in suppression efficiency as compared to non-treated HEK293 cells. Parallel to our present research, Carnes et al. reported a slight enhancement of natural nonsense read-through after 90 % silencing of eRF1 transcripts in human cells [36]. These experiments were done in the absence of artificial suppressor tRNAs. On the basis of our study we are now able to confirm a positive influence of eRF1 silencing also on artificial nonsense codon suppression.

In general, increased read-through might be problematic for the specific incorporation of unnatural amino acids when using cell lines exhibiting a strong natural suppression; in such a situation the

amount of proteins translated without the desired synthetic amino acid incorporation would increase relatively to the labeled protein. However we determined natural amber codon suppression to be very low in HEK293 as compared to some other cell lines (Chapter II.4), making them well suited for labeling experiments. By silencing eRF1 transcripts down to 40 % of the original level we could achieve an increased artificial amber suppression without enhancing natural read-through.

In our hands, further silencing of eRF1 by using the strong interfering RNA “si1187” [36] lead to changes in cell morphology as indicated by their detachment from the growth surface, thus impairing microinjection experiments and subsequent subcellular investigations by fluorescence confocal microscopy (not shown).

The prospects for suppression of nonsense codons in prokaryotes as well as in eukaryotes might be influenced by the same strategy involving the downregulation or deactivation of intrinsic translation termination factors. This was demonstrated in previous *in vitro* experiments by the group of Sidney Hecht [6]: partial heat deactivation of a thermosensitive mutant of the prokaryotic release factor 1 (RF1) increased amber codon suppression by chemically misacylated suppressor tRNAs in cell-free *E.coli* extracts using dehydropholate reductase (DHFR) as a reporter protein.

Here, we provided a general and efficient method to enhance the yield of artificial nonsense suppression in live human cells. This finding in combination with the presented EGFP suppression assay is expected to make the suppressor tRNA labeling technique accessible to a wide range of cell types, which are more suitable for structural and functional studies than classically used *E.coli* or *Xenopus* oocytes.

II.5.6 References

1. Cload, S.T., Liu, D.R., Froland, W.A. and Schultz, P.G. (1996) Development of improved tRNAs for in vitro biosynthesis of proteins containing unnatural amino acids. *Chem Biol*, **3**, 1033-1038.
2. Noren, C.J., Anthony-Cahill, S.J., Suich, D.J., Noren, K.A., Griffith, M.C. and Schultz, P.G. (1990) In vitro suppression of an amber mutation by a chemically aminoacylated transfer RNA prepared by runoff transcription. *Nucleic Acids Res*, **18**, 83-88.
3. Karginov, V.A., Mamaev, S.V. and Hecht, S.M. (1997) In vitro suppression as a tool for the investigation of translation initiation. *Nucleic Acids Res*, **25**, 3912-3916.
4. Kurzchalia, T.V., Wiedmann, M., Breter, H., Zimmermann, W., Bauschke, E. and Rapoport, T.A. (1988) tRNA-mediated labelling of proteins with biotin. A nonradioactive method for the detection of cell-free translation products. *Eur J Biochem*, **172**, 663-668.
5. Hohsaka, T., Kajihara, D., Ashizuka, Y., Murakami, H. and Sisido, M. (1998) Efficient Incorporation of Nonnatural Amino Acids with Large Aromatic Groups into Streptavidin in In Vitro Protein Synthesizing Systems. *J Am Chem Soc*, **121**, 34-40.
6. Short, G.F., 3rd, Golovine, S.Y. and Hecht, S.M. (1999) Effects of release factor 1 on in vitro protein translation and the elaboration of proteins containing unnatural amino acids. *Biochemistry*, **38**, 8808-8819.
7. Liu, D.R. and Schultz, P.G. (1999) Progress toward the evolution of an organism with an expanded genetic code. *Proc Natl Acad Sci U S A*, **96**, 4780-4785.
8. Wang, L., Brock, A., Herberich, B. and Schultz, P.G. (2001) Expanding the genetic code of *Escherichia coli*. *Science*, **292**, 498-500.
9. Wang, L., Brock, A. and Schultz, P.G. (2002) Adding L-3-(2-Naphthyl)alanine to the genetic code of *E. coli*. *J Am Chem Soc*, **124**, 1836-1837.
10. Liu, D.R., Magliery, T.J., Pastrnak, M. and Schultz, P.G. (1997) Engineering a tRNA and aminoacyl-tRNA synthetase for the site-specific incorporation of unnatural amino acids into proteins in vivo. *Proc Natl Acad Sci U S A*, **94**, 10092-10097.
11. Turcatti, G., Nemeth, K., Edgerton, M.D., Knowles, J., Vogel, H. and Chollet, A. (1997) Fluorescent labeling of NK2 receptor at specific sites in vivo and fluorescence energy transfer analysis of NK2 ligand-receptor complexes. *Receptors Channels*, **5**, 201-207.
12. Turcatti, G., Nemeth, K., Edgerton, M.D., Meseth, U., Talabot, F., Peitsch, M., Knowles, J., Vogel, H. and Chollet, A. (1996) Probing the structure and function of the tachykinin

- neurokinin-2 receptor through biosynthetic incorporation of fluorescent amino acids at specific sites. *J Biol Chem*, **271**, 19991-19998.
13. Chollet, A., Turcatti, G., Nemeth, K. and Vogel, H. (1998) In Slavik, J. (ed.), *Fluorescence Microscopy and Fluorescent Probes*. Plenum Press, New York, Vol. 2, pp. 87-92.
 14. Beene, D.L., Brandt, G.S., Zhong, W., Zacharias, N.M., Lester, H.A. and Dougherty, D.A. (2002) Cation- π Interactions in Ligand Recognition by Serotonergic (5-HT_{3A}) and Nicotinic Acetylcholine Receptors: The Anomalous Binding Properties of Nicotine. *Biochemistry*, **41**, 10262-10269.
 15. Cohen, B.E., McAnaney, T.B., Park, E.S., Jan, Y.N., Boxer, S.G. and Jan, L.Y. (2002) Probing protein electrostatics with a synthetic fluorescent amino acid. *Science*, **296**, 1700-1703.
 16. Ilegems, E., Pick, H.M. and Vogel, H. (2002) Monitoring mis-acylated tRNA suppression efficiency in mammalian cells via EGFP fluorescence recovery. *Nucleic Acids Res*, **30**, e128.
 17. Monahan, S.L., Lester, H.A. and Dougherty, D.A. (2003) Site-specific incorporation of unnatural amino acids into receptors expressed in Mammalian cells. *Chem Biol*, **10**, 573-580.
 18. Carnes, J., Frolova, L., Zinnen, S., Drugeon, G., Phillippe, M., Justesen, J., Haenni, A.L., Leinwand, L., Kisselev, L.L. and Yarus, M. (2000) Suppression of eukaryotic translation termination by selected RNAs. *Rna*, **6**, 1468-1479.
 19. Bertram, G., Bell, H.A., Ritchie, D.W., Fullerton, G. and Stansfield, I. (2000) Terminating eukaryote translation: domain 1 of release factor eRF1 functions in stop codon recognition. *Rna*, **6**, 1236-1247.
 20. Bertram, G., Innes, S., Minella, O., Richardson, J. and Stansfield, I. (2001) Endless possibilities: translation termination and stop codon recognition. *Microbiology*, **147**, 255-269.
 21. Drugeon, G., Jean-Jean, O., Frolova, L., Le Goff, X., Philippe, M., Kisselev, L. and Haenni, A.L. (1997) Eukaryotic release factor 1 (eRF1) abolishes readthrough and competes with suppressor tRNAs at all three termination codons in messenger RNA. *Nucleic Acids Res*, **25**, 2254-2258.
 22. Le Goff, X., Philippe, M. and Jean-Jean, O. (1997) Overexpression of human release factor 1 alone has an antisuppressor effect in human cells. *Mol Cell Biol*, **17**, 3164-3172.
 23. Czaplinski, K., Ruiz-Echevarria, M.J., Paushkin, S.V., Han, X., Weng, Y., Perlick, H.A., Dietz, H.C., Ter-Avanesyan, M.D. and Peltz, S.W. (1998) The surveillance complex

- interacts with the translation release factors to enhance termination and degrade aberrant mRNAs. *Genes Dev*, **12**, 1665-1677.
24. Hilleren, P. and Parker, R. (1999) Mechanisms of mRNA surveillance in eukaryotes. *Annu Rev Genet*, **33**, 229-260.
 25. McManus, M.T. and Sharp, P.A. (2002) Gene silencing in mammals by small interfering RNAs. *Nat Rev Genet*, **3**, 737-747.
 26. Chiu, Y.L. and Rana, T.M. (2002) RNAi in human cells: basic structural and functional features of small interfering RNA. *Mol Cell*, **10**, 549-561.
 27. Elbashir, S.M., Lendeckel, W. and Tuschl, T. (2001) RNA interference is mediated by 21- and 22-nucleotide RNAs. *Genes Dev*, **15**, 188-200.
 28. Elbashir, S.M., Harborth, J., Lendeckel, W., Yalcin, A., Weber, K. and Tuschl, T. (2001) Duplexes of 21-nucleotide RNAs mediate RNA interference in cultured mammalian cells. *Nature*, **411**, 494-498.
 29. Milligan, J.F., Groebe, D.R., Witherell, G.W. and Uhlenbeck, O.C. (1987) Oligoribonucleotide synthesis using T7 RNA polymerase and synthetic DNA templates. *Nucleic Acids Res*, **15**, 8783-8798.
 30. Yu, J.Y., DeRuiter, S.L. and Turner, D.L. (2002) RNA interference by expression of short-interfering RNAs and hairpin RNAs in mammalian cells. *Proc Natl Acad Sci U S A*, **99**, 6047-6052.
 31. Jordan, M., Schallhorn, A. and Wurm, F.M. (1996) Transfecting mammalian cells: optimization of critical parameters affecting calcium-phosphate precipitate formation. *Nucleic Acids Res*, **24**, 596-601.
 32. Ramakers, C., Ruijter, J.M., Deprez, R.H. and Moorman, A.F. (2003) Assumption-free analysis of quantitative real-time polymerase chain reaction (PCR) data. *Neurosci Lett*, **339**, 62-66.
 33. Donze, O. and Picard, D. (2002) RNA interference in mammalian cells using siRNAs synthesized with T7 RNA polymerase. *Nucleic Acids Res*, **30**, e46.
 34. Breitschopf, K., Achsel, T., Busch, K. and Gross, H.J. (1995) Identity elements of human tRNA(Leu): structural requirements for converting human tRNA(Ser) into a leucine acceptor in vitro. *Nucleic Acids Res*, **23**, 3633-3637.
 35. Raftery, L.A. and Yarus, M. (1987) Systematic alterations in the anticodon arm make tRNA(Glu)-Suoc a more efficient suppressor. *Embo J*, **6**, 1499-1506.
 36. Carnes, J., Jacobson, M., Leinwand, L. and Yarus, M. (2003) Stop codon suppression via inhibition of eRF1 expression. *Rna*, **9**, 648-653.

III

Conclusions and outlook

III – Conclusions and outlook

III.1.1 Conclusions and outlook

In the context of this thesis I investigated the versatility of fluorescently-labeled proteins. In the first part, I showed that the fusion of proteins having completely different original biological functions could create a chimera exhibiting interesting novel optical properties. The 5-HT₃R was fused to variants of the green fluorescent protein (GFP), without losing its characteristic ligand binding properties and channel activities. The fluorescent 5-HT₃R permitted to follow its trafficking during an entire biogenesis in live cells, from the assembly of its subunits to cell membrane integration and finally to its agonist-induced internalization. Moreover, the fluorescence intensity emitted from the GFP-derived proteins was directly proportional to the number of 5-HT₃Rs, permitting to collect quantitative information about overall spatial organization of the receptors.

In addition, the 5-HT₃R was shown to be still functional in both “native vesicles” and detergent-solubilized form. This finding opens further bioanalytic applications such as functional screening. The 5-HT₃R function could be assessed in both cases via fluorescence: by confocal microscopy imaging of a calcium-sensitive dye, and by measuring binding of a fluorescent ligand via fluorescence resonance energy transfer, respectively.

The production of native vesicles from living cells represents a novel approach allowing the miniaturization of cell-based assays. The exemplary study on the 5-HT₃R indicates that plasma membrane receptors in the native vesicles retain their original cellular location, orientation and function. Another important finding is that native vesicles preserve cellular signal detection and transduction processes as demonstrated by 5-HT₃R-mediated calcium signaling upon agonist application. Because a single mammalian cell delivers about 50 native vesicles, which can be isolated and addressed as individuals, this concept allows multiple analyses of the functions of single, for example primary cells, which are hampered by limited availability.

Changes in the receptor fluorescence properties upon binding a non-fluorescent agonist could also be detected, supporting the general idea of a ligand-induced conformational change of the receptor. The possibility of quantifying agonist-receptor interactions by simple measurements of changes in receptor-intrinsic GFP fluorescence intensities has the potency for high-throughput applications.

The structural similarity among ligand-gated ion channels might allow analogous strategies for other members of this receptor family.

In the second part of this thesis I focused on adapting the mis-acylated tRNA technology to cultured mammalian cells. In principle, this methodology could lead to the incorporation of much smaller probes based on single unnatural amino acids, as compared to the large GFP fused to the receptor protein.

I found that tRNA sequences coming from genetically different cells such as *Escherichia coli* can be suitable for unnatural amino acid incorporations in mammalian cells, minimizing the probability of endogenous acylation by the host cell while still being accepted by the ribosome translational machinery. Compared to normal translation, we obtained an efficiency of amino acid incorporation using mis-acylated suppressor tRNA in the order of 15%. I then investigated which cell lines and codon-anticodon pairs could be more appropriate for this methodology, in respect to the existence of natural nonsense-codon readthrough [1-5] potentially competing with the unnatural amino acid incorporation by inserting natural amino acids at the position of interest. Both HEK293 and N1E-115 cells showed low natural suppression for all three stop codons (UAG, UAA, UGA), with the exception of the opal codon (UGA) in the case of HEK293 cells. After reduction of background nonsense codon readthrough by selecting most suited cells and codon-anticodon pair, I elaborated a general approach for increasing the efficiency of unnatural amino acid mutagenesis. This was achieved by *in vivo* siRNA-induced down-regulation of the eRF1, which is the sole release factor in eukaryotic cells catalyzing translation termination at all three stop codons. I obtained a five-fold increase of artificial amber codon suppression in cultured human cells, using endogenously aminoacylated suppressor tRNAs. Due to the inferior stability of *in vitro* aminoacylated suppressor tRNA compared to the *in vivo* aminoacylated suppressor tRNA we used, as well as its “unique” usage in the ribosome, the efficiency improvement of unnatural amino acid incorporation might not be multiplied by the same factor of five, but should nevertheless be noticeable.

For each case, I investigated various cell transfection techniques and defined the best adapted one to transfer the different molecules needed for the mis-acylated suppressor tRNA methodology.

In conclusion, I established the essential basis for efficient site-specific incorporation of unnatural amino acids in cultured mammalian cells. This technique has the potential to introduce very small amino acid modifications [6], fluorescent or photoactivatable amino acids [7-10], or even nonproteinogenic D-amino acids [11], in order to study specific biological processes. Future choice of an unnatural amino acid should be mainly driven by the research objective, but also by its

potential acceptance by the ribosomal translational machinery and its stability. Indeed, some chemical properties of amino acids can affect the stability of aminoacylated tRNAs [12,13], and too large sizes are a physical limitation for the ribosome processing [14].

Single or multiple unnatural amino acid incorporation using different codon-anticodon pairs [15], or together with complementary orthogonal labeling methods such as FLASH [16], oligohistidine-NTA chromophores [17] or the human alkylguanine transferase procedure [18], this approach will offer many applications to investigate selective molecular interactions allowing the elucidation of structure-function relationships in live biological cells. More specifically, as I already could observe ligand-induced structural modifications in the 5-HT₃R by fusing EGFP molecules near the channel opening, it can be foreseen that the introduction of small fluorescent probes into the channel pore itself could lead to much stronger modifications of the fluorescence signals that could be followed over time. Although this is a speculative notion, it may be offered as an additional stimulus to future investigations of the 5-HT₃R structure and function.

III.1.2 References

1. Berteaux, V., Rousset, J.P. and Cassan, M. (1991) UAG readthrough is not increased in vivo by Moloney murine leukemia virus infection. *Biochimie*, **73**, 1291-1293.
2. Burke, J.F. and Mogg, A.E. (1985) Suppression of a nonsense mutation in mammalian cells in vivo by the aminoglycoside antibiotics G-418 and paromomycin. *Nucleic Acids Res*, **13**, 6265-6272.
3. Sedivy, J.M., Capone, J.P., RajBhandary, U.L. and Sharp, P.A. (1987) An inducible mammalian amber suppressor: propagation of a poliovirus mutant. *Cell*, **50**, 379-389.
4. Capone, J.P., Sedivy, J.M., Sharp, P.A. and RajBhandary, U.L. (1986) Introduction of UAG, UAA, and UGA nonsense mutations at a specific site in the Escherichia coli chloramphenicol acetyltransferase gene: use in measurement of amber, ochre, and opal suppression in mammalian cells. *Mol Cell Biol*, **6**, 3059-3067.
5. Cassan, M., Berteaux, V., Angrand, P.O. and Rousset, J.P. (1990) Expression vectors for quantitating in vivo translational ambiguity: their potential use to analyse frameshifting at the HIV gag-pol junction. *Res Virol*, **141**, 597-610.
6. Mamaev, S.V., Laikhter, A.L., Arslan, T. and Hecht, S.M. (1996) Firefly Luciferase: Alteration of the Color of Emitted Light Resulting from Substitutions at Position 286. *J Am Chem Soc*, **118**, 7243-7244.
7. Cornish, V.W., Benson, D.R., Altenbach, C.A., Hideg, K., Hubbell, W.L. and Schultz, P.G. (1994) Site-specific incorporation of biophysical probes into proteins. *Proc Natl Acad Sci U S A*, **91**, 2910.
8. Turcatti, G., Nemeth, K., Edgerton, M.D., Meseth, U., Talabot, F., Peitsch, M., Knowles, J., Vogel, H. and Chollet, A. (1996) Probing the structure and function of the tachykinin neurokinin-2 receptor through biosynthetic incorporation of fluorescent amino acids at specific sites. *J Biol Chem*, **271**, 19991-19998.
9. Taki, M., Hohsaka, T., Murakami, H., Taira, K. and Sisido, M. (2001) A non-natural amino acid for efficient incorporation into proteins as a sensitive fluorescent probe. *FEBS Lett*, **507**, 35-38.
10. Zhang, Z., Smith, B.A., Wang, L., Brock, A., Cho, C. and Schultz, P.G. (2003) A New Strategy for the Site-Specific Modification of Proteins in Vivo. *Biochemistry*, **42**, 6735-6746.
11. Dedkova, L.M., Fahmi, N.E., Golovine, S.Y. and Hecht, S.M. (2003) Enhanced D-amino acid incorporation into protein by modified ribosomes. *J Am Chem Soc*, **125**, 6616-6617.

12. Hentzen, D., Mandel, P. and Garel, J.P. (1972) Relation between aminoacyl-tRNA stability and the fixed amino acid. *Biochim Biophys Acta*, **281**, 228-232.
13. Stepanov, V.G. and Nyborg, J. (2002) Thermal stability of aminoacyl-tRNAs in aqueous solutions. *Extremophiles*, **6**, 485-490.
14. Hohsaka, T., Sato, K., Sisido, M., Takai, K. and Yokoyama, S. (1993) Adaptability of nonnatural aromatic amino acids to the active center of the E. coli ribosomal A site. *FEBS Lett*, **335**, 47-50.
15. Kohrer, C., Yoo, J.H., Bennett, M., Schaack, J. and RajBhandary, U.L. (2003) A possible approach to site-specific insertion of two different unnatural amino acids into proteins in mammalian cells via nonsense suppression. *Chem Biol*, **10**, 1095-1102.
16. Adams, S.R., Campbell, R.E., Gross, L.A., Martin, B.R., Walkup, G.K., Yao, Y., Llopis, J. and Tsien, R.Y. (2002) New biarsenical ligands and tetracysteine motifs for protein labeling in vitro and in vivo: synthesis and biological applications. *J Am Chem Soc*, **124**, 6063-6076.
17. Guignet, E.G., Hovius, R. and Vogel, H. (2004) Reversible site-selective labeling of membrane proteins in live cells. *Nat Biotechnol*.
18. Keppler, A., Gendreizig, S., Gronemeyer, T., Pick, H., Vogel, H. and Johnsson, K. (2003) A general method for the covalent labeling of fusion proteins with small molecules in vivo. *Nat Biotechnol*, **21**, 86-89.

IV

Appendix

IV – Appendix

IV.1 Murine 5-HT_{3A} receptor cDNA

```

      1   2   3   4   5   6   7   8   9   10  11  12  13  14  15  16
5' – ATG CGG CTC TGC ATC CCG CAG GTG CTG TTG GCC TTG TTC CTT TCC ATG

17  18  19  20  21  22  23  24  25  26  27  28  29  30  31  32  33
CTG ACA GCC CCG GGA GAA GGC AGC CGG AGG AGG GCC ACC CAG GAG GAT ACC

34  35  36  37  38  39  40  41  42  43  44  45  46  47  48  49  50
ACC CAG CCT GCT CTA CTA AGG CTG TCA GAC CAC CTC CTG GCT AAC TAC AAG

51  52  53  54  55  56  57  58  59  60  61  62  63  64  65  66  67
AAG GGG GTG CGG CCT GTG CGG GAC TGG AGG AAG CCT ACT ACT GTC TCC ATT

68  69  70  71  72  73  74  75  76  77  78  79  80  81  82  83  84
GAT GTC ATC ATG TAT GCC ATC CTC AAC GTG GAT GAG AAG AAC CAG GTT CTG

85  86  87  88  89  90  91  92  93  94  95  96  97  98  99  100 101
ACC ACC TAC ATA TGG TAC CGG CAG TAC TGG ACT GAT GAG TTT CTG CAG TGG

102 103 104 105 106 107 108 109 110 111 112 113 114 115 116 117 118
ACT CCT GAG GAC TTC GAC AAT GTC ACC AAA TTG TCC ATC CCC ACA GAC AGC

119 120 121 122 123 124 125 126 127 128 129 130 131 132 133 134 135
ATC TGG GTC CCT GAC ATT CTC ATC AAT GAG TTT GTG GAC GTG GGG AAG TCT

136 137 138 139 140 141 142 143 144 145 146 147 148 149 150 151 152
CCG AAC ATT CCT TAT GTG TAC GTG CAT CAT CGA GGT GAA GTT CAG AAC TAC

153 154 155 156 157 158 159 160 161 162 163 164 165 166 167 168 169
AAG CCC TTG CAA TTG GTG ACC GCC TGT AGC CTT GAC ATC TAC AAC TTC CCC

170 171 172 173 174 175 176 177 178 179 180 181 182 183 184 185 186
TTT GAT GTG CAG AAC TGT TCT CTG ACT TTC ACC AGC TGG CTG CAC ACC ATC

187 188 189 190 191 192 193 194 195 196 197 198 199 200 201 202 203
CAG GAC ATC AAC ATT ACT CTG TGG CGA TCA CCG GAA GAA GTG AGG TCT GAC

204 205 206 207 208 209 210 211 212 213 214 215 216 217 218 219 220
AAG AGC ATC TTC ATA AAT CAG GGC GAG TGG GAG CTG CTG GAG GTG TTC CCC

221 222 223 224 225 226 227 228 229 230 231 232 233 234 235 236 237
CAG TTC AAG GAG TTC AGC ATA GAT ATC AGT AAC AGC TAT GCA GAA ATG AAG

```

238 239 240 241 242 243 244 245 246 247 248 249 250 251 252 253 254
 TTC TAC GTG ATC ATC CGC CGG AGG CCT TTA TTC TAT GCA GTC AGC CTC TTG
 1

255 256 257 258 259 260 261 262 263 264 265 266 267 268 269 270 271
 CTG CCC AGT ATC TTC CTC ATG GTC GTG GAC ATT GTG GGC TTT TGC CTG CCC

272 273 274 275 276 277 278 279 280 281 282 283 284 285 286 287 288
 CCG GAC AGT GGT GAG AGA GTC TCT TTC AAG ATC ACA CTC CTT CTG GGA TAC
 2

289 290 291 292 293 294 295 296 297 298 299 300 301 302 303 304 305
 TCA GTC TTC CTC ATC ATC GTG TCA GAC ACA CTG CCG GCA ACG ATC GGT ACC

306 307 308 309 310 311 312 313 314 315 316 317 318 319 320 321 322
 CCC CTC ATT GGT GTC TAC TTT GTG GTG TGC ATG GCT CTG CTA GTG ATA AGC
 3

323 324 325 326 327 328 329 330 331 332 333 334 335 336 337 338 339
 CTC GCT GAG ACC ATC TTC ATT GTG CGG CTG GTG CAT AAG CAG GAC CTA CAG

340 341 342 343 344 345 346 347 348 349 350 351 352 353 354 355 356
 CGG CCA GTA CCT GAC TGG CTG AGG CAC CTG GTC CTA GAC AGA ATA GCC TGG

357 358 359 360 361 362 363 364 365 366 367 368 369 370 371 372 373
 ATA CTC TGC CTA GGG GAG CAG CCT ATG GCC CAT AGA CCC CCA GCC ACC TTC

374 375 376 377 378 379 380 381 382 383 384 385 386 387 388 389 390
 CAA GCC AAC AAG ACT GAT GAC TGC TCA GCC ATG GGA AAC CAC TGC AGC CAT

391 392 393 394 395 396 397 398 399 400 401 402 403 404 405 406 407
 GTT GGA GGA CCT CAG GAC TTG GAG AAG ACC CCA AGG GGC AGA GGT AGC CCT

408 409 410 411 412 413 414 415 416 417 418 419 420 421 422 423 424
 CTT CCA CCA CCA AGG GAG GCC TCA CTG GCT GTG CGT GGT CTC TTG CAA GAG

425 426 427 428 429 430 431 432 433 434 435 436 437 438 439 440 441
 CTA TCC TCC ATC CGC CAC TTC CTG GAG AAG CGG GAT GAG ATG CGG GAG GTG

442 443 444 445 446 447 448 449 450 451 452 453 454 455 456 457 458
 GCA AGG GAC TGG CTG CGG GTG GGA TAC GTG CTG GAC AGG CTG CTG TTC CGC
 4

459 460 461 462 463 464 465 466 467 468 469 470 471 472 473 474 475
 ATC TAC CTG CTG GCT GTG CTC GCT TAC AGC ATC ACC CTG GTC ACT CTC TGG

476 477 478 479 480 481
 TCC ATT TGG CAT TAT TCT TGA -3'

Short splicing variant of the murine 5-HT_{3A} receptor – SwissProt entry p23979.[1] The membrane targeting signal sequence is indicated in italics, and the four coding regions for the transmembrane domains are underlined.

IV.2 Bioluminescent proteins cDNAs

IV.2.1 Fluorescent proteins derived from *Aequorea victoria* GFP

Enhanced green fluorescent protein (EGFP) sequence:

```

1      2  3  4  5  6  7  8  9  10 11 12 13 14 15
5' - ATG GTG AGC AAG GGC GAG GAG CTG TTC ACC GGG GTG GTG CCC ATC CTG

16 17 18 19 20 21 22 23 24 25 26 27 28 29 30 31 32
GTC GAG CTG GAC GGC GAC GTA AAC GGC CAC AAG TTC AGC GTG TCC GGC GAG

33 34 35 36 37 38 39 40 41 42 43 44 45 46 47 48 49
GGC GAG GGC GAT GCC ACC TAC GGC AAG CTG ACC CTG AAG TTC ATC TGC ACC

50 51 52 53 54 55 56 57 58 59 60 61 62 63 64 65 66
ACC GGC AAG CTG CCC GTG CCC TGG CCC ACC CTC GTG ACC ACC CTG ACC TAC

67 68 69 70 71 72 73 74 75 76 77 78 79 80 81 82 83
GGC GTG CAG TGC TTC AGC CGC TAC CCC GAC CAC ATG AAG CAG CAC GAC TTC

84 85 86 87 88 89 90 91 92 93 94 95 96 97 98 99 100
TTC AAG TCC GCC ATG CCC GAA GGC TAC GTC CAG GAG CGC ACC ATC TTC TTC

101 102 103 104 105 106 107 108 109 110 111 112 113 114 115 116 117
AAG GAC GAC GGC AAC TAC AAG ACC CGC GCC GAG GTG AAG TTC GAG GGC GAC

118 119 120 121 122 123 124 125 126 127 128 129 130 131 132 133 134
ACC CTG GTG AAC CGC ATC GAG CTG AAG GGC ATC GAC TTC AAG GAG GAC GGC

135 136 137 138 139 140 141 142 143 144 145 146 147 148 149 150 151
AAC ATC CTG GGG CAC AAG CTG GAG TAC AAC TAC AAC AGC CAC AAC GTC TAT

152 153 154 155 156 157 158 159 160 161 162 163 164 165 166 167 168
ATC ATG GCC GAC AAG CAG AAG AAC GGC ATC AAG GTG AAC TTC AAG ATC CGC

169 170 171 172 173 174 175 176 177 178 179 180 181 182 183 184 185
CAC AAC ATC GAG GAC GGC AGC GTG CAG CTC GCC GAC CAC TAC CAG CAG AAC

186 187 188 189 190 191 192 193 194 195 196 197 198 199 200 201 202
ACC CCC ATC GGC GAC GGC CCC GTG CTG CTG CCC GAC AAC CAC TAC CTG AGC

203 204 205 206 207 208 209 210 211 212 213 214 215 216 217 218 219
ACC CAG TCC GCC CTG AGC AAA GAC CCC AAC GAG AAG CGC GAT CAC ATG GTC

220 221 222 223 224 225 226 227 228 229 230 231 232 233 234 235 236
CTG CTG GAG TTC GTG ACC GCC GCC GGG ATC ACT CTC GGC ATG GAC GAG CTG

237 238
TAC AAG TAA -3'

```

The usual numbering (as presented here) reflects amino acid positions in the original GFP (before addition of valine at position 2, modification in all the enhanced versions). The enhanced green fluorescent protein (EGFP) encodes the GFPmut1 variant [2], optimized for brighter fluorescence. The mutations from the original GFP are indicated in bold letters.

Cyan- and yellow-shifted variations are obtained by amino acid substitutions:

Specific ECFP (cyan) mutations [3]:	66	TAC ->CAC
	146	AAC->ATC
	153	ATG->ACC
	163	GTG->GCC
Specific EYFP (yellow) mutations [4]:	64	CTG ->TTC
	65	ACC->GGC
	68	GTG->CTG
	72	AGC->GCC
	203	ACC->TAC

The coding sequence of these genes contains additionally hundreds of silent base mutations corresponding to human codon usage preferences [5], for enhanced expression in mammalian cells.

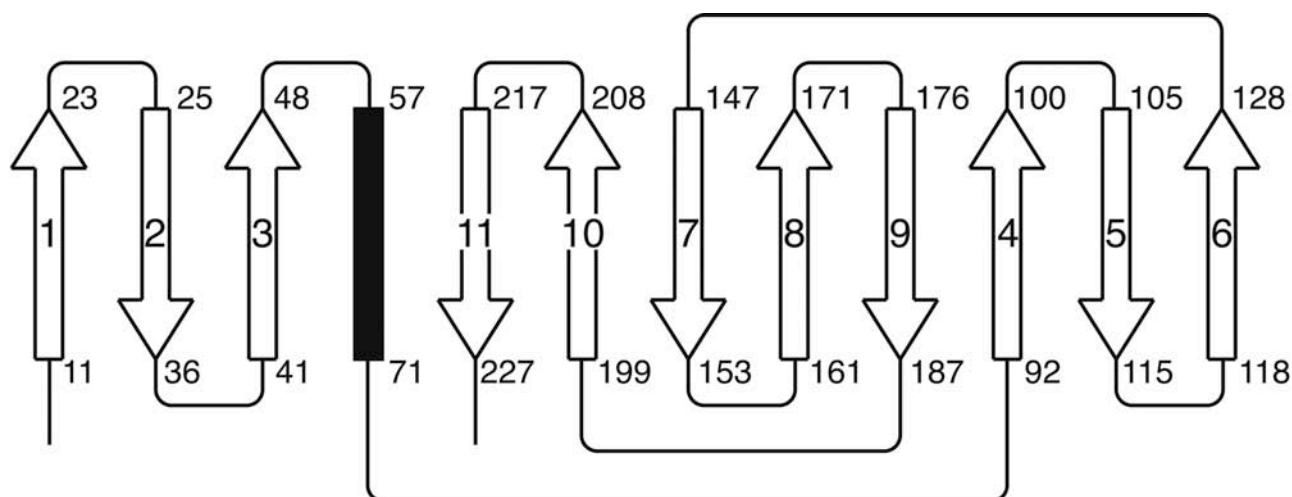


Figure IV.1 Schematic drawing of the overall fold of the fluorescent proteins derived from the GFP. The 11 strands forming the walls of the β barrel-shaped protein are shown as arrows, and the fluorescent core is depicted by a black rectangle (adapted from M. Ormö [3] and F. Yang [6]).

IV.2.2 DsRed Express cDNA derived from *Discosoma sp.* Red Fluorescent Protein

```

      1   2   3   4   5   6   7   8   9   10  11  12  13  14  15  16
5' - ATG GCC TCC TCC GAG GAC GTC ATC AAG GAG TTC ATG CGC TTC AAG GTG

17  18  19  20  21  22  23  24  25  26  27  28  29  30  31  32  33
CGC ATG GAG GGC TCC GTG AAC GGC CAC GAG TTC GAG ATC GAG GGC GAG GGC

34  35  36  37  38  39  40  41  42  43  44  45  46  47  48  49  50
GAG GGC CGC CCC TAC GAG GGC ACC CAG ACC GCC AAG CTG AAG GTG ACC AAG

51  52  53  54  55  56  57  58  59  60  61  62  63  64  65  66  67
GGC GGC CCC CTG CCC TTC GCC TGG GAC ATC CTG TCC CCC CAG TTC CAG TAC

68  69  70  71  72  73  74  75  76  77  78  79  80  81  82  83  84
GGC TCC AAG GTG TAC GTG AAG CAC CCC GCC GAC ATC CCC GAC TAC AAG AAG

85  86  87  88  89  90  91  92  93  94  95  96  97  98  99  100 101
CTG TCC TTC CCC GAG GGC TTC AAG TGG GAG CGC GTG ATG AAC TTC GAG GAC

102 103 104 105 106 107 108 109 110 111 112 113 114 115 116 117 118
GGC GGC GTG GTG ACC GTG ACC CAG GAC TCC TCC CTG CAG GAC GGC TCC TTC

119 120 121 122 123 124 125 126 127 128 129 130 131 132 133 134 135
ATC TAC AAG GTG AAG TTC ATC GGC GTG AAC TTC CCC TCC GAC GGC CCC GTA

136 137 138 139 140 141 142 143 144 145 146 147 148 149 150 151 152
ATG CAG AAG AAG ACT ATG GGC TGG GAG GCC TCC ACC GAG CGC CTG TAC CCC

153 154 155 156 157 158 159 160 161 162 163 164 165 166 167 168 169
CGC GAC GGC GTG CTG AAG GGC GAG ATC CAC AAG GCC CTG AAG CTG AAG GAC

170 171 172 173 174 175 176 177 178 179 180 181 182 183 184 185 186
GGC GGC CAC TAC CTG GTG GAG TTC AAG TCC ATC TAC ATG GCC AAG AAG CCC

187 188 189 190 191 192 193 194 195 196 197 198 199 200 201 202 203
GTG CAG CTG CCC GGC TAC TAC TAC GTG GAC TCC AAG CTG GAC ATC ACC TCC

204 205 206 207 208 209 210 211 212 213 214 215 216 217 218 219 220
CAC AAC GAG GAC TAC ACC ATC GTG GAG CAG TAC GAG CGC GCC GAG GGC CGC

221 222 223 224 225
CAC CAC CTG TTC CTG TAG -3'

```

The nine mutations on the original DsRed sequence [7] are marked in bold letters. Their purpose is to improve the solubility of the protein, shorten the folding time to that of the EGFP and reduce the level of green emission [8]. A large number of silent mutations are also present to optimize the sequence to human codon usage [4].

IV.3 Subcellular targeting sequences

IV.3.1 Nucleus

Tandem repeat of the nuclear localization signal (NLS) to be fused at C-terminus:

```

      1   2   3   4   5   6   7   8   9   10  11  12  13  14  15  16
5' – GAT CCA AAA AAG AAG AGA AAG GTA GAT CCA AAA AAG AAG AGA AAG GTA
      17  18  19  20  21  22  23  24
GAT CCA AAA AAG AAG AGA AAG GTA –3'

```

The reiteration of the NLS sequence of the simian virus 40 large T-antigen [9,10] significantly increases the efficiency of translocation into the nucleus of mammalian cells [11].

IV.3.2 Endoplasmic reticulum

Endoplasmic reticulum (ER) targeting sequence of calreticulin [12] to be cloned at the 5' end:

```

      1   2   3   4   5   6   7   8   9   10  11  12  13  14  15  16
5' – ATG CTG CTA TCC GTG CCG TTG CTG CTC GGC CTC CTC GGC CTG GCC GTC
      17
GCC –3'

```

and the sequence encoding the ER retrieval sequence, KDEL [13,14] (2, 3), cloned at the 3' end:

```

      1   2   3   4
5' – AAG GAC GAG CTG –3'

```

IV.3.3 Golgi

Golgi apparatus to be fused at N-terminus:

```

      1   2   3   4   5   6   7   8   9   10  11  12  13  14  15  16
5' – ATG AGG CTT CGG GAG CCG CTC CTG AGC GGC AGC GCC GCG ATG CCA GGC
      17  18  19  20  21  22  23  24  25  26  27  28  29  30  31  32  33
GCC TCC CTA CAG CGG GCC TGC CGC CTG CTC GTG GCC GTC TGC GCT CTG CAC
      34  35  36  37  38  39  40  41  42  43  44  45  46  47  48  49  50
CTT GGC GTC ACC CTC GTT TAC TAC CTG GCT GGC CGC GAC CTG AGC CGC CTG
      51  52  53  54  55  56  57  58  59  60  61  62  63  64  65  66  67
CCC CAA CTG GTC GGA GTC TCC ACA CCG CTG CAG GGC GGC TCG AAC AGT GCC

```

68 69 70 71 72 73 74 75 76 77 78 79 80 81 82
 GCC GCC ATC GGG CAG TCC TCC GGG GAG CTC CGG ACC GGA GGG GCC -3'

The sequence encoding the N-terminal 81 amino acids of human beta 1,4-galactosyltransferase (GT; [15]) contains the membrane-anchoring signal peptide that targets the fusion protein to the trans-medial region of the Golgi apparatus [16-18].

IV.3.4 Actin

Human cytoplasmic beta-actin [19,20] to be fused at C-terminus:

	1	2	3	4	5	6	7	8	9	10	11	12	13	14	15	16
5' -	ATG	GAT	GAT	GAT	ATC	GCC	GCG	CTC	GTC	GTC	GAC	AAC	GGC	TCC	GGC	ATG
17	18	19	20	21	22	23	24	25	26	27	28	29	30	31	32	33
TGC	AAG	GCC	GGC	TTC	GCG	GGC	GAC	GAT	GCC	CCC	CGG	GCC	GTC	TTC	CCC	TCC
34	35	36	37	38	39	40	41	42	43	44	45	46	47	48	49	50
ATC	GTG	GGG	CGC	CCC	AGG	CAC	CAG	GGC	GTG	ATG	GTG	GGC	ATG	GGT	CAG	AAG
51	52	53	54	55	56	57	58	59	60	61	62	63	64	65	66	67
GAT	TCC	TAT	GTG	GGC	GAC	GAG	GCC	CAG	AGC	AAG	AGA	GGC	ATC	CTC	ACC	CTG
68	69	70	71	72	73	74	75	76	77	78	79	80	81	82	83	84
AAG	TAC	CCC	ATC	GAG	CAC	GGC	ATC	GTC	ACC	AAC	TGG	GAC	GAC	ATG	GAG	AAA
85	86	87	88	89	90	91	92	93	94	95	96	97	98	99	100	101
ATC	TGG	CAC	CAC	ACC	TTC	TAC	AAT	GAG	CTG	CGT	GTG	GCT	CCC	GAG	GAG	CAC
102	103	104	105	106	107	108	109	110	111	112	113	114	115	116	117	118
CCC	GTG	CTG	CTG	ACC	GAG	GCC	CCC	CTG	AAC	CCC	AAG	GCC	AAC	CGC	GAG	AAG
119	120	121	122	123	124	125	126	127	128	129	130	131	132	133	134	135
ATG	ACC	CAG	ATC	ATG	TTT	GAG	ACC	TTC	AAC	ACC	CCA	GCC	ATG	TAC	GTT	GCT
136	137	138	139	140	141	142	143	144	145	146	147	148	149	150	151	152
ATC	CAG	GCT	GTG	CTA	TCC	CTG	TAC	GCC	TCT	GGC	CGT	ACC	ACT	GGC	ATC	GTG
153	154	155	156	157	158	159	160	161	162	163	164	165	166	167	168	169
ATG	GAC	TCC	GGT	GAC	GGG	GTC	ACC	CAC	ACT	GTG	CCC	ATC	TAC	GAG	GGG	TAT
170	171	172	173	174	175	176	177	178	179	180	181	182	183	184	185	186
GCC	CTC	CCC	CAT	GCC	ATC	CTG	CGT	CTG	GAC	CTG	GCT	GGC	CGG	GAC	CTG	ACT
187	188	189	190	191	192	193	194	195	196	197	198	199	200	201	202	203
GAC	TAC	CTC	ATG	AAG	ATC	CTC	ACC	GAG	CGC	GGC	TAC	AGC	TTC	ACC	ACC	ACG
204	205	206	207	208	209	210	211	212	213	214	215	216	217	218	219	220
GCC	GAG	CGG	GAA	ATC	GTG	CGT	GAC	ATT	AAG	GAG	AAG	CTG	TGC	TAC	GTC	GCC

221 222 223 224 225 226 227 228 229 230 231 232 233 234 235 236 237
 CTG GAC TTC GAG CAA GAG ATG GCC ACG GCT GCT TCC AGC TCC TCC CTG GAG
 238 239 240 241 242 243 244 245 246 247 248 249 250 251 252 253 254
 AAG AGC TAC GAG CTG CCT GAC GGC CAG GTC ATC ACC ATT GGC AAT GAG CGG
 255 256 257 258 259 260 261 262 263 264 265 266 267 268 269 270 271
 TTC CGC TGC CCT GAG GCA CTC TTC CAG CCT TCC TTC CTG GGC ATG GAG TCC
 272 273 274 275 276 277 278 279 280 281 282 283 284 285 286 287 288
 TGT GGC ATC CAC GAA ACT ACC TTC AAC TCC ATC ATG AAG TGT GAC GTG GAC
 289 290 291 292 293 294 295 296 297 298 299 300 301 302 303 304 305
 ATC CGC AAA GAC CTG TAC GCC AAC ACA GTG CTG TCT GGC GGC ACC ACC ATG
 306 307 308 309 310 311 312 313 314 315 316 317 318 319 320 321 322
 TAC CCT GGC ATT GCC GAC AGG ATG CAG AAG GAG ATC ACT GCC CTG GCA CCC
 323 324 325 326 327 328 329 330 331 332 333 334 335 336 337 338 339
 AGC ACA ATG AAG ATC AAG ATC ATT GCT CCT CCT GAG CGC AAG TAC TCC GTG
 340 341 342 343 344 345 346 347 348 349 350 351 352 353 354 355 356
 TGG ATC GGC GGC TCC ATC CTG GCC TCG CTG TCC ACC TTC CAG CAG ATG TGG
 357 358 359 360 361 362 363 364 365 366 367 368 369 370 371 372 373
 ATC AGC AAG CAG GAG TAT GAC GAG TCC GGC CCC TCC ATC GTC CAC CGC AAA
 374 375
 TGC TTC TAG –3'

IV.3.5 Tubulin

Human alpha-tubulin [21,22] to be fused at C-terminus:

1 2 3 4 5 6 7 8 9 10 11 12 13 14 15 16
 5' – GTG CGT GAG TGC ATC TCC ATC CAC GTT GGC CAG GCT GGT GTC CAG ATT
 17 18 19 20 21 22 23 24 25 26 27 28 29 30 31 32 33
 GGC AAT GCC TGC TGG GAG CTC TAC TGC CTG GAA CAC GGC ATC CAG CCC GAT
 34 35 36 37 38 39 40 41 42 43 44 45 46 47 48 49 50
 GGC CAG ATG CCA AGT GAC AAG ACC ATT GGG GGA GGA GAT GAC TCC TTC AAC
 51 52 53 54 55 56 57 58 59 60 61 62 63 64 65 66 67
 ACC TTC TTC AGT GAG ACG GGC GCT GGC AAG CAC GTG CCC CGG GCT GTG TTT
 68 69 70 71 72 73 74 75 76 77 78 79 80 81 82 83 84
 GTA GAC TTG GAA CCC ACA GTC ATT GAT GAA GTT CGC ACT GGC ACC TAC CGC

ILEGEMS

85 86 87 88 89 90 91 92 93 94 95 96 97 98 99 100 101
 CAG CTC TTC CAC CCT GAG CAG CTC ATC ACA GGC AAG GAA GAT GCT GCC AAT

 102 103 104 105 106 107 108 109 110 111 112 113 114 115 116 117 118
 AAC TAT GCC CGA GGG CAC TAC ACC ATT GGC AAG GAG ATC ATT GAC CTT GTG

 119 120 121 122 123 124 125 126 127 128 129 130 131 132 133 134 135
 TTG GAC CGA ATT CGC AAG CTG GCT GAC CAG TGC ACC GGT CTT CAG GGC TTC

 136 137 138 139 140 141 142 143 144 145 146 147 148 149 150 151 152
 TTG GTT TTC CAC AGC TTT GGT GGG GGA ACT GGT TCT GGG TTC ACC TCC CTG

 153 154 155 156 157 158 159 160 161 162 163 164 165 166 167 168 169
 CTC ATG GAA CGT CTC TCA GTT GAT TAT GGC AAG AAG TCC AAG CTG GAG TTC

 170 171 172 173 174 175 176 177 178 179 180 181 182 183 184 185 186
 TCC ATT TAC CCA GCA CCC CAG GTT TCC ACA GCT GTA GTT GAG CCC TAC AAC

 187 188 189 190 191 192 193 194 195 196 197 198 199 200 201 202 203
 TCC ATC CTC ACC ACC CAC ACC ACC CTG GAG CAC TCT GAT TGT GCC TTC ATG

 204 205 206 207 208 209 210 211 212 213 214 215 216 217 218 219 220
 GTA GAC AAT GAG GCC ATC TAT GAC ATC TGT CGT AGA AAC CTC GAT ATC GAG

 221 222 223 224 225 226 227 228 229 230 231 232 233 234 235 236 237
 CGC CCA ACC TAC ACT AAC CTT AAC CGC CTT ATT AGC CAG ATT GTG TCC TCC

 238 239 240 241 242 243 244 245 246 247 248 249 250 251 252 253 254
 ATC ACT GCT TCC CTG AGA TTT GAT GGA GCC CTG AAT GTT GAC CTG ACA GAA

 255 256 257 258 259 260 261 262 263 264 265 266 267 268 269 270 271
 TTC CAG ACC AAC CTG GTG CCC TAC CCC CGC ATC CAC TTC CCT CTG GCC ACA

 272 273 274 275 276 277 278 279 280 281 282 283 284 285 286 287 288
 TAT GCC CCT GTC ATC TCT GCT GAG AAA GCC TAC CAT GAA CAG CTT TCT GTA

 289 290 291 292 293 294 295 296 297 298 299 300 301 302 303 304 305
 GCA GAG ATC ACC AAT GCT TGC TTT GAG CCA GCC AAC CAG ATG GTG AAA TGT

 306 307 308 309 310 311 312 313 314 315 316 317 318 319 320 321 322
 GAC CCT CGC CAT GGT AAA TAC ATG GCT TGC TGC CTG TTG TAC CGT GGT GAC

 323 324 325 326 327 328 329 330 331 332 333 334 335 336 337 338 339
 GTG GTT CCC AAA GAT GTC AAT GCT GCC ATT GCC ACC ATC AAA ACC AAG CGC

 340 341 342 343 344 345 346 347 348 349 350 351 352 353 354 355 356
 AGC ATC CAG TTT GTG GAT TGG TGC CCC ACT GGC TTC AAG GTT GGC ATC AAC

 357 358 359 360 361 362 363 364 365 366 367 368 369 370 371 372 373
 TAC CAG CCT CCC ACT GTG GTG CCT GGT GGA GAC CTG GCC AAG GTA CAG AGA

```

374 375 376 377 378 379 380 381 382 383 384 385 386 387 388 389 390
GCT GTG TGC ATG CTG AGC AAC ACC ACA GCC ATT GCT GAG GCC TGG GCT CGC

391 392 393 394 395 396 397 398 399 400 401 402 403 404 405 406 407
CTG GAC CAC AAG TTT GAC CTG ATG TAT GCC AAG CGT GCC TTT GTT CAC TGG

408 409 410 411 412 413 414 415 416 417 418 419 420 421 422 423 424
TAC GTG GGT GAG GGG ATG GAG GAA GGC GAG TTT TCA GAG GCC CGT GAA GAT

425 426 427 428 429 430 431 432 433 434 435 436 437 438 439 440 441
ATG GCT GCC CTT GAG AAG GAT TAT GAG GAG GTT GGT GTG GAT TCT GTT GAA

442 443 444 445 446 447 448 449 450 451
GGA GAG GGT GAG GAA GAA GGA GAG GAA TAC TAA -3'

```

IV.3.6 Endosomes

Human rhoB GTPase [23] to be fused at C-terminus:

```

      1   2   3   4   5   6   7   8   9   10  11  12  13  14  15  16
5' - CGG AAG AAA CTG GTG GTT GTT GGT GAT GGA GCC TGT GGA AAG ACA TGC

17  18  19  20  21  22  23  24  25  26  27  28  29  30  31  32  33
TTG CTC ATA GTC TTC AGC AAG GAC GAG TTC CCA GAG GTG TAT GTG CCC ACA

34  35  36  37  38  39  40  41  42  43  44  45  46  47  48  49  50
GTG TTT GAG AAC TAT GTG GCA GAT ATC GAG GTG GAT GGA AAG CAG GTA GAG

51  52  53  54  55  56  57  58  59  60  61  62  63  64  65  66  67
TTG GCT TTG TGG GAC ACA GCT GGC CAG GAG GAC TAC GAC CGC CTG CGG CCG

68  69  70  71  72  73  74  75  76  77  78  79  80  81  82  83  84
CTC TCC TAC CCG GAC ACC GAC GTC ATT CTC ATG TGC TTC TCG GTG GAC AGC

85  86  87  88  89  90  91  92  93  94  95  96  97  98  99  100 101
CCG GAC TCG CTG GAG AAC ATC CCC GAG AAG TGG GTC CCC GAG GTG AAG CAC

102 103 104 105 106 107 108 109 110 111 112 113 114 115 116 117 118
TTC TGT CCC AAT GTG CCC ATC ATC CTG GTG GCC AAC AAA AAA GAC CTG CGC

119 120 121 122 123 124 125 126 127 128 129 130 131 132 133 134 135
AGC GAC GAG CAT GTC CGC ACA GAG CTG GCC CGC ATG AAG CAG GAA CCC GTT

136 137 138 139 140 141 142 143 144 145 146 147 148 149 150 151 152
CGC ACG GAT GAC GGC CGC GCC ATG GCC GTG CGC ATC CAA GCC TAC GAC TAC

153 154 155 156 157 158 159 160 161 162 163 164 165 166 167 168
CTC GAG TGC TCT GCC AAG ACC AAG GAA GGC GTG CGC GAG GTC TTC GAG -3'

```

IV.4 References

1. Maricq, A.V., Peterson, A.S., Brake, A.J., Myers, R.M. and Julius, D. (1991) Primary structure and functional expression of the 5HT3 receptor, a serotonin-gated ion channel. *Science*, **254**, 432-437.
2. Cormack, B.P., Valdivia, R.H. and Falkow, S. (1996) FACS-optimized mutants of the green fluorescent protein (GFP). *Gene*, **173**(1), 33-38.
3. Ormö, M., Cubitt, A.B., Kallio, K., Gross, L.A., Tsien, R.Y. and Remington, S.J. (1996) Crystal structure of the *Aequorea victoria* green fluorescent protein. *Science*, **273**, 1392-1395.
4. Heim, R., Prasher, D.C. and Tsien, R.Y. (1994) Wavelength mutations and posttranslational autoxidation of green fluorescent protein. *Proc Natl Acad Sci U S A*, **91**, 12501-12504.
5. Haas, J., Park, E.C. and Seed, B. (1996) Codon usage limitation in the expression of HIV-1 envelope glycoprotein. *Curr Biol*, **6**, 315-324.
6. Yang, F., Moss, L.G. and Phillips, G.N., Jr. (1996) The molecular structure of green fluorescent protein. *Nat Biotechnol*, **14**, 1246-1251.
7. Matz, M.V., Fradkov, A.F., Labas, Y.A., Savitsky, A.P., Zaraisky, A.G., Markelov, M.L. and Lukyanov, S.A. (1999) Fluorescent proteins from nonbioluminescent Anthozoa species. *Nat Biotechnol*, **17**, 969-973.
8. Bevis, B.J. and Glick, B.S. (2002) Rapidly maturing variants of the *Discosoma* red fluorescent protein (DsRed). *Nat Biotechnol*, **20**, 83-87.
9. Kalderon, D., Roberts, B.L., Richardson, W.D. and Smith, A.E. (1984) A short amino acid sequence able to specify nuclear location. *Cell*, **39**, 499-509.
10. Lanford, R.E., Kanda, P. and Kennedy, R.C. (1986) Induction of nuclear transport with a synthetic peptide homologous to the SV40 T antigen transport signal. *Cell*, **46**, 575-582.
11. Fischer-Fantuzzi, L. and Vesco, C. (1988) Cell-dependent efficiency of reiterated nuclear signals in a mutant simian virus 40 oncoprotein targeted to the nucleus. *Mol Cell Biol*, **8**, 5495-5503.
12. Fliegel, L., Burns, K., MacLennan, D.H., Reithmeier, R.A. and Michalak, M. (1989) Molecular cloning of the high affinity calcium-binding protein (calreticulin) of skeletal muscle sarcoplasmic reticulum. *J Biol Chem*, **264**, 21522-21528.
13. Munro, S. and Pelham, H.R. (1987) A C-terminal signal prevents secretion of luminal ER proteins. *Cell*, **48**, 899-907.

14. Pelham, H.R. (1996) The dynamic organisation of the secretory pathway. *Cell Struct Funct*, **21**, 413-419.
15. Watzele, G. and Berger, E.G. (1990) Near identity of HeLa cell galactosyltransferase with the human placental enzyme. *Nucleic Acids Res*, **18**, 7174.
16. Llopis, J., McCaffery, J.M., Miyawaki, A., Farquhar, M.G. and Tsien, R.Y. (1998) Measurement of cytosolic, mitochondrial, and Golgi pH in single living cells with green fluorescent proteins. *Proc Natl Acad Sci U S A*, **95**, 6803-6808.
17. Yamaguchi, N. and Fukuda, M.N. (1995) Golgi retention mechanism of beta-1,4-galactosyltransferase. Membrane-spanning domain-dependent homodimerization and association with alpha- and beta-tubulins. *J Biol Chem*, **270**, 12170-12176.
18. Gleeson, P.A., Teasdale, R.D. and Burke, J. (1994) Targeting of proteins to the Golgi apparatus. *Glycoconj J*, **11**, 381-394.
19. Ponte, P., Ng, S.Y., Engel, J., Gunning, P. and Kedes, L. (1984) Evolutionary conservation in the untranslated regions of actin mRNAs: DNA sequence of a human beta-actin cDNA. *Nucleic Acids Res*, **12**, 1687-1696.
20. Westphal, M., Jungbluth, A., Heidecker, M., Muhlbauer, B., Heizer, C., Schwartz, J.M., Marriott, G. and Gerisch, G. (1997) Microfilament dynamics during cell movement and chemotaxis monitored using a GFP-actin fusion protein. *Curr Biol*, **7**, 176-183.
21. Kimble, M., Kuzmiak, C., McGovern, K.N. and de Hostos, E.L. (2000) Microtubule organization and the effects of GFP-tubulin expression in dictyostelium discoideum. *Cell Motil Cytoskeleton*, **47**, 48-62.
22. Neujahr, R., Albrecht, R., Kohler, J., Matzner, M., Schwartz, J.M., Westphal, M. and Gerisch, G. (1998) Microtubule-mediated centrosome motility and the positioning of cleavage furrows in multinucleate myosin II-null cells. *J Cell Sci*, **111 (Pt 9)**, 1227-1240.
23. Adamson, P., Paterson, H.F. and Hall, A. (1992) Intracellular localization of the P21rho proteins. *J Cell Biol*, **119**, 617-627.

Acknowledgments

Je tiens à remercier toutes les personnes qui ont participé de près ou de loin à l'élaboration de cette thèse:

Je remercie mon directeur de thèse - le Professeur Horst Vogel - pour m'avoir proposé ce projet inspirant et permis de réaliser mon travail dans son groupe, pour sa compétence scientifique et son esprit critique. La confiance dont il a fait preuve à mon égard m'a permis d'entreprendre les expériences les plus risquées du point de vue résultats, dont les plus abouties font partie de ce présent rapport.

J'exprime une très particulière gratitude envers le docteur Horst Pick, qui a supervisé avec engagement mon travail durant les nombreuses années nécessaires à son accomplissement. Son initiation à la biologie moléculaire et cellulaire fait partie des fondations indispensables au développement de ce travail de thèse. En plus de sa participation dans l'élaboration d'articles, il a corrigé de manière critique une grande partie de cette thèse. Je le remercie chaleureusement pour son support constant, sa patience et son amabilité.

Une grande reconnaissance aussi à Cédric Deluz, dont l'assistance enthousiaste et dévouée m'a aidé à venir à bout des nombreux projets s'accumulant à la fin de mon travail de thèse. Merci également à Verena Tabet pour son immense patience et son assistance administrative, et aux nombreux membres du LCPPM pour leur contribution à l'atmosphère stimulante du groupe.

Ce travail a aussi profité du savoir faire appréciable de Stephan Kellenberger, qui a fait les mesures électrophysiologiques de toutes mes constructions basées sur le 5-HT₃R, de Frédéric Grosjean pour les mesures au FACS, et de Yann Karlen et Michael Ilegems pour leur initiation à la real-time PCR. Claudio Arrivoli a participé activement au projet de recherche sur la suppression naturelle dans le cadre de son travail de diplôme en collaboration avec Cyrille Denarie, que je remercie également pour sa compétence dans le domaine de la chimie des ARNt.

Je remercie les experts pour avoir lu et corrigé de manière critique cette présente thèse.

Je remercie mes parents. Bien que n'ayant pas participé à mes manipulations au laboratoire, ils ont le mérite d'avoir contribué à ce travail de par leur éducation, leur soutien et leur amour.

Finalement je te remercie profondément, Gabriela, pour ton amour et pour avoir fait preuve de patience et d'entendement durant mes longues années de doctorat aux horaires imprévisibles.

Ce travail a été financé par le Fonds National Suisse de la Recherche Scientifique.

Curriculum Vitae

- 1973 Born in Summit, NJ, USA
- 1991 Maturité fédérale C, Gymnase CESSRIVE in Lausanne, Switzerland
- 1994-1998 Study of Chemistry at the University of Lausanne, Switzerland
- 1998 Diploma work in the group of Pr. Horst Vogel at the Laboratoire de chimie physique des polymères et membranes (LCPPM), EPFL:
“Epitope tagging of the murine serotonin receptor 5-HT₃ for structural analysis and surface immobilization”
- 1998 Novartis Prize for the highest grade point average at final exams in the Chemistry Department
- 1999-2004 Thesis under the supervision of Pr. Horst Vogel, LCPPM/EPFL:
“*In vivo* protein labeling for structural and functional investigation of the 5-HT_{3A} neurotransmitter receptor”

Publications

Ilegems, E., Pick, H.M. and Vogel, H. (2002) Monitoring mis-acylated tRNA suppression efficiency in mammalian cells via EGFP fluorescence recovery. *Nucleic Acids Res*, **30**, e128.

Rigler, P., Ulrich, W.P., Hovius, R., Ilegems, E., Pick, H. and Vogel, H. (2003) Downscaling Fourier transform infrared spectroscopy to the micrometer and nanogram scale: secondary structure of serotonin and acetylcholine receptors. *Biochemistry*, **42**, 14017-14022.

Pick, H.M., Schmid, E.L., Tairi, A.P., Ilegems, E., Preuss, A., Hovius, R. and Vogel, H. (2004) Downscaling bioanalytics to the submicrometer and attoliter range by probing cellular signaling reactions in single native vesicles. Manuscript submitted for publication.

Ilegems, E., Pick, H.M. and Vogel, H. (2004) RNA interference targeting eRF1 in human cells increases mis-acylated suppression efficiency. Manuscript submitted for publication.

Ilegems, E., Pick, H.M., Deluz, C., Kellenberger, S. and Vogel, H (2004) Noninvasive imaging of 5-HT₃ receptor trafficking in live cells: from biosynthesis to endocytosis. Manuscript submitted for publication.